EFFECTS OF GEOMETRIC DEVIATIONS AND NONLINEARITIES IN COHERENT OPTICAL DATA PROCESSORS

Under NASA Research Grant
NGR-34-002-038/S1
June 30, 1968

PROGRESS REPORT
GRANT NGR-34-002-038/S1
June 30, 1968

"EFFECTS OF GEOMETRIC DEVIATIONS AND NONLINEARITIES IN COHERENT OPTICAL DATA PROCESSORS"

to

The National Aeronautics and Space Administration, Washington, D. C.

North Carolina State University
Raleigh, North Carolina

Submitted: Frederick J. Tischer

Dr. Frederick J. Tischer, Professor
Principal Investigator

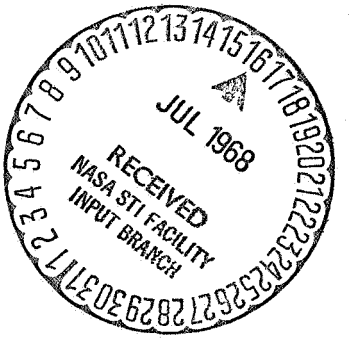

SUMMARY

This report represents the final report on work carried out under Grant NGR-34-002-038 during the period ending June 30, 1968. The report deals with the effects of geometric deviations and nonlinearities in coherent optical data processors. The study was carried out by James P. Moffatt under the direction of Dr. Frederick J. Tischer. The material was presented in part in previous interim reports. The resulting report was submitted by Mr. Moffatt as a dissertation for the degree of Doctor of Philosophy at the North Carolina State University at Raleigh, N. C.

The study deals with signal distortions in optical data processors, particularly optical correlators, caused by departures of signal-carrying surfaces from specified geometry (geometric deviations) and by nonlinearities. The nonlinearities are incurred in signal recording. It is the first phase of a more comprehensive investigation of error effects in data processing and holography. In the reported study, methods are developed for the description of the error effects. An equivalent noise-to-signal ratio is introduced for the description of the severity of the signal distortions. This method allows numerical comparisons and evaluations of the various effects. It also facilitates optimization of data processing and holographic reproduction systems. Effects of geometric deviations and nonlinearities were evaluated by this method. The results are presented in this report.

A novel method of analyzing nonlinearities encountered in optical signal recording is also developed in the present study. The method is based on Tchebyscheff expansions of nonlinear characteristics. In a comparison of various expansion methods, Tchebyscheff polynomials were found to be particularly well suited to this problem. It should be mentioned that the Tchebyscheff expansion method also can be applied for considering nonlinear effects in other nonoptical subject areas. Numerical methods and a computer program for the determination of the Tchebyscheff coefficients are developed. The program is then applied to an analysis of the characteristic curves of Type 649-F spectroscopic plates.

It was indicated above that the present study represents the first phase of a more comprehensive investigation. The reason for this statement is the fact that the methods developed and described in this report open ways for further studies which could not be carried out in the past since they led to excessively complicated relationships. Evaluation and comparison of photographic characteristic curves and of other optical recording principles, distortions in "noisy" optical systems, the effects of nonlinearities in specialized data processing systems and in holography are topics under continued investigation.

TABLE OF CONTENTS

TABLE OF CONTENTS (Continued)

TABLE OF CONTENTS (Continued)

LIST OF TABLES

LIST OF FIGURES

LIST OF FIGURES (Continued)

LIST OF FIGURES (Continued)

1. INTRODUCTION

Research in the area of optical data processing has existed for at least two decades. The advent of the laser as a convenient source of coherent quasi-monochromatic light, however, has increased interest in the subject. With the assumption of coherent light such as obtained from a laser, imaging properties of lenses in optical systems can be described by two-dimensional complex Fourier transforms. Image forms in such systems can thus be directly related to frequency and time domain representations of equivalent electrical signals. Because of this relation, optical systems employing coherent light can conveniently perform a wide variety of data processing operations.

This investigation is concerned with the analysis of two sources of signal distortions in optical data processors employing coherent light. The first of these can be described as deviations from optimum geometry of the surfaces on which signals are introduced to such processors. The deviations exist because of alignment errors and mechanical tolerances that are incurred in the construction of the processor. Specific models for these geometric deviations are introduced, and the signal distortions resulting from the models are derived. The distortions are quantitatively related to the parameters which characterize the geometry of the models.

The second source of signal distortions consists of nonlinearities which are incurred in the recording of signals in

optical form. A method of analysis is developed which allows determination of the extent to which the nonlinearities affect data processing. The method is implemented in the form of a digital computer program which facilitates rapid and thorough analysis of nonlinear transfer characteristics and allows determination of conditions under which nonlinear effects are minimized. The program is used to analyze the nonlinearities of type 649-F spectroscopic plates which are widely used in optical data processing.

2. REVIEW OF THE LITERATURE

2.1 Coherent Optical Data Processors

In a number of recent papers (Cutrona, 1960, 1964; Preston, 1965) the use of optical systems for data processing operations has been described. More specifically, systems employing coherent illumination have been shown to be capable of performing operations such as: spectral analysis, frequency domain filtering, crosscorrelation, autocorrelation, and convolution. A conceptual model of a optical system employing coherent illumination is abstracted from the above literature. By assuming various input and output devices, the model is able to perform the data processing operations mentioned. The model serves as an introduction to coherent optical data processors and provides a basis for discussing the literature reviewed in the next section.

In optical systems employing coherent light, image forms in sucessive focal planes are approximately related by two-dimensional Fourier trahsforms. This property allows such systems to process data spatially and constitutes one of their primary advantages. The Fourier transform imaging properties of such systems have been known for some time (Rhodes, 1953) but the lack of a convenient source of coherent illumination has hindered their development. With the advent of the laser, however, this difficulty has been overcome.

Figure 2.1 shows the geometric configuration of the optical system model. A point source of monochromatic illumination is placed at the left-hand focus of lens L_1 and imaging occurs in the system from left to right. The planes P_1 through P_4 coincide with the focal planes of the lenses. The focal length of each lens is f. Because of the imaging properties of the lenses, sucessive focal planes are illuminated by the two-dimensional Fourier transforms of the complex light amplitude distributions emerging from their predecessors. Various light and electro-optic modulating devices can thus be placed in the planes to perform data processing operations. In the following description of the operation of various configurations of the system, the Fourier transform relations are assumed in one dimension only. This allows direct analogies to be made to electrical systems.

The imaging properties of lens L_1 cause a uniform distribution of light to appear at the left-hand surface of plane P_1. The amplitude distribution in the x_1 direction can be described in complex presentation as

$$d_1'(x_1) = d_0 e^{j\frac{2\pi c}{\lambda} t} , \qquad (2.1)$$

where c is the velocity of light, λ is the wavelength of the coherent source, t is time, and d_o is an amplitude constant related to the intensity of the source.

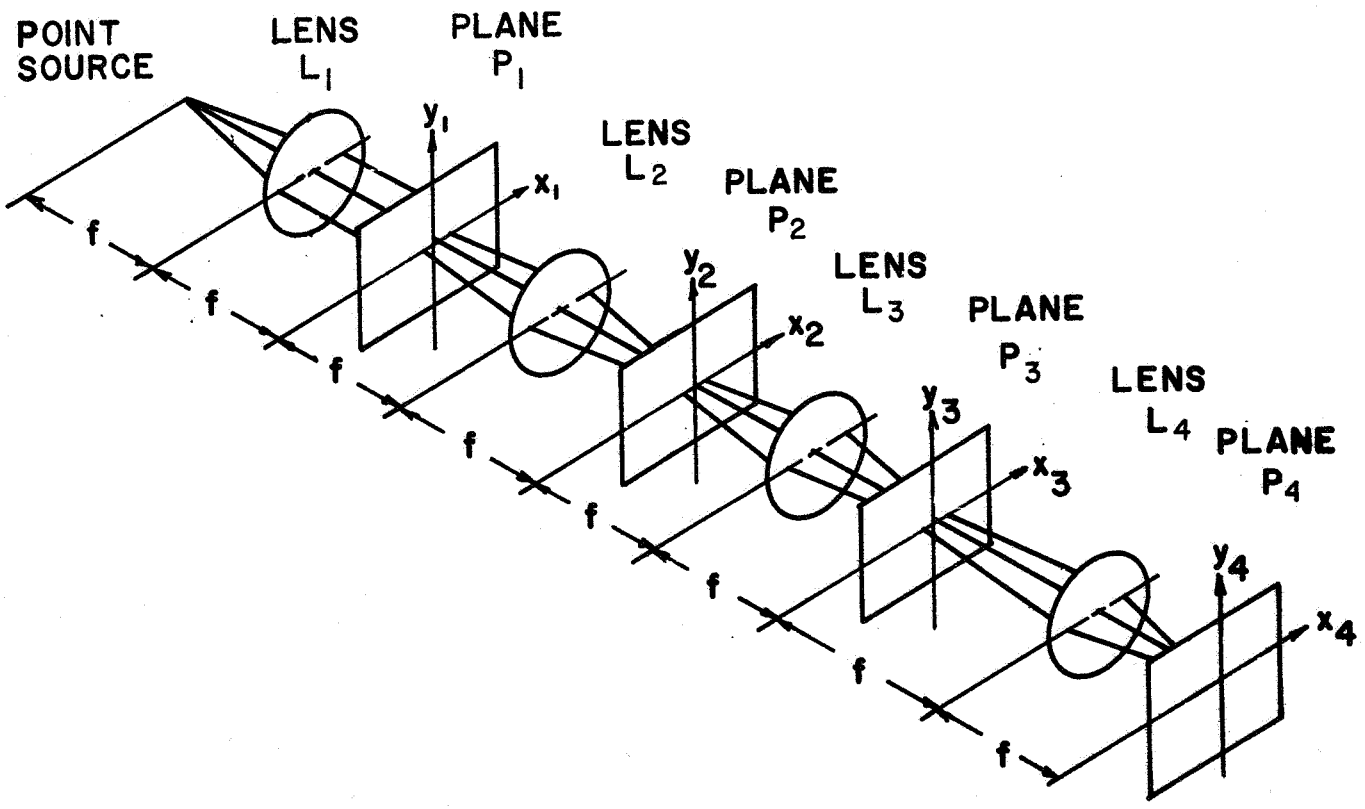

Figure 2.1 An optical system employing coherent light for data processing

A photographic transparency placed in plane P_1 serves as a means of modulating the distribution d_1'. The transparency can be described by an amplitude transmittance function $s_1(x_1)$ which relates the amplitude of the illumination transmitted by the transparency to that which is incident. The functional form of s_1 represents a signal which has been previously optically recorded with the addition of a bias such that $0 < s_1 < 1$. With the distribution d_1' incident on the transparency, the complex amplitude distribution on the right-hand side of plane P_1 becomes

$$d_1(x_1) = d_o s_1(x_1) e^{j\frac{2\pi c}{\lambda} t} . \tag{2.2}$$

In order to simplify the presentation, the constant d_o is assumed to be unity and the exponential time function is suppressed. Equation (2.2) then becomes

$$d_1(x_1) = s_1(x_1). \tag{2.3}$$

The imaging properties of lens L_2 cause a distribution corresponding to the Fourier transform of $d_1(x_1)$ to appear at the left-hand side of plane P_2. This can be written as

$$d_2'(w_2) = F[s_1(x_1)] = S_1(w_2), \tag{2.4}$$

where F represents the Fourier transformation, S_1 the transform of s_1 and the radian frequency w_2 is related to x_2 by

$$w_2 = \frac{2\pi}{\lambda f} x_2 . \tag{2.5}$$

A light sensor, such as a photocell, placed in plane P_2 can be used to obtain information about the frequency function S_1. If the output of the sensor is proportional to the intensity of the incident illumination and the sensor is moved along the x_2 axis, an output given by

$$V(w_2) = S_1(w_2)\ S_1^*(w_2), \tag{2.6}$$

appears (the asterisk denotes the complex conjugate). Inspection of Eq. (2.6) shows that the sensor's output corresponds to the spectral density of S_1. The operation of spectral analysis can thus be performed in the plane P_2.

If a photographic transparency having an amplitude transmittance function described by $S_2(w_2)$ is placed in the plane P_2 and the distribution d_2' is incident, the light emerging from the transparency is described by

$$d_2(w_2) = S_1(w_2)\ S_2(w_2). \tag{2.7}$$

This expression corresponds to the passage of the signal S_1 through a filter having a transfer function $S_2(w_2)$. Although the amplitude transmittance function of a transparency is restricted to be real such that $0 < S_2 < 1$, both negative and complex values for S_2 can be introduced in the plane P_2 by the use of phase modulating media such as thermoplastic films. The operation of frequency domain filtering can thus be performed in plane P_2. The lens L_3 causes a distribution given by

$$d_3'(x_3) = F[S_1(w_2)\ S_2(w_2)], \tag{2.8}$$

to appear at the left-hand side of plane P_3. Since the Fourier transform has the properties

$$F^{-1}\{F[s(x)]\} = s(x) \ , \tag{2.9}$$

and

$$F\{F[s(x)]\} = s(-x), \tag{2.10}$$

the distribution d_3' corresponds to a reflection about $x = 0$ of the inverse transform of the product S_1S_2. If the reflection is neglected, d_3' becomes

$$d_3'(x_3) = \int s_1(x_3 - p)\ S_2(p)\ dp \tag{2.11}$$

where

$$s_2 = F^{-1}[S_2] \ . \tag{2.12}$$

The convolution expression (2.11) corresponds to the output of the filter and S_2 represents its impulse response. If a light sensor responding linearly to light amplitude is placed in plane P_3 and traversed along the x_3 axis, the output corresponds to Eq. (2.11).

The optical system can be used to perform operations of convolution and correlation by placing transparencies containing signal functions in planes P_1 and P_3. If, as before, the amplitude transmittance of the transparency in plane P_1 is described by $s_1(x_1)$, so that

$$d_1(x_1) = s_1(x), \tag{2.13}$$

the lenses L_2 and L_3 cause a reflected image (double Fourier

transform) of d_1 to appear at the left-hand side of P_3. If the reflection is neglected,

$$d_3'(x_3) = s_1(x_3). \tag{2.14}$$

With the amplitude transmittance of the transparency in plane P_3 given by $s_3(x_3)$, the light emerging from the plane is described by

$$d_3(x_3) = s_1(x_3)\ s_3(x_3). \tag{2.15}$$

If the transparency in plane P_1 is translated in the negative x_1 direction by an amount u, Eq. (2.15) becomes

$$d_3(x_3) = s_1(x_3 + u)\ s_3(x_3). \tag{2.16}$$

The lens L_4 causes the Fourier transform of Eq. (2.16) to appear at the left-hand side of P_4 so that

$$d_4'(w_4) = F[s_1(x_3 + u)\ s_3(x_3)]\ , \tag{2.17}$$

where w_4 is related to x_4 by an expression similar to Eq. (2.5). Equation (2.17) can also be written

$$d_4'(w_4) = \int s_1(x_3 + u)\ s_3(x_3) e^{jw_4x_3} dx_3\ , \tag{2.18}$$

so that

$$d_4'(0) = \int s_1(x_3 + u)\ s_3(x_3) dx_3\ . \tag{2.19}$$

This last expression is recognized as the crosscorrelation of the functions s_1 and s_3 evaluated at u. Thus, a light sensor

placed in plane P_4 at the origin of the x_4 axis can be used to obtain the correlation of s_1 and s_3 as s_1 is translated parallel to the x axis. When s_1 and s_3 are different functions, the operation corresponds to crosscorrelation. When they are the same, autocorrelation results.

2.2 Imaging Errors Due to Geometric Deviations

In an optical system such as that shown in Fig. 2.1, the Fourier transform relation holds only between the various planes P_1, P_2, etc. If a transparency or light sensor placed in the processor deviates in position from one of these planes, errors in the optical imaging and resultant processor output occur. It is thus important to know what the effects of such deviations are and to what extent they affect the operation of the system as a data processor.

In a paper concerned with the mathematical description of the formation of optical images, J. E. Rhodes (1953) described phase distortions resulting from defocused images which can be readily interpreted in terms of the notation and geometry of the optical system described in the previous section. In Rhodes' paper the Fourier transform relation between the complex light amplitude distributions in the two focal planes of a lens was derived. Assume, for example, that the derived Fourier transformation exists between the planes P_1 and P_2 of Figure 2.1. Using the notation of the previous section, the complex light amplitude distributions

in the two planes are related by

$$d_2'(w_2) = F[d_1(x_1)] \ , \tag{2.20}$$

where F denotes the Fourier transform operation and w_2 is related to x_2 by Eq. (2.5). Rhodes described imaging errors in plane P_2 as the plane P_1 is displaced by a distance Δz along the optic axis.

The result was

$$d_2'(w_2) = F[d_1(x_1)]e^{-j\frac{\lambda w_2^2}{4\pi}\Delta z} \ , \tag{2.21}$$

where Δz represents the displacement of the plane P_1 and λ is the wavelength of the illumination. Equation (2.21) shows that the imaging error corresponds to a frequency dependent phase delay. The Fourier transform of $d_1(x_1)$ is thus distorted by this factor as the plane P_1 is displaced from the focal plane of the lens L_2.

Vander Lugt (1967) described some effects of small displacements of spatial filters on signal-to-noise ratios in coherent optical processors. The results of this work can be interpreted in terms of the optical processor model presented in the previous section. With a processor configuration similar to that described for frequency domain filtering, effects of displacing the transparency in plane P_2 both transversely and longitudinally along the optic (z) axis were considered. Assuming the transparency in plane P_1 to contain a signal $s_1(x_1)$ accompanied by an additive noise

$n_1(x_1)$ having uniform spectral density, the complex light amplitude distribution corresponding to that emerging from P_1 was described by

$$d_1(x_1) = s_1(x_1) + n_1(x_1). \tag{2.22}$$

The distribution incident on plane P_2 was then described by

$$d_2'(w_2) = S_1(w_2) + N_1(w_2), \tag{2.23}$$

where S_1 and N_1 represent, respectively, the Fourier transforms of s_1 and n_1 due to the imaging of lens L_2. In the plane P_2 a matched filter having a complex amplitude transmittance function

$$H_2(w_2) = C \frac{S_1^*(w_2)}{N_1(w_2)\ N_1^*(w_2)}, \tag{2.24}$$

was assumed, where the asterisk denotes the complex conjugate and C is a constant.

A transverse displacement of the filter by an amount Δw_2 was considered. The light distribution emerging from plane P_2 was described by a term corresponding to the signal given by

$$d_{s2}(w_2, \Delta w_2) = \frac{S_1(w_2)\ S_1^*(w_2 + \Delta w_2)}{N_1(w_2 + \Delta w_2)\ N_1^*(w_2 + \Delta w_2)}, \tag{2.25}$$

and a noise term

$$d_{n2}(w_2, \Delta w_2) = \frac{N_1(w_2)\ S_1^*(w_2 + \Delta w_2)}{N_1(w_2 + \Delta w_2)\ N_1^*(w_2 + \Delta w_2)}. \tag{2.26}$$

In the plane corresponding to P_3, the transforms of (2.25) and (2.26) appear so that the light distribution there is described by

$$d_3'(x_3,\Delta w_2) = F^{-1}[d_{s2}(w_2,\Delta w_2)] + F^{-1}[d_{n2}(w_2,\Delta w_2)], \tag{2.27}$$

when the reflection about $x_3 = 0$ is neglected. The two terms appearing in (2.27) thus correspond to the signal and noise components of the output of the displaced matched filter. A signal-to-noise power ratio was then formulated from these two components. With the assumption of a signal form which maximizes the degradation of the performance of the filter as it is displaced, the noise-to-signal ratio was shown to have the form

$$SNR(\Delta w_2) = SNR_o \left[\frac{\sin(\frac{\Delta w_2 L}{2})}{(\frac{\Delta w_2 L}{2})}\right]^2, \tag{2.28}$$

where SNR_o is the noise-to-signal ratio for zero displacement and ΔL is the spatial extent of the signal s_1. This relation was considered as a measure of the performance of the displaced filter. The function in the brackets of (2.28) is of the sin x/x type which occurs frequently in communication theory. The maximum value occurs for x (i.e. Δw_2) equal to zero, and the function is similar to a damped cosine wave. Equation (2.28) thus demonstrates the degradation of the

SNR as Δw_2 increases. The effect of the lateral displacement Δw_2 on the filter's operation is thus apparent.

Vander Lugt then considered a longitudinal displacement of the filter Δz which corresponds to the displacement of the plane P_2 of Figure 2.1 along the optic axis. He showed that the effect of such a displacement could be described by an equation identical to (2.28) with the effective Δw_2 given by

$$\Delta w_2 = \frac{2\pi x_o}{\lambda f^2} \Delta z \ , \qquad (2.29)$$

where the wavelength λ and focal length F follow the notation of the previous section, and x_o corresponds to the position of the signal s_1 on the x_1 axis of plane P_1.

2.3 Nonlinearities in Optical Data Processors

2.3.1 The Zero-Memory Model and Methods of Analysis

D. H. Kelly (1960) introduced a three-stage model for the analysis of photographic imaging processes. In the first stage, the light scattering properties of the emulsion are accounted for. The scattering prevents the emulsion from faithfully reproducing images of sharp edges or exposure patterns where the incident intensity varies considerably over small spatial dimensions. This effect is analogous to the low-pass filtering of electrical signals. The first stage of the model corresponds to image filtering of this type. A similar filtering operation occurs during the

development of the photographic material. The third stage characterizes this effect. Nonlinearities in the photographic process are accounted for in the second stage. A pointwise nonlinear transformation is used to relate the so-called latent image density (input to third stage) to the effective exposure (output of first stage). The transformation is termed pointwise since the latent image density at a given point on the emulsion surface is dependent only on the effective exposure at that point. An analogous situation occurs in the area of electrical engineering when signals are passed through nonlinear devices. If the instantaneous output of the device depends only on the instantaneous input, the nonlinearity is said to be of the zero-memory type (Middleton, 1960). The function describing the nonlinear transformation is termed the characteristic function, the transfer characteristic, or simply the characteristic.

In the literature on optical data processing and holography,methods of analyzing zero-memory nonlinearities have followed two general approaches. In the first, characteristic functions are represented by their Fourier or Laplace integral transforms. These methods have been widely used in the field of communication theory. They allow the determination of nonlinear effects on a wide variety of signal or image forms and have been applied primarily to the analysis of analytic models of actual nonlinear

characteristics. The models allow qualitative understanding of the effects of the nonlinearities that they represent and are quite useful in theoretical studies. In the second approach, the nonlinear characteristics, or models for them, are analyzed directly. In most applications, Taylor or power series expansions are employed which allow the nonlinear effects to be computed for sinusoidal signals. The direct methods have been applied to the analysis of empirically obtained characteristics. They can be readily applied to such characteristics and yield quantitative results with a minimum of computational complexity.

2.3.2 Transform Methods

Davenport and Root (1958) described the use of Transform methods for the analysis of zero-memory nonlinear characteristics. In their description, the output of a nonlinear device is expressed as

$$y = f(x) \tag{2.30}$$

where x represents the input of the device and f represents the zero-memory characteristic. The input of the device is assumed to be a function of some other variable t so that

$$y(t) = f[x(t)]. \tag{2.31}$$

If the function f is sectionally smooth and

$$\int_{-\infty}^{\infty} |f(x)| \, dx < +\infty , \tag{2.32}$$

exists, the Fourier transform of f exists and is given by

$$F(v) = \int_{-\infty}^{\infty} f(x)e^{-jvx}dx. \tag{2.33}$$

The output of the nonlinear device can then be expressed as

$$y = f(x) = \frac{1}{2\pi}\int_{-\infty}^{\infty} F(v)e^{jvx}dv. \tag{2.34}$$

For a given input, x(t), y becomes

$$y(t) = \frac{1}{2\pi}\int_{-\infty}^{\infty} F(v)e^{jvx(t)}dv. \tag{2.35}$$

This expression is used to obtain the form of y(t) from the input function x(t).

In some cases the characteristic function f may not meet the condition (2.32) but may satisfy

$$|f(x)| \leq M_1 e^{U_1 x} \ , \ x > 0 \tag{2.36}$$

and

$$|f(x)| \leq M_2 e^{-U_2 x} \ , \ x < 0 \tag{2.37}$$

where M_1, M_2, U_1, U_2 are positive constants. In such cases f can be represented by a pair of unilateral Laplace transforms given by

$$f_+(p) = \int_0^{\infty} f(x)e^{-px}dx \ , \tag{2.38}$$

and

$$F_-(p) = \int_{-\infty}^{\infty} f(x)e^{-px}dx, \tag{2.39}$$

where $p = u + jv$. The output of the nonlinear device is then given by

$$y = f(x) = \frac{1}{2\pi j}\left[\int_{\sigma_1 - j\infty}^{\sigma_1 + j\infty} F_+(p)e^{xp}\,dp + \int_{\sigma_2 - j\infty}^{\sigma_2 + j\infty} F_-(p)e^{xp}\,dp\right] \tag{3.40}$$

where $\sigma_1 > U_1$ and $\sigma_2 < U_2$. For a given $x(t)$, the output is expressed as

$$y(t) = \frac{1}{2\pi j}\left[\int_{\sigma_1 - j\infty}^{\sigma_1 + j\infty} F_+(p)e^{px(t)}\,dp + \int_{\sigma_2 - j\infty}^{\sigma_2 + j\infty} F_-(p)e^{px(t)}\,dp\right]. \tag{2.41}$$

In either Eq. (2.35) or (2.41). the form of $y(t)$ is usually obtained by expanding the exponentials containing $x(t)$ and computing the inverse transform termwise.

Kozma (1966) employed the Fourier transform method to describe some general effects of nonlinearities encountered in the photographic recording of spatially modulated coherent light. He considered the recording of a one-dimensional interference pattern created by two monochromatic wavefronts. One of these was a reference wave having a complex representation

$$r(x) = ke^{jbx}, \tag{2.42}$$

where k is the amplitude of the wave, b is a constant, and x is the spatial variable on the photographic material. The second wavefront contained signal information that was to be subsequently extracted from the photographic recording. The complex amplitude of this wave was described by

$$s(x) = a(x)e^{-j\phi(x)} , \tag{2.43}$$

where the functions $a(x)$ and $\phi(x)$ contain the information to be extracted. The interference pattern of these wavefronts was shown to create a modulation of the exposure of the recording medium given by

$$E(x) = ta^2(x) + 2tka(x) \cos[bx + \phi(x)] , \tag{2.44}$$

where t is the exposure time.

A zero-memory nonlinearity having functional form G was assumed to relate the amplitude transmittance of the photographic material to its exposure. Thus the spatial variation of the amplitude transmittance was given by

$$g(x) = G[E(x)] . \tag{2.45}$$

Using a Fourier transform representation for the nonlinearity G, Kozma showed that the form of $E(x)$ given in (2.44) results in an expression for $g(x)$ that can be written as

$$g(x) = \sum_{m=o}^{\infty} H_m(x) \cos \left\{ m[bx + \phi(x)] \right\} \tag{2.46}$$

where the various terms of the series result from the expansion of the exponential in the inverse transform. The

similarity of the first two terms of this series to the two terms in (2.44) is evident. An error-function-limiter model was assumed for the nonlinearities. G was thus given by

$$G(E) = \frac{L}{S}\sqrt{\frac{2}{\pi}}\int_{o}^{E} e^{-y^2/2S^2}\, dy \qquad (2.47)$$

where L and S are constants. The introduction of this model yielded expressions for H_0 and H_1 given by

$$H_0(x) = (\frac{L}{S}\sqrt{\frac{2}{\pi}})[ta^2(x)]\ f(x)\ , \qquad (2.48)$$

$$H_1(x) = (\frac{2L}{S}\sqrt{\frac{2}{\pi}})[2tka(x)]\ f(x)\ , \qquad (2.49)$$

and

$$f(x) = e^{-[tka(x)/s]^2}\ I_o\{[tka(x)/s]^2\}\ , \qquad (2.50)$$

where I_o represents the zero-order modified Bessel function of the first type. Thus, the first two terms of Eq. (2.46) correspond to Eq. (2.44) except for the amplitude distortion factor f(x). The form of this distortion factor was studied for cases of mild and severe nonlinear distortion. For mild distortions represented by tka(x) << S, a series expansiom of Eq. (2.50) gave

$$H_o(x) = (\frac{L}{S}\sqrt{\frac{2}{\pi}})\{ta^2(x) - tk^2[\frac{ta^2(x)}{s}]^2+...\}\ , \qquad (2.51)$$

and

$$H_1(x) = (\frac{2L}{S}\sqrt{\frac{2}{\pi}})\{2tka(x) - \frac{s}{4}[\frac{2tka(x)}{s}]^2+...\}\ . \qquad (2.52)$$

The leading terms in these expressions are identical to the

terms in the exposure expression. Kozma concluded that for mild nonlinear distortions, both the functions $a(x)$ and $\phi(x)$ can be recovered from the photographic recording. For severe distortions represented by $tka(x) >> S$, an asymptotic expansion of Eq. (2.50) yielded

$$H_o(x) = \left(\frac{L}{\pi}\right)\left\{\frac{a(x)}{k} + \frac{1}{8}\left(\frac{tk^2}{s}\right)^2 \frac{a(x)}{k} + \ldots\right\}, \tag{2.53}$$

and

$$H_1(x) = \left(\frac{4L}{\pi}\right)\left\{1 + \frac{1}{2}\left[\frac{2tka(x)}{s}\right]^2 + \ldots\right\} . \tag{2.54}$$

These expressions contain no terms with amplitude fluctuations similar to those of Eq. (2.44) and amplitude information is therefore lost. The phase function $\phi(x)$, however, still appears in the second term of Eq. (2.46). Thus Kozma concluded that even with severe nonlinearities in photographic processes, phase information in a recorded signal of the form of (2.43) can be recovered. These results demonstrate that spatial filters for use in optical data processors can be feasibly made by photographically recording interference patterns of reference and signal waves as given by (2.42) and (2.43).

Friesem and Zelenka (1967) used the Laplace transform method to describe the effects of photographic nonlinearities in holography. They assumed exposure of the photographic material to a monochromatic reference beam with complex representation

$$r(x) = A_r e^{j\theta_r(x)} , \tag{2.55}$$

where A_r is a constant and $\theta_r(x)$ is a linear function of x, and a signal beam given by

$$s(x) = A_1 e^{j\theta_1(x)} + A_2 e^{j\theta_2(x)} , \tag{2.56}$$

where A_1, A_2 are constants such that $A_1 >> A_2$ and $\theta_1(x), \theta_2(x)$ are linear functions of x. A signal beam of the form Eq. (2.56) occurs when the "scene" of the hologram contains two point sources of different intensities. The resulting amplitude transmittance of the hologram was described by

$$v(x) = g[u(x)] , \tag{2.57}$$

where g represents the nonlinear characteristic of the photographic process, and u(x) represents the modulation of the exposure resulting from the interference of Eqs. (2.55) and (2.56). The form of v(x) was obtained by the Laplace transform method and assuming g to be an odd power-law function of the form

$$g(u) = u|u|^{\nu-1} \tag{2.58}$$

where $\nu \geq 0$. The resulting amplitude transmittance function was shown to have terms which yield an output image corresponding to an array of point sources. Two of the point sources correspond to the reconstruction of the images of the object points, and the others correspond to false images. For severe nonlinearities, the false images of the stronger source are of intensity comparable to that of the reconstructed weak source. Experimental results included in the paper demonstrated the occurrence of the false images.

2.3.3 Direct Methods

In the area of optical data processing, direct methods of analyzing zero-memory characteristics have been applied in two ways. In the first, nonlinearities in photographic processes have been modeled by so-called gamma-law characteristics. That is, the intensity transmittance of a transparency is assumed to be related to its exposure by an equation of the form

$$T = KE^{-\gamma} , \tag{2.59}$$

where T represents the intensity transmittance, E the exposure, and K and γ are constants. This relation assumes the nonlinear characteristic to be representable by a power-law curve. With the exposure given as a sinusoidal function of a spatial variable, a power series expansion of the term $E^{-\gamma}$ is used to obtain an approximate expression for the resultant spatial variation of the intensity transmittance. Direct methods have also been applied to photographic nonlinearities without the assumption of gamma-law models. The functional relation between the intensity transmittance and exposure of a transparency is represented by a polynomial approximation. The polynomial representation is used to express the spatial variation of the intensity transmittance when a sinusoidal exposure pattern is assumed.

In a paper concerned with the application of sine-wave response techniques to photographic processes, R. L. Lamberts

(1961) employed the gamma-law model. Nonlinearities in photographic processes were described by an equation of the form of (2.59(. An exposure of the form

$$E(x) = 1\text{-}A \cos x \ , \tag{2.60}$$

was assumed where A is a constant less than one. The resultant intensity transmittance was described by

$$T(x) = K(1\text{-}A \cos x)^{-\gamma} \ . \tag{2.61}$$

A binomial expansion of the factor $(1\text{-}A \cos x)^{-\gamma}$ was used to give an expression of the form

$$T(x) = K[1 + \binom{\gamma}{1} A\cos x + \binom{\gamma}{2} A^2\cos^2 x + \ldots], \tag{2.62}$$

where the parentheses represent binomial coefficients. By expanding the powers of the cosine function, this expression becomes

$$T(x) = K[\, Q_0 + Q_1 \cos x + Q_2 \cos(2x) + \ldots] \ , \tag{2.63}$$

where the Q coefficients are obtained from the parameters A and γ. Lamberts presented a table giving the Q coefficients of orders zero through eight for values of A ranging from 0.1 to 0.7 and gammas between 0.5 amd 2.0. The Q coefficients of second and higher orders gave the amplitudes of the harmonic distortions of the sinusoidal exposure based on the gamma-law model. Lamberts' paper did not contain experimental results directly related to the Q coefficients.

R. E. Little (1966) employed the gamma-law model in a paper concerned with the suppression of harmonic distortion in photographic images. The resultant intensity transmittance of a negative-positive photographic process was related to the exposure by

$$T = KE^{\gamma_1\gamma_2} \tag{2.64}$$

where K is a constant and γ_1 and γ_2 represent respectively, the gammas of the negative and positive photographic materials. Following a development similar to Lamberts'. Little showed that an exposure of the form

$$E(x) = a + b \sin x \ , \tag{2.65}$$

where a and b are constants such that $a \geq b$, leads to a resultant intensity transmittance given by

$$T(x) = A\left[1 + \frac{B}{A} \sin x + \frac{C}{A} \cos 2x + \ldots\right] \ , \tag{2.66}$$

where the constants A, B, and C can be evaluated in terms of the parameters K, a, b, γ_1, and γ_2. Little computed the values of the fundamental and second harmonic coefficients in (2.66) for a range of values of the parameters. He compared the calculated fundamental amplitudes to those resulting from experiment. The comparison showed that for relatively high levels of average exposure, results from the gamma-law model were fairly accurate. For lower average exposure levels, the fundamental amplitudes obtained from the gamma-law model

differed from those obtained experimentally by considerable amounts (10 to 75%).

D. C. Espley (1933) described a method of calculating the effects of zero-memory nonlinearities on sinusoidal signals that is based on polynomial approximations. It has been subsequently employed in the area of optical data processing. In a paper concerned with the determination of harmonic distortions produced by vacuum tubes, Espley represented the plate-current grid-voltage characteristic of a tube by a polynomial approximation. The approximation was obtained from the functional values of the characteristic at a set of equally spaced values of grid voltage. A typical polynomial is given by

$$i_p = a_0 + a_1 e_g + \ldots + a_{n-1} e_g^{n-1} \quad , \tag{2.67}$$

where i_p represents the plate current, e_g the grid voltage, and the a coefficients are constants. Values for the a coefficients were obtained from the solution of the set of n simultaneous equations resulting from the evaluation of Eq. (2.67) at the n equally spaced values of e_g. By assuming a grid-voltage signal

$$e_g = K \sin(wt) \quad , \tag{2.68}$$

where K is an amplitude constant, w is the radian frequency of the signal, and t is time; Equation (2.67) becomes

$$i_p(t) = b_0 + b_1 \sin(wt) + \ldots + b_{n-1} \sin[(n-1)wt] \quad , \tag{2.69}$$

where the b coefficients are given explicitly in terms of the a coefficients and K. The b coefficients of second and higher orders thus correspond to harmonic distortions. Espley derived equations giving these directly in terms of the n equally spaced functional values of the characteristic and the constant K. Versions of this method are described in a number of recent books on elementary electronic circuit theory (Ryder, 1964 and Chirlian, 1965).

J. S. Wilczynski (1961) employed Espley's method for the determination of harmonic distortions resulting from the exposure of photographic plates to sinusoidal intensity patterns. By exposing a number of plates to patterns of the form

$$E(x) = a + b \sin(w_x x), \tag{2.70}$$

where a, b, and w_x are constants ($a \geq b$), Wilczynski compared the resultant variation of the opacity of the plates to that computed by applying Espley's method to the measured opacity-exposure characteristic curves. By fitting fourth and sixth order polynomials to the characteristic curves, the fundamental and harmonic amplitudes of orders two through four were obtained. The results agreed well in the experiment for a wide range of exposure conditions of the plates. However, in instances when high contrast sinusoidal patterns were recorded, higher order harmonics showed some variation from the calculated values. Wilczynski ascribed these

differences to a development effect which was not accounted for in his measurement of the opacity-exposure characteristics.

In recent studies, F. J. Tischer[1/] indicated that the representation of a nonlinear characteristic by Tchebyscheff polynomials can lead to simplification of the computational procedures with which the harmonic distortions of sinusoidal signals are obtained. By properly expanding a given characteristic into a series of Tchebyscheff polynomials, the amplitude of each harmonic of a distorted signal was shown to be equal to the expansion coefficient of corresponding order. This is in contrast to the Taylor series expansion where the amplitude of each harmonic is given by an infinite series of the expansion coefficients.

[1/] F. J. Tischer. September 15, 1967. Interim Progress Report, National Aeronautics and Space Administration Grant NGR 34-002-038/S2, Department of Electrical Engineering, North Carolina State University, Raleigh, North Carolina. (Unpublished)

3. IMAGING ERRORS DUE TO GEOMETRIC DEVIATIONS

3.1 Introduction

In coherent optical data processors, signals are recorded on signal carriers such as photographic transparencies, photochromic glasses, or other media capable of light modulation. A beam of coherent light passes through the signal carrier surface and the data processing is accomplished optically. If the geometry of the signal carrier surface deviates by a small amount from that which is optimum, distortions result in the optical imaging within the processor. These distortions, in turn, cause signal distortions to appear in the processor output. Geometric deviations of signal carrier surfaces can be caused by imperfections in the shape of the surfaces or by alignment errors in the optical system.

In this chapter, imaging distortions for several types of geometric deviations are derived. These deviations model those that can occur in actual processors. The distortions are interpreted in terms of the Fourier transforms of the signals recorded on the signal carrier surfaces and are shown to correspond to attenuation, frequency shifts, and phase errors in electronic systems. The Kirchhoff integral solution of the scalar wave equation is used to derive quantitative relations between the distortions and the parameters describing the deviations of the signal carrier surface geometry.

Figure 3.1 introduces a portion of a typical coherent processor model. The three planes shown are transverse to

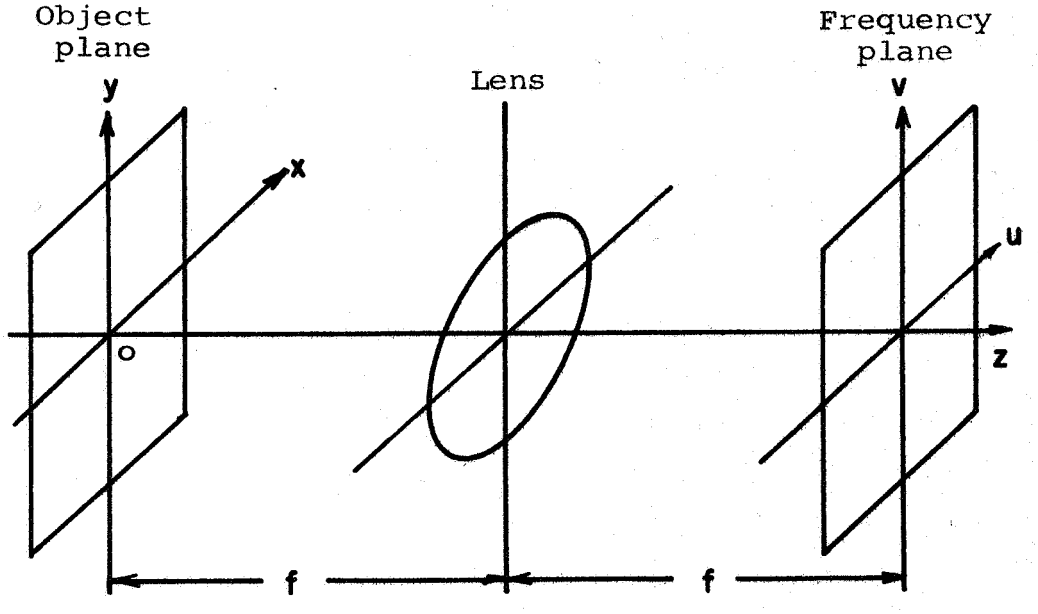

Figure 3.1 Model of a portion of a typical optical data processor

the z axis and coherent light is assumed to be propagating in the positive direction along this axis. The object and frequency planes coincide with the two focal planes of the lens. A one-dimensional signal is assumed to be introduced to the processor on a signal carrier surface that ideally coincides with the object plane. The signal is assumed to have negligible width and is recorded as a function of a spatial variable x' as shown in the figure. The remainder of the signal carrier surface is assumed to be opaque. The signal is represented by the amplitude transmittance function t(x').

Figures 3.2 through 3.4 introduce the geometric deviations of the signal carrier surface that are considered. In Figure 3.2, the signal carrier surface is a plane which is tilted with respect to the object plane. This geometry can be used to model alignment errors in actual processors. In Figures 3.3 and 3.4, the signal carrier surface corresponds to cylindrical and spherical sections. This geometry models signal carrier surfaces having slight warps and bends. Such surfaces occur since manufacturing tolerances limit the attainable flatness of actual signal carriers.

The results of this chapter can be used in at least two types of applications. If alignment errors and other geometric deviations are known for a given processor, the resulting attenuation, frequency shifts and phase errors in the processor output can be estimated. Conversely, if the allowable data processing errors are specified for a system that

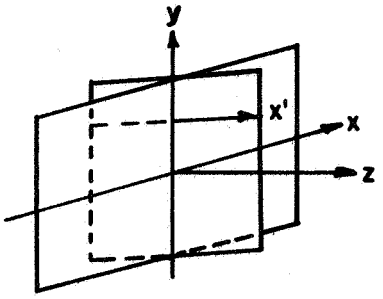

(a) tilt with respect to x axis

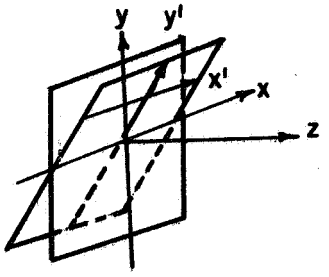

(b) tilt with respect to y axis

Figure 3.2 Signal carrier surface as a tilted plane

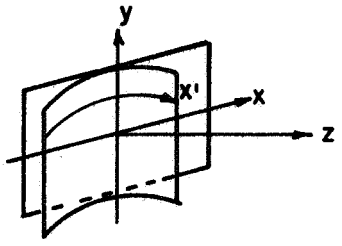

(a) cylinder tangent to y axis

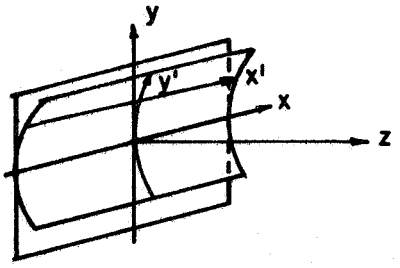

(b) cylinder tangent to x axis

Figure 3.3 Signal carrier surface as a circular cylinder

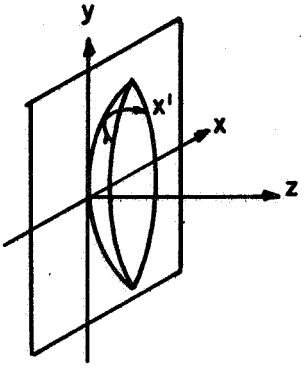

Figure 3.4 Signal carrier surface as a sphere tangent to origin of object plane

is being designed, tolerances can be set on the alignment and flatness of signal carriers within the system.

Parallel displacements of the signal carrier surface from the object plane are not considered here. The paper by Rhodes (1953) which is summarized in the literature review essentially covers this case.

3.2 Application of the Kirchhoff Integral to the Optical Processor Model

Figure 3.5 introduces the model of the lens that is used in the following calculations. The assumed imaging properties of the lens are:

(1) All rays entering the lens at an angle α with respect to the optic axis (see Figure 3.2) are imaged into the same point of the u axis;

(2) The optical path lengths of all rays entering the lens at angle α are equal when measured from any line drawn perpendicular to their direction of propagation to the point of focus on the u axis (in the figure, r_o = ABC = DEC = FGC);

(3) The aperture of the lens is large enough so that all rays exiting from the object plane at angle α pass through it;

(4) All light impinging on the lens is assumed to be transmitted (no reflections).

These assumptions are essentially those used by Born and Wolf (1965) in the description of Fraunhofer diffraction with a "well corrected lens." Using this model for the lens, the complex light amplitude l(u) in the frequency plane can be calculated from the knowledge of the complex light amplitude l(x') on the right hand signal carrier surface (x' is taken as the spatial variable along this surface).

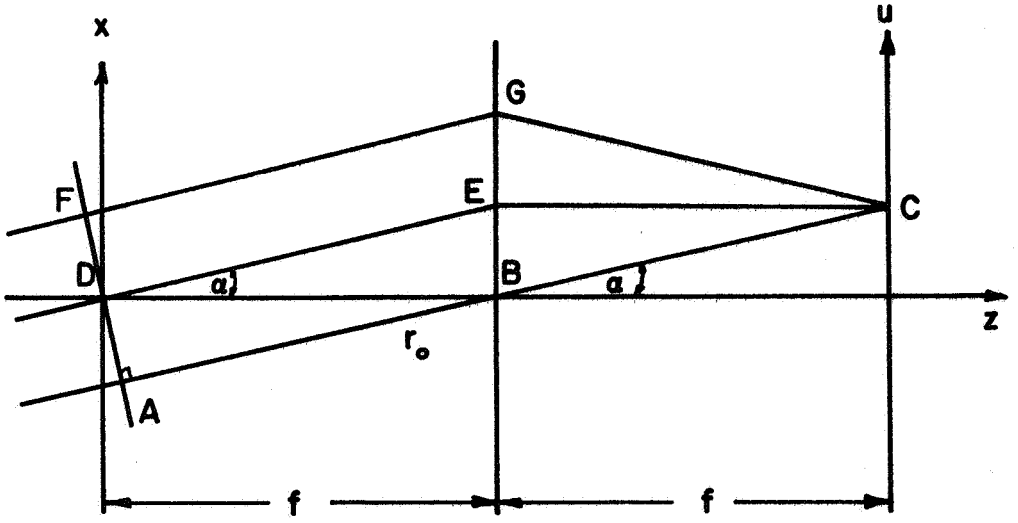

Figure 3.5 Imaging properties of the lens

The calculation of $l(u)$ from $l(x')$ is accomplished by means of the Kirchhoff integral (Tischer, 1965). With the assumption that the incident light amplitude is uniform across the width of the recorded signal, the Kirchhoff integral can be written as (see Figure 3.6):

$$l(u) = \frac{b}{4\pi} \int_{-a}^{a} \left\{ \frac{\partial l(x')}{\partial n} - l(x') \left[\frac{1}{r(x')} + j\frac{2\pi}{\lambda} \right] \cos\theta \right\} \frac{e^{-j\frac{2\pi}{\lambda} r(x')}}{r(x')} \, dx' \,, \tag{3.1}$$

where $\frac{\partial}{\partial n}$ is a directional derivative taken normal to the signal carrier surface (as defined in Figure 3.6),

$r(x')$ is the ray path length from a point x' on the transparency surface to the image point on u,

$\theta = \emptyset + \alpha$ is the angle between the normal to the signal carrier surface and the ray path under consideration,

λ is the wavelength of the light employed,

$-a$ and a are the aperture limits of the processor,

b is the width of the signal, and

$$j = \sqrt{-1} \tag{3.2}$$

Several simplifying approximations may be made in calculations of Eq. (3.1). These approximations are extensively used in the literature on optical imaging (Rhodes, 1953) and are as follows. In any practical imaging system (processor)

$$\frac{1}{r(x')} << \frac{2\pi}{\lambda} \,, \tag{3.3}$$

thus

$$\left[\frac{1}{r(x')} + j\frac{2\pi}{\lambda}\right] \approx j\frac{2\pi}{\lambda} \quad . \tag{3.4}$$

Since r(x') varies only by a small amount, the r(x') appearing in the denominator of the integrand is replaced by some nominal value r_o (shown in Figure 3.5). Equation (3.1) thus becomes

$$l(u) = \frac{b}{4\pi r_o} \int_{-a}^{a} \left[\frac{\partial l(x')}{\partial n} - j\frac{2\pi}{\lambda}\, l(x')\, \cos\theta\right] e^{-j\frac{2\pi}{\lambda}r(x')}\, dx'. \tag{3.5}$$

This expression may be further simplified by writing l(x') and $\frac{\partial l(x')}{\partial n}$ in terms of: the incident light wavefront, the amplitude transmittance function t(x'), and the geometry of the signal carrier surface. Assuming a plane, monochromatic wavefront of amplitude L_o propagating in the positive z direction, the complex light amplitude to the left of the signal carrier surface is

$$l_o(x,z) = L_o\, e^{-j\frac{2\pi}{\lambda} z} \quad , \tag{3.6}$$

where the complex exponential represents the phase variation of the wavefront with z. The geometry of the signal carrier surface can be characterized, as shown in Figure 3.7, by

$$z = z'(x') \quad . \tag{3.7}$$

Thus, the complex light amplitude incident on the transparency surface can be written as

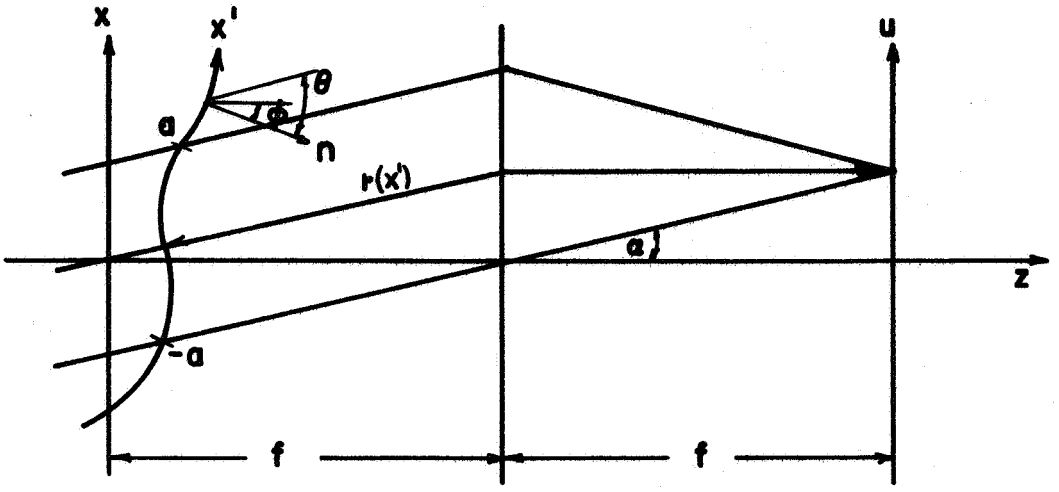

Figure 3.6 Application of the Kirchhoff integral to the processor model

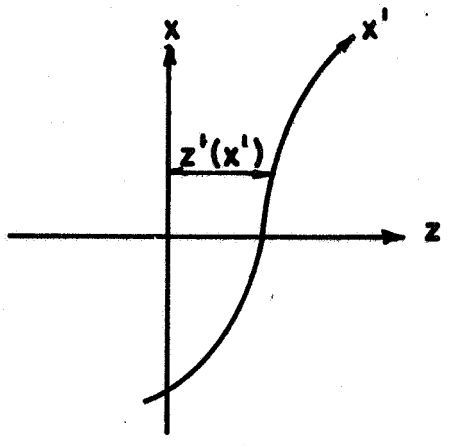

Figure 3.7 Parameters describing the signal carrier surface

$$l_o(x') = L_o\, e^{-j\frac{2\pi}{\lambda} z'(x')} . \tag{3.8}$$

Multiplying this expression by the transmittance function of the carrier surface $t(x')$ yields

$$l(x') = L_o t(x')\, e^{-j\frac{2\pi}{\lambda} z'(x')} , \tag{3.9}$$

which is the complex light amplitude on the right-hand surface of the signal carrier.

The term $\frac{\partial l(x')}{\partial n}$ in Eq. (3.5) can be evaluated as in the calculation of radiation from surface wave antennas (Tischer, 1965). If the transmittance function $t(x')$ does not vary appreciably within lengths of the order of λ[1/], the complex light amplitude immediately to the right of a small region of the transparency surface can be written

$$l(x,z) = L_o t(x_o')\, e^{-j\frac{2\pi}{\lambda} z} , \tag{3.10}$$

where $t(x_o')$ is the transmittance of the transparency near the region. From the geometry of Figure 3.6,

$$\frac{\partial l(x')}{\partial n} = \frac{\partial l(x')}{\partial z}\frac{\partial z}{\partial n} + \frac{\partial l(x')}{\partial x}\frac{\partial x}{\partial n} . \tag{3.11}$$

This can be written as

$$\frac{\partial l(x')}{\partial n} = \frac{\partial l(x')}{\partial z}\cos\phi + \frac{\partial l(x')}{\partial x}\sin\phi . \tag{3.12}$$

[1/] This assumption restricts the spatial frequency spectrum of $t(x')$ to frequencies of several hundred lines per millimeter and less.

Substitution of Eq. (3.10) in Eq. (3.12) gives

$$\frac{\partial l(x_o')}{\partial n} = \left(-j\ \frac{2\pi}{\lambda}\right) L_o\ t(x_o')\ \cos\ \phi\ e^{-j\frac{2\pi}{\lambda}\ z'(x_o')}, \qquad (3.13)$$

so that for an arbitrary x',

$$\frac{\partial l(x')}{\partial n} = \left(-j\frac{2\pi}{\lambda}\right) \cos\ \phi\ L_o\ t(x')\ e^{-j\frac{2\pi}{\lambda}\ z'(x')}. \qquad (3.14)$$

Equations (3.9) and (3.14) can be substituted into Eq. (3.5) to give

$$l(u) = -j\frac{I_o b}{2r_o}\int_{-a}^{a} t(x')(\cos\theta + \cos\phi)e^{-j\frac{2\pi}{\lambda}[z'(x')+r(x')]}dx'. \qquad (3.15)$$

In the derivations which follow, trigonometric functions of the angle α occur frequently. Since in any practical processor α is limited to small values, the following approximations are made (see Figure 3.5).

$$\sin\ \alpha = \frac{u}{(f^2+u^2)^{\frac{1}{2}}} \approx \frac{u}{f} = \tan\ \alpha, \qquad (3.16)$$

$$\cos\ \alpha = \frac{f}{(f^2+u^2)^{\frac{1}{2}}} \approx \left(1 - \frac{u^2}{2f^2}\right), \qquad (3.17)$$

$$(\cos\ \alpha)^{-1} = \frac{(f^2+u^2)^{\frac{1}{2}}}{f} = \left(1 + \frac{u^2}{2f^2}\right), \qquad (3.18)$$

These approximations represent the first several terms of the series expansions of the trigonometric functions. The approximations are computed in terms of u and f which correspond to physical lengths in the processor.

The value of r_o appearing in Eq. (3.15) can be calculated with the help of Figure 3.5. Inspection of the figure shows

$$r_o = (\cos \alpha)f + (\cos \alpha)^{-1}f. \tag{3.19}$$

Use of Eqs. (3.17) and (3.18) gives

$$r_o = f(1 - \frac{u^2}{2f^2}) + f(1 + \frac{u^2}{2f^2}), \tag{3.20}$$

or

$$r_o = 2f. \tag{3.21}$$

Use of Eq. (3.21) allows r(x') to be written as

$$r(x') = r_o - \Delta r(x'), \tag{3.22}$$

or

$$r(x') = 2f - \Delta r(x'), \tag{3.23}$$

where $\Delta r(x')$ is defined as shown in Figure 3.8. Introduction of Eqs. (3.21) and (3.23) in Eq. (3.15) yields

$$l(u) = (-je^{-j\frac{4\pi}{\lambda}f}) \frac{L_o b}{4f} \int_{-a}^{a} t(x')[\cos \theta + \cos \phi]$$

$$e^{-j\frac{2\pi}{\lambda}[z'(x') - \Delta r(x')]}dx'. \tag{3.24}$$

Since the phase shift $(-je^{-j\frac{4\pi}{\lambda}f})$ is constant over the image plane, it may be neglected so that

$$l(u) = \frac{L_o b}{4f} \int_{-a}^{a} t(x')(\cos\theta+\cos\phi)e^{-j\frac{2\pi}{\lambda}[z'(x')-\Delta r(x')]}dx' . \tag{3.25}$$

This equation can be applied to the "ideal" processor where

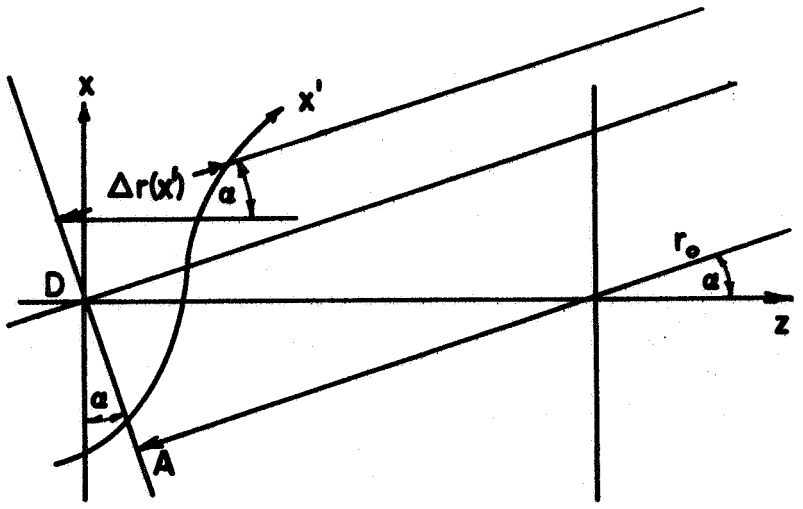

Figure 3.8 Geometry for the calculation of r'(x)

the transparency surface is coincident with the object plane (xy-plane). Inspection of Figure 3.9 shows that for this case;

$$x' = x, \tag{3.26}$$

$$z' = 0, \tag{3.27}$$

$$\Delta r = x \sin \alpha \tag{3.28}$$

and

$$\phi = 0. \tag{3.29}$$

Using Eq. (3.16), Eq. (3.28) becomes

$$\Delta r = \frac{xu}{f} . \tag{3.30}$$

Substitution of Eqs. (3.26), (3.27), (3.29) and (3.30) into Eq. (3.25) yields

$$1(u) = \frac{L_o b}{4f} \int_{-a}^{a} t(x)(\cos \alpha + 1) e^{j\frac{2\pi}{\lambda f}ux} dx. \tag{3.31}$$

Equation (3.31) thus describes the imaging in the frequency plane of the processor (uv-plane). If the factor cos α in Eq. (3.31) is assumed to be unity, the equation becomes

$$1(u) = \frac{L_o b}{2f} \int_{-a}^{a} t(x) e^{j(\frac{2\pi}{\lambda f})ux} dx, \tag{3.32}$$

which is in the form of a Fourier transformation. By defining

$$\frac{2\pi}{\lambda f} = 2\pi f_x = w_x, \tag{3.33}$$

where f_x represents a spatial frequency and w_x the corresponding radian frequency, Eq. (3.32) becomes

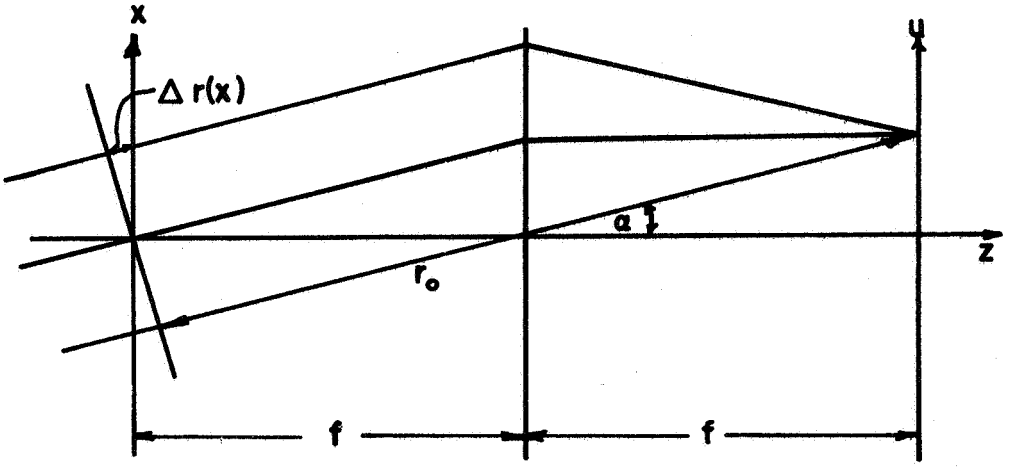

Figure 3.9 Geometry for signal carrier surface coincident with object plane

$$l(u) = \frac{L_o b}{2f} \int_{-a}^{a} t(x)\ e^{jw_x x} dx. \qquad (3.34)$$

Equation (3.32) thus represents the desired or ideal imaging relation between the object and frequency planes of the processor. In actual processors this relation holds as an approximation since α is a small angle. Since this development is concerned only with the imaging errors due to the geometric deviations of the signal carrier surface from the object plane, the factor cos θ in Eq. (3.25) is replaced by cos ϕ. The equation thus becomes

$$l(u) = \frac{L_o b}{2f} \int_{-a}^{a} t(x')\ \cos\phi\ e^{-j\frac{2\pi}{\lambda}[z'(x') - \Delta r(x')]} dx'. \qquad (3.35)$$

By evaluating Eq. (3.35) in terms of the geometry of the signal carrier surface and comparing the results to Eq. (3.32), the imaging errors introduced by the geometry become apparent. In the following sections, this process is carried out.

3.3 The Signal Carrier Surface as a Tilted Plane

3.3.1 Axis of Tilt Normal to Direction of Processing

When the signal carrier surface consists of a plane which is inclined at some angle γ with respect to the x axis, the geometry corresponds to that of Figures 3.2a and 3.10. In this case, the angle ϕ is equal to γ and does not vary with x'. Thus

$$\cos\phi = \cos\gamma\ . \qquad (3.36)$$

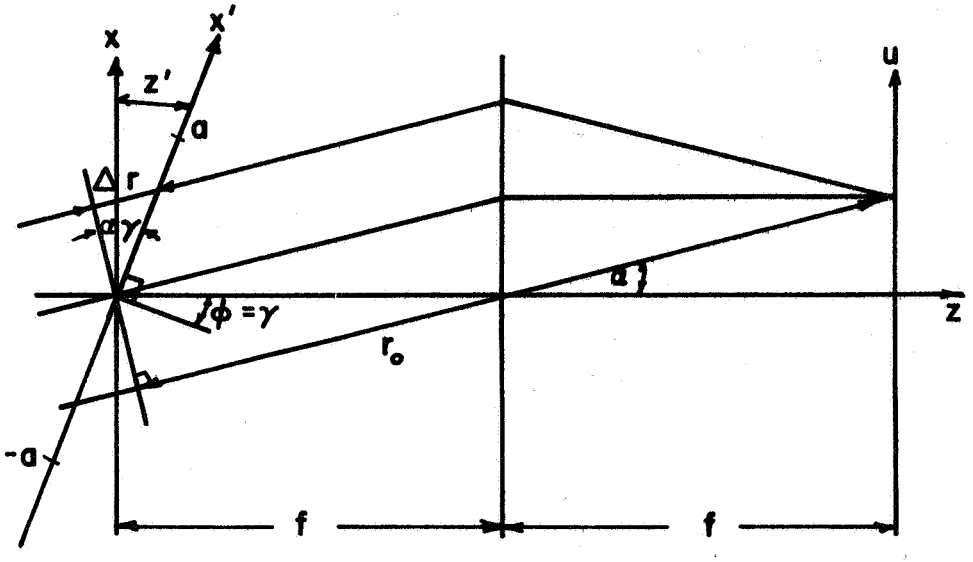

Figure 3.10 Signal carrier surface tilted with respect to x axis

By inspection of Figure 3.10,

$$z'(x') = x' \sin \gamma, \tag{3.37}$$

and

$$\Delta r(x') = x' \sin(\gamma + \alpha). \tag{3.38}$$

By expanding the sine function,

$$\Delta r(x') = x'(\sin \gamma \cos \alpha + \sin \alpha \cos \gamma). \tag{3.39}$$

Using the approximations of Eqs. (3.16) and (3.17),

$$\Delta r(x') = x'[\sin \gamma(1 - \frac{u^2}{2f^2}) + \frac{u}{f} \cos \gamma], \tag{3.40}$$

and

$$z'(x') - \Delta r(x') = x'(-\frac{u}{f} \cos \gamma + \frac{u^2}{2f^2} \sin \gamma). \tag{3.41}$$

Substitution of Eqs. (3.36) amd (3.41) in Eq. (3.35) yields

$$l(u) = \frac{L_o b \cos\gamma}{2f} \int_{-a}^{a} t(x') e^{j\frac{2\pi}{\lambda f}(x'u\cos \gamma - \frac{x'u^2}{2f} \sin \gamma)} dx'. \tag{3.42}$$

Comparison of this expression to Eq. (3.32) points up the following effects in the imaging of the tilted surface; (1) the amplitude of $l(u)$ is reduced by the factor $\cos \gamma$, (2) the spatial frequency variable (u or f_x) is scaled by the factor $\cos \gamma$, and (3) an additional phase term ($-j\frac{\pi x'u^2}{\lambda f^2} \sin \gamma$) is introduced into the exponential. Effects (1) and (2) can be insignificant if γ is a small angle since, then

$$\cos (\gamma) \approx 1 - \frac{\gamma^2}{2}, \tag{3.43}$$

and the angle enters as a second order effect. Effect (3) consists of a phase distortion of the complex light amplitude

in the uv-plane. If this distortion is to be held to within ρ radians,

$$\rho \geq \frac{\pi x'_{max}\, u^2_{max}}{\lambda f^2} \sin\gamma \ . \tag{3.44}$$

Inspection of Figure 3.10 shows

$$x'_{max} = a. \tag{3.45}$$

The quantity u_{max} corresponds to the maximum spatial frequency ($f_{x\ max}$) appearing in the uv-plane. Equation (3.44) can thus be written as

$$\sin\gamma \leq \frac{\rho}{\pi\lambda\alpha f^2_{x\ max}} \ . \tag{3.46}$$

The inequality is thus expressed in terms of the aperture length of the processor, the wavelength of the light employed, and the maximum spatial frequency to be processed. Equation (3.46) expresses the maximum allowable tilt of the object plane (about an axis normal to the direction of processing) in terms of the maximum allowable phase distortion in the frequency plane. Similar equations can be derived for effects (1) and (2). As an example, application of Eq. (3.46) to a processor where

$$a = 15 \text{ mm.}, \tag{3.47}$$

$$\lambda = 6328 \text{ Å}, \tag{3.48}$$

$$f_{x\ max} = 100 \text{ lines/mm.}, \tag{3.49}$$

and

$$\rho = \pi/4 \tag{3.50}$$

yields

$$\sin \gamma \leq 0.0026 \tag{3.51}$$

or

$$\gamma \leq 0.15^{o} . \tag{3.52}$$

3.3.2 Axis of Tilt Parallel to Direction of Processing

If the signal carrier surface is a plane inclined at angle γ with respect to the y axis of the processor, the geometry can be represented by Figures 3.2b and 3.11. Because of the tilt,

$$\cos \phi = \cos \gamma . \tag{3.53}$$

If the x' axis is displaced from the z axis by an amount y' (y' is the spatial variable normal to x' in the tilted plane), then by anology to Eq. (3.37) and Figure 3.10,

$$z' = y' \sin \gamma. \tag{3.54}$$

From inspection of Figure 3.11,

$$\Delta r(x') = (x \sin \alpha + \frac{z'}{\cos \alpha}). \tag{3.55}$$

Since

$$x = x' - z' \tan \alpha, \tag{3.56}$$

Eq. (3.55) becomes

$$\Delta r(x') = x' \sin \alpha - z' \left(\frac{\sin^2 \alpha}{\cos \alpha} - \frac{1}{\cos \alpha}\right) , \tag{3.57}$$

or

$$\Delta r(x') = x' \sin \alpha + z' \cos \alpha. \tag{3.58}$$

Using the approximations of Eqs. (3.16) and (3.17) in

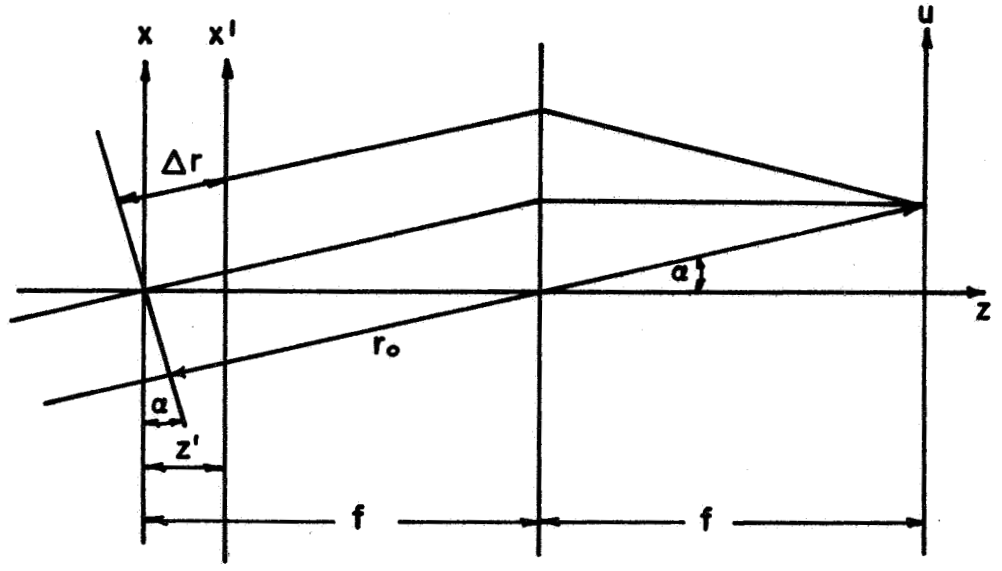

Figure 3.11 Signal carrier surface tilted with respect to y axis

Eq. (3.58) gives

$$\Delta r(x') = x' \frac{u}{f} + z'(1 - \frac{u^2}{2f^2}), \tag{3.59}$$

or

$$\Delta r(x') = \frac{x'u}{f} - y' \sin\gamma(1 - \frac{u^2}{2f^2}). \tag{3.60}$$

Substitution of Eqs. (3.53), (3.55) and (3.60) into Eq. (3.35) yields

$$l(u) = \frac{L_o b \cos\gamma}{2f} \int_{-a}^{a} t(x') e^{j\frac{2\pi}{\lambda}(\frac{x'u}{f} - \frac{y'u^2}{2f^2}\sin\gamma)} dx' . \tag{3.61}$$

This shows that when the axis of tilt is parallel to the direction of processing, the only frequency-dependent effect is a phase distortion which increases as the off axis distance of the function being processed increases.

Comparison of Eq. (3.61) with Eq. (3.32) shows that the tilt introduces: (1) an amplitude reduction of l(u) given by cos γ, and (2) a frequency dependent phase distortion given by $\exp(-j\frac{2\pi y'y^2}{\lambda\ 2f^2}\sin\gamma)$.[2/] If the phase distortion is to be kept within ρ radians,

$$\rho \geq \frac{\pi y' u^2_{max}}{\lambda\ f^2} \sin\gamma \tag{3.62}$$

or

$$\sin\gamma \leq \frac{\rho}{\pi\lambda y' f^2_{x\ max}} . \tag{3.63}$$

[2/] As in the previous case, effect (1) can be insignificant since for small tilts γ enters as a second order effect.

This last expression limits the maximum allowable tilt (about the y axis of the processor) in terms of the maximum allowable phase distortion in the frequency plane.

3.4 The Signal Carrier Surface as a Cylinder

3.4.1 Axis of Cylinder Normal to Direction of Processing

Figures 3.3a and 3.12 show the geometry existing in the processor if the signal carrier surface forms a circular cylinder of radius R tangent to the y axis. Inspection of Figure 3.12 shows

$$\cos \phi = \cos \frac{x'}{R} , \tag{3.64}$$

$$z'(x') = R(1-\cos \frac{x'}{R}), \tag{3.65}$$

and

$$\Delta r(x') = (x_1 \sin \alpha + \frac{z'}{\cos \alpha}). \tag{3.66}$$

Also,

$$\frac{x_o}{R} = \sin \phi = \sin \frac{x'}{R} , \tag{3.67}$$

or

$$x_o = R \sin \frac{x'}{R} , \tag{3.68}$$

and

$$x_1 = x_o - z' \tan \alpha. \tag{3.69}$$

Thus,

$$\Delta r(x') = R[\sin\frac{x'}{R} \sin \alpha + (1-\cos\frac{x'}{R}) \cos \alpha]. \tag{3.70}$$

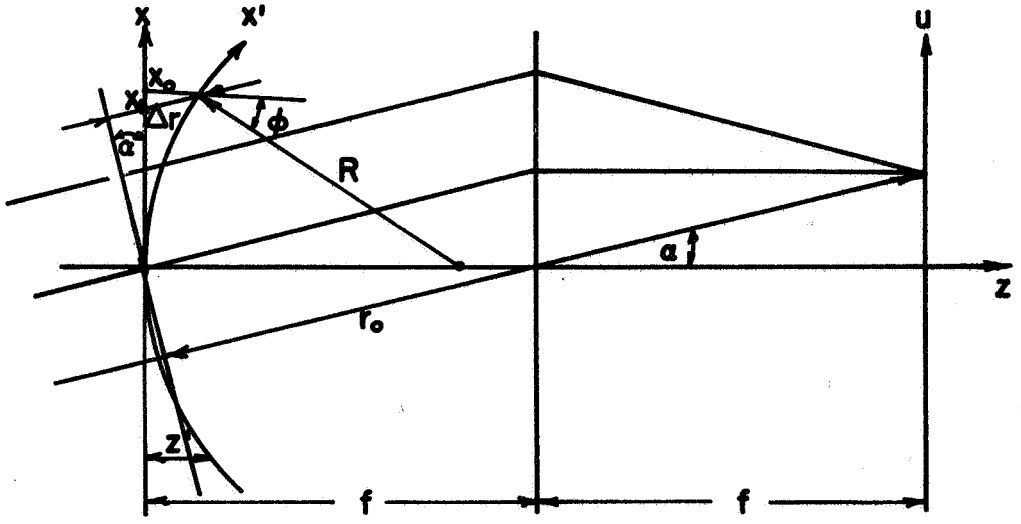

Figure 3.12 Cylindrical signal carrier surface tangent to y axis

Using the approximations of Eqs. (3.16) and (3.17),

$$\Delta r(x') = R[\frac{u}{f} \sin \frac{x'}{R} + (1 - \frac{u^2}{2f^2})(1- \cos\frac{x'}{R})]. \qquad (3.71)$$

Substitutions of Eqs. (3.64), (3.65) and (3.71) into Eq. (3.35) yields

$$l(u) = \frac{L_o b}{2f} \int_{-a}^{a} t(x') \cos(\frac{x'}{R}) \cdot e^{j\frac{2\pi}{\lambda}R[\frac{u}{f} \sin \frac{x'}{R} - \frac{u^2}{2f^2} (1-\cos\frac{x'}{R})]} dx' . \qquad (3.72)$$

Comparison of Eq. (3.72) with Eq. (3.32) shows that the cylindrical surface introduces the following distortions; (1) a signal attenuation dependent on x' ($\cos \frac{x'}{R}$); (2) a frequency scaling factor dependent on x' ($R \sin \frac{x'}{R}$); (3) an additional phase term in the complex exponential given by $[j\frac{\pi R u^2}{\lambda f^2}(1-\cos \frac{x'}{R})]$. For small deviations of the geometry from plane-form, $x' < R$. Thus,

$$\cos \frac{x'}{R} \approx 1 - \frac{x'^2}{2R^2} , \qquad (3.73)$$

$$\sin \frac{x'}{R} \approx \frac{x'}{R} , \qquad (3.74)$$

and Eq. (3.72) can be written as

$$l(u) = \frac{L_o b}{2f} \int_{-a}^{a} t(x')(1- \frac{x'^2}{2R^2}) e^{j\frac{2\pi}{\lambda}(\frac{x'u}{f} - \frac{x'^2u^2}{4Rf^2})} dx' . \qquad (3.75)$$

In this case the distortion (2) is negligable and (1) corresponds to a second order effect. If the phase distortion in

the frequency plane is to be limited to ρ radians, then

$$\rho = \frac{\pi x'^2_{max}\, u^2_{max}}{2R\lambda f^2}, \tag{3.76}$$

or

$$R \geq \frac{\pi\lambda a^2 f^2_{x\ max}}{2\rho} \tag{3.77}$$

(with the notation used previously).

This expression can be used to determine the minimum radius of the cylinder if λ, ρ, a, and $f_{x\ max}$ are given. For example, if

$$\lambda = 6328\ \text{Å}, \tag{3.78}$$

$$a = 15\ \text{mm.}, \tag{3.79}$$

$$f_{x\ max} = 100\ \text{lines/mm.}, \tag{3.80}$$

and

$$\rho = \pi/4, \tag{3.81}$$

then

$$R \geq 2.85\ \text{m}, \tag{3.82}$$

yields the desired level of phase distortion.

3.4.2. Axis of Cylinder Parallel to Direction of Processing

When the signal carrier surface forms a cylinder of radius R tangent to the x axis, the geometry corresponds to that of Figures 3.3b and 3.13. By analogy to Figure 3.12 and Eq. (3.65),

$$z' = R\left(1 - \cos\frac{y'}{R}\right). \tag{3.83}$$

Inspection of Figure 3.13 shows,

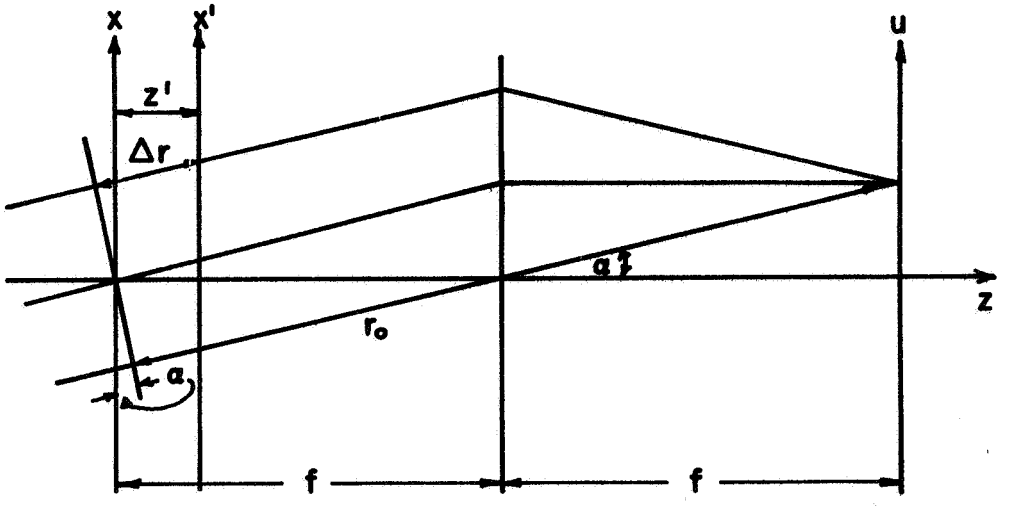

Figure 3.13 Projection of cylindrical signal carrier surface (tangent to x axis) onto xz-plane

$$\cos \phi = \cos \frac{y'}{R} \quad , \tag{3.84}$$

and

$$\Delta r = (x \sin \alpha + \frac{z'}{\cos \alpha}) . \tag{3.85}$$

As in Eq. (3.56),

$$x = x' - z'(\tan \alpha), \tag{3.86}$$

so that

$$\Delta r = (x' \sin \alpha + z' \cos \alpha). \tag{3.87}$$

Application of Eq. (3.83) and the approximations of Eqs. (3.16) and (3.17) yields

$$\Delta r = [\frac{x'u}{f} + (1 - \frac{u^2}{2f^2}) R(1 - \cos \frac{y'}{R})]. \tag{3.88}$$

Substitution of Eqs. (3.83), (3.84), and (3.88) into Eq. (3.35) gives

$$l(u) = \frac{L_o b \cos \frac{y'}{R}}{2f} \int_{-a}^{a} t(x') e^{j\frac{2\pi}{\lambda} [\frac{x'u}{f} - \frac{u^2}{2f^2} R(1-\cos\frac{y'}{R})]} dx'. \tag{3.89}$$

Comparison of this equation with Eq. (3.32) shows that the imaging distortions are: (1) an amplitude attenuation $\cos \frac{y'}{R}$ and (2) an additional phase term in the exponential. For small deviations of the geometry from planer form, $y' < R$. Thus

$$\cos \frac{y'}{R} \approx (1 - \frac{y'^2}{2R^2}), \tag{3.90}$$

and Eq. (3.89) can be written as

$$l(u) = \frac{L_o b \cos \frac{y'}{R}}{2f} \int_{-a}^{a} t(x') e^{j\frac{2\pi}{\lambda} (\frac{x'u}{f} - \frac{u^2 y'^2}{4Rf^2})} dx' \quad . \tag{3.91}$$

Requiring the phase distortion to be limited to ρ radians gives

$$\rho \geq \frac{\pi u^2_{max}\, y'^2}{2\lambda R f^2}, \tag{3.92}$$

or

$$R \geq \frac{\pi \lambda y'^2 f^2_{x\ max}}{2\rho}. \tag{3.93}$$

Thus, the minimum radius of the cylinder can be determined from: the wavelength of the light, the off axis distance of the signal (y'), the maximum frequency to be processed and the maximum allowable phase distortion.

3.5 The Signal Carrier Surface as a Sphere

If the signal carrier surface is a sphere of radius R_o, tangent to the origin of the object plane, the geometry can be represented as shown in Figures 3.4 and 3.14 through 3.16. The x' axis corresponds to the intersection of a plane parallel to the xz-plane with the sphere. Although the angle $\emptyset$ lies neither in the xz- nor the yz-plane, application of the law of cosines to the angles γ and Δ of Figure 3.15 and 3.16 yields

$$\cos \emptyset = \cos \gamma \cos \Delta, \tag{3.94}$$

or

$$\cos \emptyset = \cos \left(\frac{x'}{R}\right) \cos \left(\frac{y'}{R_o}\right). \tag{3.95}$$

By inspection of Figure 3.16

$$R = R_o \cos x = R_o \cos \left(\frac{y'}{R_o}\right), \tag{3.96}$$

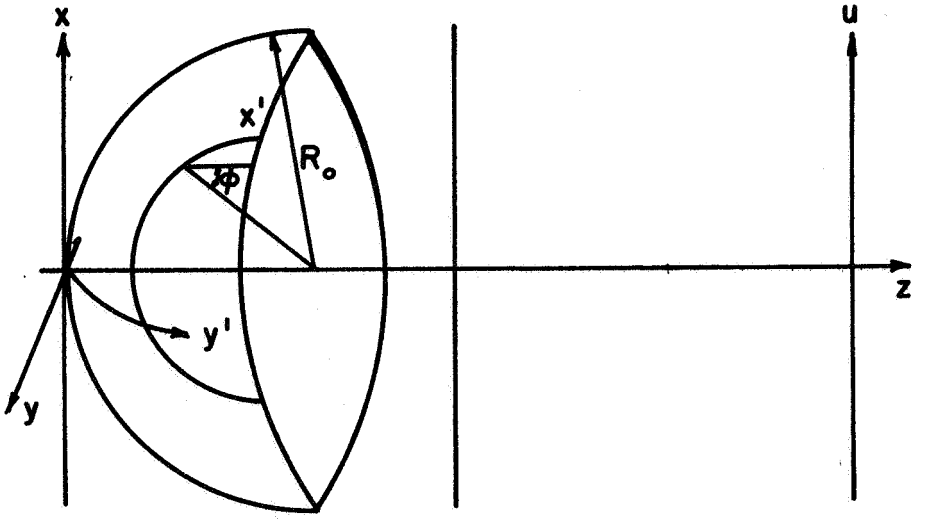

Figure 3.14 Spherical signal carrier surface

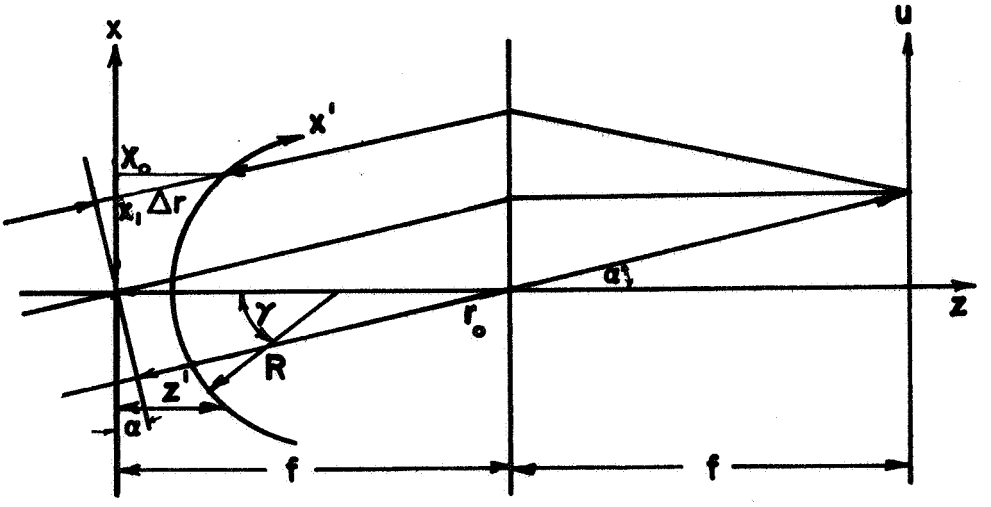

Figure 3.15 Projection of spherical surface into xz-plane

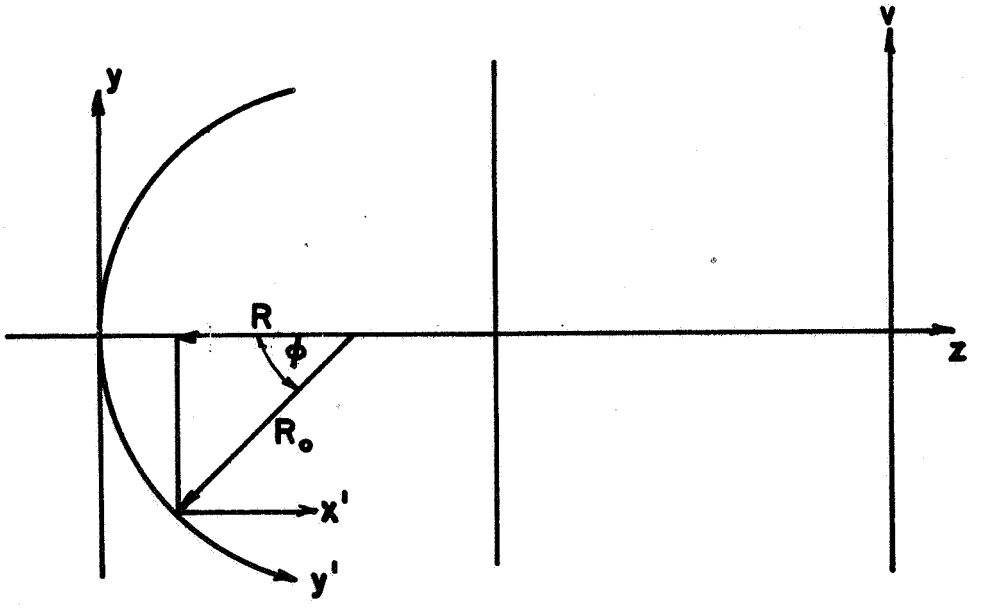

Figure 3.16 Projection of spherical surface onto yz-plane

so that

$$\cos \phi = \cos \left[\frac{x'}{R_o \cos\left(\frac{y'}{R_o}\right)}\right] \cos \left(\frac{y'}{R_o}\right). \tag{3.97}$$

Inspection of Figure 3.15 shows

$$z' = R_o - R \cos \left(\frac{x'}{R}\right), \tag{3.98}$$

$$\Delta r = \frac{z'}{\cos \alpha} + x_1 \sin \alpha \ , \tag{3.99}$$

$$x_1 = x_o - z' \tan \alpha, \tag{3.100}$$

and

$$x_o = R \sin \left(\frac{x'}{R}\right). \tag{3.101}$$

Thus,

$$z'(x') = R_o \left[1 - \cos\left(\frac{y'}{R_o}\right) \cos \left(\frac{x'}{R}\right)\right] \tag{3.102}$$

and

$$\Delta r(x') = \left[R \sin\left(\frac{x'}{R}\right) \sin \alpha + z'(x') \cos \alpha\right]. \tag{3.103}$$

Introduction of the approximations of Eqs. (3.16) and (3.17) into Eq. (3.103) and subtraction of the result from Eq. (3.102) yields

$$z'(x') - \Delta r(x') =$$

$$-\left\{ R \frac{u}{f} \sin\left(\frac{x'}{R}\right) - R_o\left[1 - \cos\left(\frac{y'}{R_o}\right) \cos\left(\frac{x'}{R}\right)\right]\frac{u^2}{2f^2}\right\}. \tag{3.104}$$

With the assumptions $x' < R$ and $y' < R_o$, the approximations

$$\cos\left(\frac{x'}{R}\right) = \left(1 - \frac{x'^2}{2R^2}\right), \tag{3.105}$$

$$\cos\left(\frac{y'}{R_o}\right) = \left(1 - \frac{y'^2}{2R_o^2}\right), \tag{3.106}$$

$$\sin\left(\frac{x'}{R}\right) = \frac{x'}{R}, \tag{3.107}$$

and

$$\sin\left(\frac{y'}{R_o}\right) = \frac{y'}{R_o}, \tag{3.108}$$

can be made. Application of these to Eqs. (3.95), (3.96) and (3.104) yields, respectively,

$$\cos \phi = \left[1 - \left(\frac{y'^2}{2R_o^2} + \frac{x'^2}{2R^2}\right)\right], \tag{3.109}$$

$$R = R_o\left(1 - \frac{y'^2}{2R_o^2}\right), \tag{3.110}$$

and

$$z'(x') - \Delta r(x') = -\left[\frac{x'u}{f} + \frac{u^2R_o}{2f^2}\left(\frac{y'^2}{2R_o^2} + \frac{x'^2}{2R^2}\right)\right], \tag{3.111}$$

when higher order terms are neglected. Substitution of Eqs.(3.109) and (3.111) into Eq. (3.35) and comparison with Eq. (3.32) shows that the spherical geometry introduces the following distortions into the frequency plane image: (1) an amplitude attenuation given by cos ϕ, and (2) a frequency-dependent phase distortion given by

$$\exp\left[\frac{\pi u^2 R_o}{\lambda f^2}\left(\frac{y'^2}{2R_o^2} + \frac{x'^2}{2R^2}\right)\right].$$

The expressions for the amplitude and phase distortion can be further simplified by use of Eq. (3.110). Substitution

of this expression into Eqs. (3.109) and (3.111) yields

$$\cos \phi = \left[1 - \frac{(x'^2 + y'^2)}{2R_o^2}\right] , \tag{3.112}$$

and

$$z'(x') - \Delta r(x') = - \left[\frac{x'u}{f} + \frac{u^2(x'^2 + y'^2)}{4f^2R_o}\right] , \tag{3.113}$$

after expansion and neglection of higher order terms. In these expressions, the only variables describing the geometry of the signal carrier surface are x', y', and R_o. As in the previous derivations, limits can now be set on the geometry in terms of the allowable distortions. The phase distortion (2) is now given by the factor

$$\exp\left[\frac{\pi u^2(x'^2 + y'^2)}{2\lambda f^2 R_o}\right] .$$

If this distortion is required to be less than ρ radians,

$$\rho \geq \frac{\pi u^2(x'^2 + y'^2)}{2\lambda f^2 R_o} . \tag{3.114}$$

Introduction of the spatial frequency f_x and the aperture a, allows Eq. (3.114) to be written as

$$R_o \geq \frac{\pi\lambda(a^2 + y'^2)f^2_{x\ max}}{2\rho} . \tag{3.115}$$

As in the previous derivations, the minimum radius of the sphere can be determined from the wavelength of the light employed, the maximum spatial frequency being processed, the off axis distance of the signal being processed, the aperture of the processor, and the maximum allowable phase error.

4. NONLINEARITIES IN OPTICAL DATA PROCESSORS

4.1 Introduction

When available signals are transformed into the forms required by optical data processors, nonlinearities are usually encountered. Nonlinear transfer characteristics occur in photographic processes as well as in electro-optic signal conversion devices such as: photocells, photomultipliers, photodiodes, cathode ray tubes, kinescopes, and retardation-type modulators based on the Kerr and Pockels effects. The nonlinearities in these signal conversion devices and methods can be described by so-called zero-memory characteristics. That is, within reasonable signal bandwidths, the nonlinear distortions can be considered as frequency independent and can be described by instantaneous (i.e., zero-memory) nonlinear input-output relations called characteristic functions. The application of zero-memory nonlinear models to photographic processes was described in the literature review. In communication theory, these models have been used to represent the operation of devices such as: biased diode modulators, square-law detectors, saturable amplifiers, and half-wave rectifiers (Middleton, 1960).

The two approaches described in the literature review have been used for the analysis of zero-memory nonlinear characteristics. The transform methods allow the assumption of fairly general types of signals but can be tractably

applied only to characteristics having rather simple functional forms. Many characteristics encountered in the use of optical data processors do not have such simple forms, and these methods are thus inappropriate for general analysis purposes. The sinusoidal signal approaches allow the analysis of a wide class of characteristics. The papers summarized in the review have established the usefullness of this type of analysis in optical data processing applications, but the accuracy of the results obtained has been limited.

This chapter and those following are concerned with the development and application of accurate methods of analyzing zero-memory characteristics using the sinusoidal signal approach. The methods of analysis which are developed are not limited to optical data processing applications. They can be used for investigations in other areas where components having nonlinear characteristics are encountered.

In this chapter, the effects of zero-memory nonlinearities on sinusoidal signals are described in a general manner. The nonlinearities are shown to create harmonic distortions of the signals; and an equivalent noise-to-signal ratio, which describes the severity of the distortions as a single quantity, is introduced.

In Chapter 5, the effects of nonlinearities on the operation of a typical optical data processor are described. Specific examples demonstrate the resulting degraded

performance. Methods of analyzing nonlinear characteristics and determining the harmonic coefficients of distorted signals are developed in Chapter 6. Taylor, Fourier, Legendre, and Tchebyscheff expansions are shown to be suitable for this purpose. The Tchebyscheff method is seen to have considerable advantages in simplicity of application. Chapters 7 and 8 deal with the application of the Tchebyscheff method to actual nonlinear problems. A numerical method for obtaining Tchebyscheff coefficients is developed and subsequently implemented in a Fortran program.

4.2 Effects of Nonlinearities on Sinusoidal Signals

The amplitude behavior of a (zero-memory) device having a nonlinear functional relation between its input and output variables may be represented in terms of a characteristic curve such as that shown in Fig. 4.1. The curve relates the output variable y to the input variable x and is a graph of the transfer function

$$y = f(x). \tag{4.1}$$

If the input variable consists of a signal varying about some value x_o, called the operating point of the device, then

$$S_1(t) = x - x_o \ , \tag{4.2}$$

where $S_1(t)$ represents the input signal which is a function of some other variable t. In general, the operating point of the device may be chosen anywhere on the characteristic.

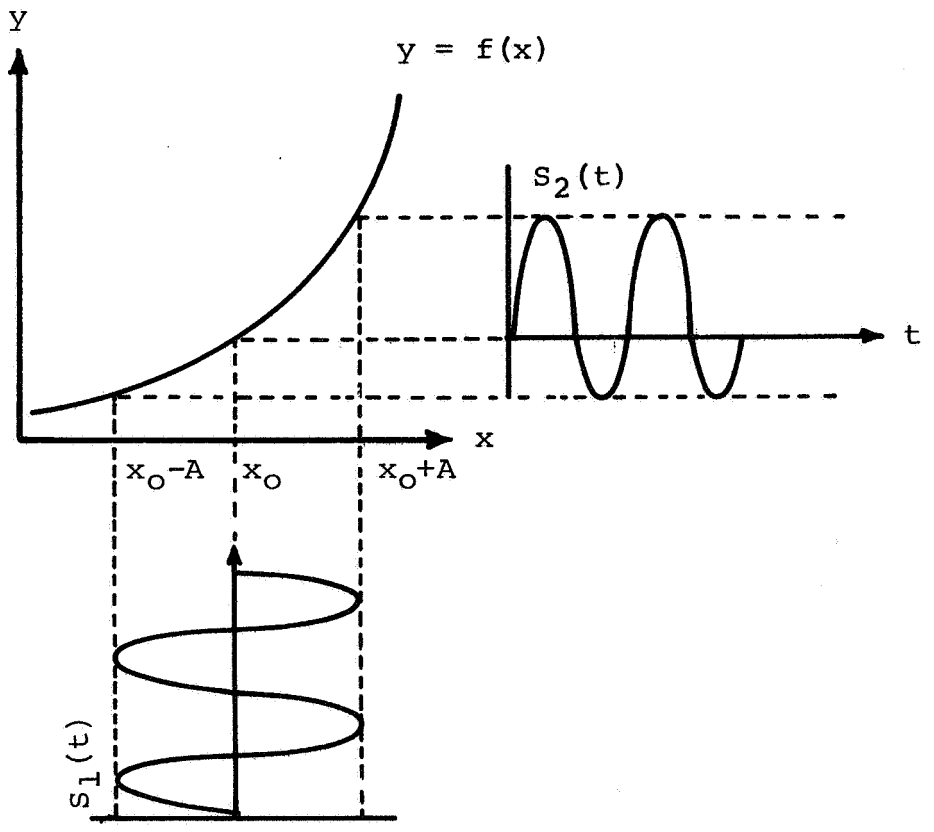

Figure 4.1 Effects of a nonlinear characteristic on a sinusoid

The form of the output signal thus depends on the location of the operating point as well as the input signal. The output can then be represented by

$$S_2[S_1(t),x_o] = y - y_o \ , \tag{4.3}$$

where S_2 represents the output signal, and y_o corresponds to the output of the device at the operating point. Substitution of Eqs. (4.1) and (4.2) into the right hand side of Eq. (4.3) yields

$$S_2[S_1(t),x_o] = f[S_1(t) + x_o] - y_o \ . \tag{4.4}$$

If $S_1(t)$ is an arbitrary sinusoidal signal given by

$$S_1(t) = A \cos(wt + \phi) \ , \tag{4.5}$$

where A is the amplitude of the signal, w is its radian frequency, and ϕ is its phase at t = 0, Eq. (4.4) may be written

$$S_2(t,A,x_o) = f[A \cos(wt + \phi) + x_o] - y_o \ , \tag{4.6}$$

where the dependence of S_2 on w and ϕ is understood. The functional form of S_2 then depends on both the operating point and the amplitude of the sinusoidal input. Equation (4.6) shows that

$$S_2(t + \frac{2\pi}{w}, A, x_o) = S_2(t, A, x_o). \tag{4.7}$$

The function S_2, thus, is periodic in t with fundamental radian frequency w. If the function f is continuous, S_2

can be expressed by a convergent Fourier series in t. The series can be written as

$$S_2(t,A,x_o) = \frac{b_o(A,x_o)}{2} + \sum_{n=1}^{\infty} b_n(A,x_o)\ \cos[nwt + \phi_n(A,x_o)], \quad (4.8)$$

where b_n and ϕ_n represent respectively the amplitude and phase of the n^{th} harmonic.

Additional information about S_2 may be obtained by letting

$$(wt + \phi) = \theta \ , \quad (4.9)$$

in Eq. (4.5). Equation (4.6) becomes

$$S_2(\theta,A,x_o) = f[A \cos \theta + x_o] - y_o \ . \quad (4.10)$$

Thus,

$$S_2(-\theta,A,x_o) = S_2(\theta,A,x_o), \quad (4.11)$$

showing that S_2 is an even function in θ. The Fourier series expansion of $S_2(\theta,A,x_o)$ in θ then contains only terms of the type $\cos(n\theta)$. Comparing this to Eq. (4.8) shows

$$n\theta = n(wt + \phi) = nwt + \phi_n \quad (4.12)$$

or

$$\phi_n = n\phi \ . \quad (4.13)$$

Thus, the phase shifts of the various harmonics of Eq. (4.8) do not depend on A, x_o, or the functional form of f(x). The series can then be written as

$$S_2(t,A,x_o) = \frac{b_o(A,x_o)}{2} + \sum_{n=1}^{\infty} b_n(A,x_o)\cos[n(wt + \phi)] \ . \quad (4.14)$$

The effects of the nonlinearity of f(x) on the input sinusoid are apparent in this expression. The term $b_1 \cos(wt + \emptyset)$ corresponds to the input S_1. The device introduces no phase shift in this signal. The term $b_o/2$ corresponds to a dc bias and the various terms $b_n \cos[n(wt + \emptyset)]$ correspond to harmonic distortions of S_1. The nonlinearity produces no subharmonics of the input sinusoid. This effect occurs only when the input consists of more than one frequency.

Equation (4.14) indicates the dependence of the harmonic coefficients on the operating point of the nonlinear device x_o, and the amplitude of the sinusoidal signal A. If such a device is used in a system where linearity is desired, knowledge of the dependence of these coefficients on x_o and A would show quantitatively the nonlinear effects and reveal optimum input conditions for their minimization. Subsequent sections present methods of obtaining these coefficients from characteristic curves.

4.3 The Description of Nonlinear Effects by a Noise-to-Signal Ratio

In the previous section, a device having a nonlinear characteristic was shown to create distortions of an input sinusoid. For a signal given by

$$S_1(t) = A \cos(wt) \ , \tag{4.15}$$

the output of the device was described by

$$S_2(t) = \frac{b_o}{2} + \sum_{n=1}^{\infty} b_n \cos(nwt), \tag{4.16}$$

where the b coefficients depend on the amplitude of the input sinusoid A and the operating point of the device. A complete description of the nonlinear effects consists of specifying these coefficients. In many instances, however, a complete description of the effects is not needed; and a single quantity describing their severity is sufficient.

In electronic circuit theory a quantity called the "total harmonic distortion" is used for describing the effects of nonlinearities on sinusoidal signals (Ryder, 1964). For a distorted sinusoid this quantity is given by the ratio of the rms value of the sum of the harmonics to that of the fundamental. In terms of Eq. (4.16), it becomes

$$D = \frac{\left[\sum_{n=2}^{\infty} b_n^2\right]^{\frac{1}{2}}}{b_1} . \tag{4.17}$$

The square of this quantity given by

$$D^2 = \frac{\sum_{n=2}^{\infty} b_n^2}{b_1^2} , \tag{4.18}$$

represents the ratio of the total power carried by the harmonics to that of the fundamental. If the harmonics are considered as an equivalent noise generated by the nonlinearity, Eq. (4.18) is equivalent to the reciprocal of the well-known signal-to-noise power ratio of communication theory (Schwartz, 1959). The term equivalent noise is used

to describe the harmonics since the usual communication theory definition of noise assumes that it is independent of the signal. The harmonics generated by nonlinearities are signal dependent and cannot strictly be called noise. The signal-to-noise ratio is defined by

$$SNR = \frac{P_s}{P_n} \quad , \tag{4.19}$$

where P_s is the signal power and P_n is the noise power. Equation (4.18) thus represents an equivalent noise-to-signal ratio or

$$NSR = \frac{P_n}{P_s} = \frac{\sum_{n=2}^{\infty} b_n^2}{b_1^2} \quad . \tag{4.20}$$

Two other quantities expressing nonlinear effects in terms of signal and equivalent noise power are defined as the "signal-power fraction"

$$SPF = \frac{P_s}{P_s + P_n} \quad , \tag{4.21}$$

and the "noise-power fraction"

$$NPF = \frac{P_n}{P_s + P_n} \quad . \tag{4.22}$$

In terms of the harmonic coefficients, these become

$$SPF = \frac{b_1^2}{\sum_{n=1}^{\infty} b_n^2} \quad , \tag{4.23}$$

and

$$NPF = \frac{\sum_{n=2}^{\infty} b_n^2}{\sum_{n=1}^{\infty} b_n^2} \quad . \tag{4.24}$$

All of these descriptions of nonlinear effects are equivalent in that they are functionally related. The knowledge of any one permits the calculation of the others without additional information.

In optical data processing systems, multiple noise sources can exist. For example photographic processes, in addition to being nonlinear, contain fluctuations in image structure known as granularity. This effect can be considered as the addition of noise to the image. If such a process is to be fully evaluated, both effects must be considered. For this reason the amenability of the above quantities to include additional noise sources was investigated. Two sources having equivalent noise powers given by N_1 and N_2 were assumed. The noise N_1 gives rise to D_1, NSR_1, SNR_1, and NPF_1 while N_2 produces D_2, NSR_2, SNR_2, SPF_2, and NPF_2. The addition of the two sources gives rise to the following expressions for the combined quantities

$$D = \sqrt{D_1^2 + D_2^2} \quad , \tag{4.25}$$

$$NSR = NSR_1 + NSR_2 \quad , \tag{4.26}$$

$$SNR = \frac{(SNR_1)(SNR_2)}{SNR_1 + SNR_2}, \tag{4.27}$$

$$SPF = \frac{(SPF_1)(SPF_2)}{SPF_1 + SPF_2 - (SPF_1)(SPF_2)}, \tag{4.28}$$

$$NPF = \frac{NPF_1 + NPF_2 - 2(NPF_1)(NPF_2)}{1 - 3(NPF_1)(NPF_2)}. \tag{4.29}$$

These equations show that the quantity NSR is most easily calculated when two sources are present. The simple addition rule indicated by Eq. (4.26) can be extended to include multiple sources. The NSR description of nonlinear effects was thus chosen for use in subsequent work.

5. NONLINEARITIES IN OPTICAL CORRELATION PROCESSORS

5.1 Introduction

In this chapter, the effects of nonlinearities on the operation of a typical optical correlator are described. The correlator is assumed to operate as part of a larger electronic system for the reception of pulse-frequency-modulation telemetry. The reception system (Rochelle, 1963) is used in satellite and space probe communications. Optical recording processes are assumed to transform the electrical signals into photographic transparencies which form the input to the correlator. These processes can contain nonlinearities which degrade the correlator operation. A description of the reception system and an idealized model of its operation with linear recording processes are first presented. Nonlinearities in the optical recording are then introduced and the resulting effects on the correlation processing described. Finally, three numerical examples are presented. In these, typical optical recording characteristics are used to demonstrate quantitative effects on the correlator operation.

5.2 Mathematical Model of the Operation of the Correlator and Reception System

The reception system receives a sequence of frequency modulated RF pulses. The pulses are of time-length T and begin at intervals of 2T. During each pulse a single RF frequency is transmitted. This frequency corresponds to

one of a set of N possible signals. The detection process consists of determining which of these signals is present in each pulse. Previous to the correlation processing, the RF pulse are demodulated to form a sequence of low-frequency, time-limited sinusoids. The sinusoids corresponding to the various signals are harmonically related. A member of the demodulated signal set can thus be represented during the occurrence of a pulse by

$$f_p(t) = A \cos(pw_o t) \ , \qquad (5.1)$$

where p is an integer ($1 \leq p \leq N$) indicating which signal is present, A is the signal amplitude, w_o is the fundamental radian frequency of the signal set, and t is time. The pulse length T is an integer number of periods of the fundamental radian frequency w_o. Under this condition, the various demodulated signals form an orthogonal set over the pulse interval.

The optical correlator acts as a channelized, matched filter for the detection of the demodulated signals. The reference transparency thus contains N channels, each having a replica of one of the sinusoids of the demodulated set. The incoming signals are continuously recorded on the signal transparency and correlated optically with the channels of the reference.

In the optical recording processes, a time-to-space transformation

$$d = v_o t \ , \tag{5.2}$$

is made where d is a spatial variable and v_o is the recording velocity. The spatial length of a recorded signal is thus

$$L = v_o T \ . \tag{5.3}$$

As a function of d, a member of the signal set becomes

$$f_p(d) = A \cos(p \frac{w_o}{v_o} d). \tag{5.4}$$

In order to clarify the equations, the quantity $(\frac{w_o}{v_o})$ is normalized to one. The spatial representation of a signal is then

$$f_p(d) = A \cos(pd) \ , \tag{5.5}$$

during the occurrence of a pulse. These functions are optically recorded. The amplitude transmittance of the resultant signal transparency is described by $S_p(x)$ where p identifies the signal present and x represents a spatial variable (in the direction of processing) on the transparency. Similarly, the transmittance of a channel of the reference transparency is given by $R_q(y)$ where q ($1 \leq q \leq N$) denotes the channel and y is the appropriate spatial variable.

The output of channel q of the correlator with signal p present is described by

$$C_{qp}(z) = \frac{1}{L} \int_{-L/2}^{L/2} S_p(y + z) R_q(y) \ dy. \tag{5.6}$$

where L is the aperture length of the correlator (spatial equivalent of the pulse length) and $S_p(y + z)$ is the image of the recorded signal at the reference transparency plane (after displacement by the correlation variable z). The quantity C_{qp} is the cross-correlation integral. Since L is an integer number of periods of the fundamental spatial frequency of the signal set, the various undistorted signals are orthogonal over the aperture.

In the remainder of this section, the effects of the pulse nature of the signals on the correlation integrals are neglected. The time limitation of the signals imparts a triangular envelope of length 2L to the periodic correlation functions described here. This simplification allows the nonlinear effects to be observed without undue complication.

If the optical recording processes are linear, the amplitude transmittance of the signal transparency is described by

$$S_p(x) = a_o + a_1 \cos(px) \ , \tag{5.7}$$

where p denotes the signal present, and a_o and a_1 are determined from the recording process used. Similarly, the transmittance of channel q of the reference transparency is

$$R_q(y) = b_o + b_1 \cos(qy) \ , \tag{5.8}$$

where b_o and b_1 are determined by its recording process. When used in Eq. (5.6), the bias terms in these equations can be neglected since the correlator is assumed to contain

a "dc stop." Substituting the resultant expressions into Eq. (5.6) gives

$$C_{qp}(z) = \frac{1}{L}\int_{-L/2}^{L/2} a_1 b_1 \cos[p(y+z)]\,\cos(qy)\,dy. \qquad (5.9)$$

Evaluation yields

$$C_{qp}(z) = \begin{cases} 0, & q \neq p \\ \frac{1}{2} a_1 b_1 \cos(pz), & q = p \end{cases}. \qquad (5.10)$$

An output thus appears in the channel of the correlator which corresponds to the input signal, and indications in the others are zero. This corresponds to normal operation of the system.

When the optical recording processes are nonlinear, the signal and reference transparencies contain harmonic distortions as described in Chapter 4. The resulting amplitude transmittance of the signal transparency with signal p present can be expressed by the series

$$S_p(x) = \frac{S_o}{2} + \sum_{m=1}^{\infty} S_m \cos(mpx)\ , \qquad (5.11)$$

where the s coefficients result from the nonlinear characteristic of the signal recording process. In a like manner the transmittance of channel q of the reference transparency is given by

$$R_q(y) = \frac{r_o}{2} + \sum_{n=1}^{\infty} r_n \cos(nqy), \tag{5.12}$$

where r coefficients result from the characteristic of the reference recording process. The harmonic distortions can be expressed as equivalent noise-to-signal ratios given by

$$NSR_s = \frac{\sum_{m=2}^{\infty} s_m^2}{s_1^2}, \tag{5.13}$$

and

$$NSR_r = \frac{\sum_{n=2}^{\infty} r_n^2}{r_1^2}, \tag{5.14}$$

where the subscripts S and r denote, respectively, the signal and reference transparencies. The correlator can thus be considered to contain two internal equivalent noise sources.

The effects of the nonlinearities on the operation of the correlator are obtained by substitution of Eqs. (5.11) and (5.12) into Eq. (5.6). This yields

$$C_{qp}(z) = \frac{1}{L} \int_{-L/2}^{L/2} \left\{ \sum_{m=1}^{\infty} S_m \cos[mp(y+z)] \right\} \left[\sum_{n=1}^{\infty} r_n \cos(nqy) \right] dy, \tag{5.15}$$

when the dc terms are omitted. This expression can be re-written as

$$C_{qp}(z) = \sum_{m=1}^{\infty} S_m \sum_{n=1}^{\infty} r_n \frac{1}{L} \int_{-L/2}^{L/2} \cos[mp(y+z)]$$

$$\cos(nqy)\, dy. \tag{5.16}$$

Due to the orthogonality properties of the cosine functions,

$$\frac{1}{L} \int_{-L/2}^{L/2} \cos[mp(y + z)] \cos(nqy)\, dy$$

$$= \begin{cases} 0, & mp \neq nq \\ \frac{1}{2} \cos(mpz), & mp = nq, \end{cases} \tag{5.17}$$

and Eq. (5.16) can be written

$$C_{qp}(z) = \frac{1}{2} \sum_{m=1}^{\infty} S_m r_n \cos(mpz)\, \delta_{mp,nq}\ , \tag{5.18}$$

where $\delta_{mp,nq}$ is one for $mp = nq$ and zero otherwise. The output of the correlator is thus non zero in those channels having a common frequency with the signal transparency. Outputs exist in channels corresponding to incorrect detection of the signal. The output of the correct or signal channel is

$$[C_{qp}(z)]_{p=q} = \frac{1}{2} \sum_{m=1}^{\infty} S_m r_m \cos(mpz)\ . \tag{5.19}$$

Two other specific cases are

$$[C_{qp}(z)]_{q=2p} = \frac{1}{2} \sum_{m=1}^{\infty} S_{2m} r_m \cos(2mpz)\ , \tag{5.20}$$

and

$$[C_{qp}(z)]_{q=\frac{p}{2}} = \frac{1}{2} \sum_{m=1}^{\infty} S_m r_{2m} \cos(mpz) \ , \qquad (5.21)$$

which indicate the output of the channels corresponding to twice and half the frequency of the signal channel. Similar expressions can be obtained for other channels.

The equivalent output powers (mean squared amplitudes) of various channels of the correlator serve as convenient measures of the severity of the nonlinear effects. Expressions for these can be obtained directly from Eq. (5.18) as

$$P_{qp} = \frac{1}{8} \sum_{m=1}^{\infty} S_m^2 \ r_n^2 \ \delta_{mp,nq} \ , \qquad (5.22)$$

where P_{qp} indicates the equivalent output power of channel q with signal p present. This quantity can be normalized with respect to the equivalent power in the signal channel. The resulting expression

$$EPR_{qp} = \frac{P_{qp}}{[P_{qp}]_{q=p}} = \frac{\sum_{m=1}^{\infty} S_m^2 \ r_n^2 \ \delta_{mp,nq}}{\sum_{m=1}^{\infty} S_m^2 \ r_m^2} \ , \qquad (5.23)$$

indicates an "error-power ratio" existing between the outputs of channel q and the signal channel. For the signal channel, the quantity becomes unity. The definition of the EPR is similar to that of the noise-to-signal ratio introduced

previously. It represents the ratio of the power of an equivalent noise source (unwanted output) to that of the desired signal.

5.3 Examples

A variety of optical recording processes can be employed to produce transparencies for use in optical correlators. The form and extent of the nonlinearities involved in these processes can vary considerably. Three examples which represent typically occuring nonlinearities are considered. In each example it is assumed that a single characteristic describes both the signal and reference recording processes. The harmonic series of the transparences resulting from each characteristic are derived and the corresponding NSR's and EPR's calculated.

The characteristic for the first example is linear. That of the second follows a square law and that of the third an exponential. A linear characteristic can result from use of a small operating region within a larger nonlinear characteristic or from using pre-distortion techniques to cancel nonlinear effects. Characteristics approaching square law and exponential curves can be obtained, respectively, from positive and negative photographic processes used in conjunction with primary electro-optic modulators such as cathode ray tubes.

The characteristics for the optical recording processes of the three examples are shown in Figures 5.1 through 5.3.

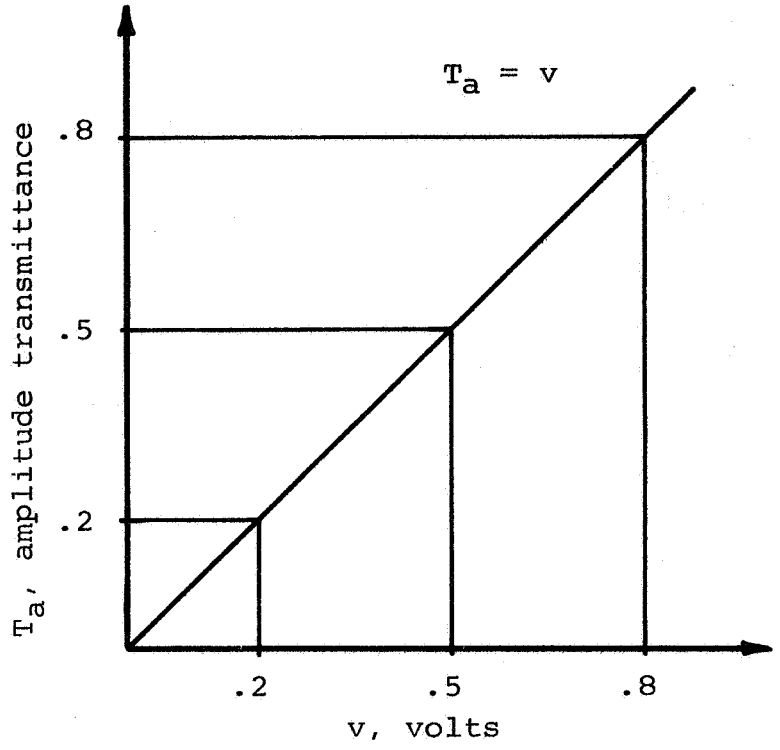

Figure 5.1 A linear characteristic

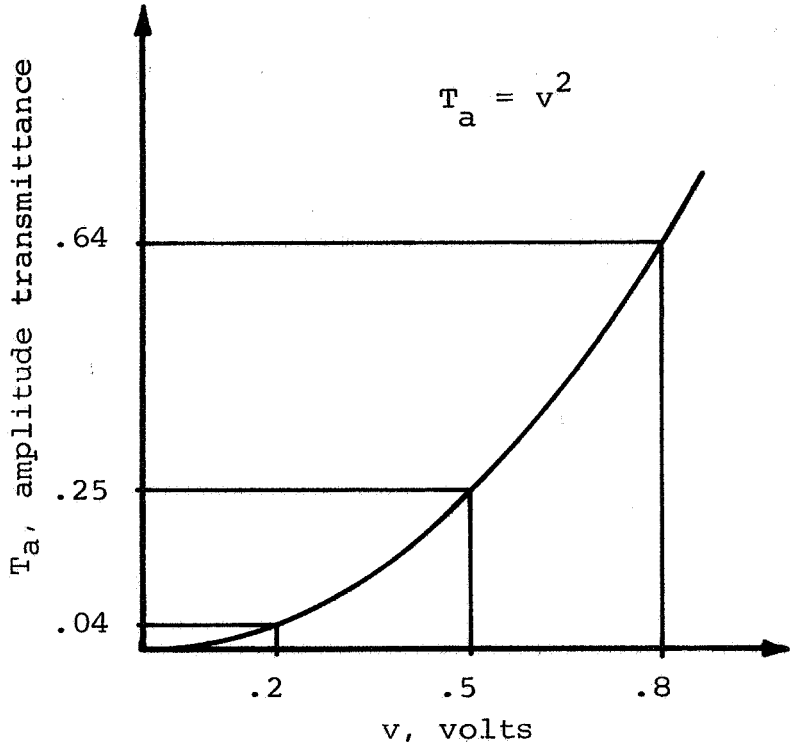

Figure 5.2 A square law characteristic

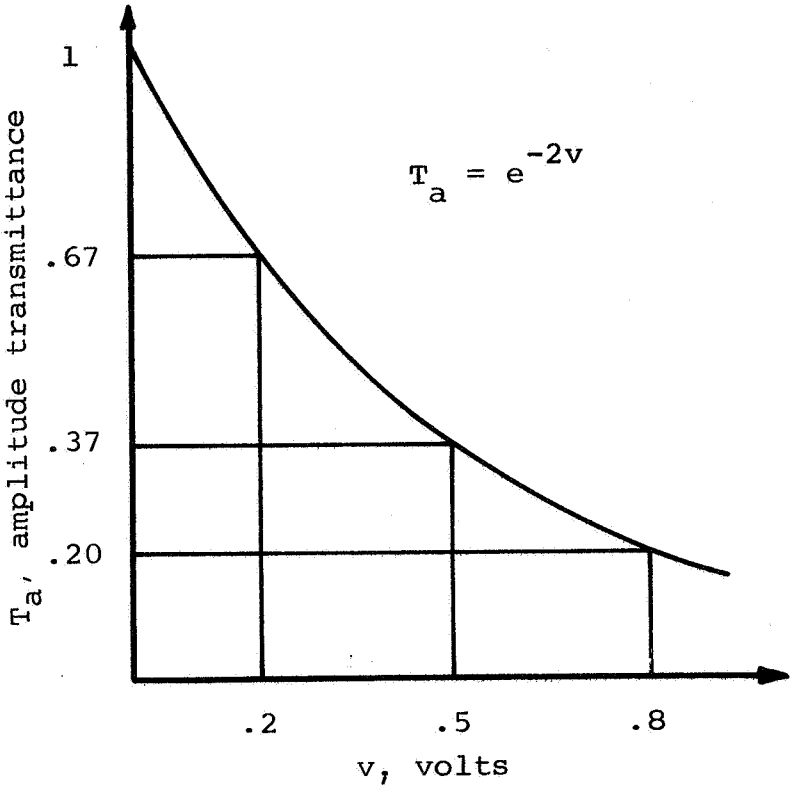

Figure 5.3 An exponential characteristic

They describe the variation of the amplitude transmittance of a resulting transparency with input voltage. In the examples, the signals are assumed to be recorded with a bias level of .5v and an amplitude of .3v. The spatial representations of the electrical inputs and thus given by

$$v_p(d) = .5 + .3 \cos(pd) \ , \tag{5.24}$$

where $1 \leq p \leq N$.

In the linear case, the amplitude transmittance of the signal transparency with signal p present becomes

$$S_p(x) = .5 + .3 \cos(px) \ , \tag{5.25}$$

and the transmittance of channel q of the reference is

$$R_q(y) = .5 + .3 \cos(qy) \ . \tag{5.26}$$

Since no distortions are present, the corresponding noise-to-signal ratios are zero. With signal p present the correlator output in the signal channel is

$$[C_{qp}(x)]_{p=q} = (.045) \cos(pz) \ . \tag{5.27}$$

Outputs of the other channels are zero, and the corresponding error-power ratios vanish as shown in Table 5.1. The correlator thus operates normally.

In the square law example, the amplitude transmittances of the transparencies are described by

$$S_p(x) = [.5 + .3 \cos(px)]^2 \ , \tag{5.28}$$

Table 5.1 Error-power ratios corresponding to three optical recording characteristics

Signal-reference channel relation q/p	Characteristic		
	Linear	Square law	Exponential
1	1.0	1.0	1.0
1/2, 2	0	$.2249 \times 10^{-1}$	$.2184 \times 10^{-1}$
1/3, 3	0	0	$.2045 \times 10^{-3}$
1/4, 4	0	0	$.1690 \times 10^{-5}$
2/3, 3/2	0	0	$.4471 \times 10^{-5}$
3/4, 4/3	0	0	$.3458 \times 10^{-9}$

and

$$R_q(y) = [.5 + .3 \cos(qy)]^2 , \tag{5.29}$$

or, after expanding,

$$S_p(x) = (.295) + (.3)\cos(px) + (.045)\cos(2px), \tag{5.30}$$

and

$$R_q(y) = (.295)+(.3)\cos(qy)+(.045)\cos(2qy). \tag{5.31}$$

The signal transparency and reference channels thus contain second harmonic distortions. The corresponding noise-to-signal ratios are

$$NSR_s = .225 \times 10^{-1} , \tag{5.32}$$

and

$$NSR_r = .225 \times 10^{-1} \ . \qquad (5.33)$$

Because of the harmonics, unwanted outputs occur in channels corresponding to twice and half the frequency of the signal channel. The resulting error-power ratios, calculated from the harmonic coefficients of Eqs. (5.30), (5.31), and (5.32) are shown in Table 5.1.

In the exponential case, the form of the recorded signal can be obtained from a Taylor series expansion of the characteristic about the bias point. Neglecting orders higher than the fourth, the amplitude transmittance is given by

$$T_a(v) = \frac{1}{e}\left[1-2(v-.5)+2(v-.5)^2 - \frac{4}{3}(v-.5)^3 + \frac{2}{3}(v-.5)^4\right] \ . \qquad (5.34)$$

Substituting Eq. (5.24) in this expression and expanding the resulting powers of the cosine function into multiple angles gives

$$S_p(x) = (.4017)-(.2307)\cos(px)+(.0341)\cos(2px) -(.0033)\cos(3\,px)+(.0003)\cos(4px) \ , \qquad (5.35)$$

for the signal transparency and a similar expression for the reference channels $R_q(y)$. The noise-to-signal ratios corresponding to these expressions are

$$NSR_s = .2206 \times 10^{-1} \ , \qquad (5.36)$$

and

$$NSR_r = .2206 \times 10^{-1} \ . \qquad (5.37)$$

Harmonics higher than the fourth do not appear in Eq. (5.35) due to the truncation of the Taylor series. The higher order terms of this series give rise to additional harmonics and small contributions to the ones retained above. These are neglected. The four harmonics of Eq. (5.35) give rise to outputs in the channels listed in Table 5.1. The error-power ratios shown were calculated from the coefficients of Eq. (5.35) and Eq. (5.23).

In this example, the Taylor series expansion was employed to obtain the harmonic coefficients of the recorded signals. Versions of this method have been used by several authors as described in the review of the literature. Other series expansion methods may be used, however. The Taylor method and a number of these are described more thoroughly in the next chapter.

6. EXPANSION METHODS FOR DETERMINING HARMONIC COEFFICIENTS

6.1 Introduction

In Chapter 4, the output of a sinusoidally excited, zero-memory nonlinear device was described by a harmonic series with a fundamental frequency equal to that of the input. The harmonic coefficients of this series may be obtained by expanding the characteristic function representing the nonlinearity. The expansion is carried out with a series of appropriate functions within the operating region spanned by the input sinusoid. In this chapter the equations necessary for using the Taylor, Fourier, Legendre, and Tchebyscheff expansions for this purpose are developed. The equations for each expansion method are obtained with relatively few restrictions on the form of the characteristic function. This establishes their use in correspondingly wide classes of application. Following the developments, applications of the various expansion methods are discussed.

Two versions of the Fourier series method are presented. In method A, a direct expansion of the nonlinear characteristic is assumed. This method has disadvantages if the characteristic is continuous within the operating region ([a,b]) but does not meet the boundary condition

$$f(a) = f(b) \tag{6.1}$$

The periodic extension of the characteristic contains discontinuities and the resulting Fourier series is slowly

convergent (Lanczos, 1966). This problem can be avoided by assuming an even extension of the characteristic about either of the end points and computing the Fourier expansion of the resulting function. Since the periodic extension of such a function is continuous, its Fourier series is more quickly convergent. This procedure is employed in method B. When successively higher derivatives of the characteristic are continuous within the operating region, more rapidly convergent Fourier series expansions can be obtained and corresponding equations for the output harmonic coefficients can be developed. Lanczos (1956) described and developed equations for a method that is rapidly convergent when the characteristic and its first derivative are continuous.

In the derivations which follow, the nonlinear characteristic is termed $f(x)$ and the operating region is assumed to be $[-1,1]$ with the input sinusoid given by

$$x = \cos \theta . \tag{6.2}$$

The output of the nonlinear device is then $f(\cos \theta)$ which is an even function of θ. Its harmonic expansion in θ can thus be written

$$f(\cos \theta) = \frac{1}{2} \sum_{k=0}^{\infty} \epsilon_k \, b_k \cos (k\theta), \tag{6.3}$$

where

$$b_k = \frac{2}{\pi} \int_0^{\pi} f(\cos \theta) \cos(k\theta) \, d\theta, \tag{6.4}$$

and the Neumann symbol ϵ_k is given by

$$\epsilon_o = 1, \tag{6.5}$$

$$\epsilon_1 = \epsilon_2 = \ldots = 2. \tag{6.6}$$

This definition of the ϵ symbol is assumed throughout this chapter.

In the drivations, the order of integration and summation of infinite series of functions are interchanged. Use of this procedure is based on Arzela's theorem as stated by Apostol (1957).

6.2 Taylor Series

The Taylor series expansion of f(x) about x = 0 is given by

$$f(x) = \sum_{n=o}^{\infty} a_n x^n , \tag{6.7}$$

where

$$a_n = \frac{1}{n!}\left[\frac{d^n}{dx^n} f(x)\right]_{x=0}. \tag{6.8}$$

If f(x) is continuous and has continuous bounded derivatives of all orders on an interval containing [-1,1], then the series (6.7) converges on [-1,1] (Apostol, 1957). Replacing x by cos θ in Eq. (6.7) gives

$$f(\cos\theta) = \sum_{n=o}^{\infty} a_n(\cos\theta)^n \tag{6.9}$$

which may be substituted into Eq. (6.4) for the k^{th} output harmonic coefficient yielding

$$b_k = \frac{2}{\pi} \int_o^{\pi} \left[\sum_{n=o}^{\infty} a_n (\cos\theta)^n \right] \cos(k\theta)\, d\theta . \qquad (6.10)$$

Since the series (6.9) is convergent for all $0 \leq \theta \leq \pi$, the order of integration and summation in (6.10) can be interchanged so that

$$b_k = \frac{2}{\pi} \sum_{n=o}^{\infty} a_n \int_o^{\pi} (\cos\theta)^n \cos(k\theta)\, d\theta . \qquad (6.11)$$

The integrals in this expression can be evaluated by using the expansions (Mangulis, 1965)

$$(\cos\theta)^n = (\tfrac{1}{2})^n \sum_{m=o,2,\ldots}^{n} \epsilon_m \binom{n}{\frac{n-k}{2}} \cos(m\theta) , \qquad (6.12)$$

for even n and

$$(\cos\theta)^n = (\tfrac{1}{2})^{n-1} \sum_{m=1,3,\ldots}^{n} \binom{n}{\frac{n-m}{2}} \cos(m\theta) , \qquad (6.13)$$

for odd n, where the large parentheses denote binomial coefficients. Substituting these into (6.11) and again interchanging orders of integration and summation gives

$$\int_o^{\pi} (\cos\theta)^n \cos(k\theta)\, d\theta =$$

$$(\tfrac{1}{2})^n \sum_{m=o,2,\ldots}^{n} \epsilon_m \binom{n}{\frac{n-m}{2}} \int_o^{\pi} \cos(m\theta) \cos(k\theta)\, d\theta , \qquad (6.14)$$

for even n and

$$\int_0^{\pi} (\cos\theta)^n \cos(k\theta)\, d\theta =$$

$$(\tfrac{1}{2})^{n-1} \sum_{m=1,3,\ldots}^{n} \binom{n}{\frac{n-m}{2}} \int_0^{\pi} \cos(m\theta)\cos(k\theta)\, d\theta, \qquad (6.15)$$

for odd n. Evaluation of the integrals in (6.14) and (6.15) yields

$$\int_0^{\pi} (\cos\theta)^n \cos(k\theta)\, d\theta = \begin{cases} 0, & n < k \\ \pi(\tfrac{1}{2})^n \binom{n}{\frac{n-m}{2}}, & n \geq k \end{cases} \qquad (6.16)$$

for all n. Substitution of this result into Eq. (6.11) yields

$$b_k = \sum_{n=k,k+2,\ldots}^{\infty} a_n (\tfrac{1}{2})^{n-1} \binom{n}{\frac{n-k}{2}}, \qquad (6.17)$$

which is the desired equation relating the Taylor expansion coefficients a_n to the output harmonic coefficients b_k.

Equation (6.17) can be written as

$$b_k = \sum_{n=k,k+2,\ldots}^{\infty} a_n g_{nk}, \qquad (6.18)$$

where

$$g_{nk} = \begin{cases} (\tfrac{1}{2})^{n-1} \binom{n}{\frac{n-k}{2}}, & (n-k) \text{ even and non negative} \\ 0, & \text{otherwise} \end{cases} \qquad (6.19)$$

The coefficients g_{nk} for $k \leq 5$ and $n \leq 10$ are shown in Table 6.1.

Table 6.1. Non-vanishing coefficients g_{nk} for the Taylor series expansion method with $k \leq 5$ and $n \leq 10$

n \ k	0	1	2	3	4	5
0	2.0000					
1		1.0000				
2	1.000		.5000			
3		.7500		.2500		
4	.7500		.5000		.1250	
5		.6250		.3125		.0625
6	.6250		.4688		.1875	
7		.5469		.3281		.0882
8	.5469		.4375		.2187	
9		.4922		.3281		.1266
10	.4922		.4102		.2344	

6.3 Fourier Series - Method A

The Fourier series expansion of f(x) on [-1,1] can be written

$$f(x) = \frac{1}{2}\sum_{n=0}^{\infty} \epsilon_n [c_n \cos(n\pi x) + d_n \sin(n\pi x)], \tag{6.20}$$

where

$$c_n = \int_{-1}^{1} f(x) \cos(n\pi x)\, dx\ , \tag{6.21}$$

$$d_n = \int_{-1}^{1} f(x) \sin(n\pi x)\, dx \ , \tag{6.22}$$

and d_o vanishes as implied by Eq. (6.22). If f(x) is continuous and square integradable on [-1,1], the series (6.20) converges on [-1,1] (Jackson, 1941). Replacing x by cos θ in Eq. (6.20) gives

$$f(\cos\theta) = \frac{1}{2} \sum_{n=o}^{\infty} \epsilon_n \left[c_n \cos(n\pi \cos\theta) + d_n \sin(n\pi \cos\theta) \right], \tag{6.23}$$

which is convergent for $0 \leq \theta \leq \pi$. Substituting the series (6.23) into Eq. (6.4) for the k^{th} output harmonic coefficient and interchanging the order of integration and summation gives

$$b_k = \frac{1}{\pi} \sum_{n=o}^{\infty} \epsilon_n \left[c_n \int_o^{\pi} \cos(n\pi \cos\theta) \cos(k\theta)\, d\theta \right.$$

$$\left. + d_n \int_o^{\pi} \sin(n\pi \cos\theta) \cos(k\theta)\, d\theta \right] . \tag{6.24}$$

The integrals in this expression can be evaluated using (Mangulis, 1965)

$$\cos(n\pi \cos\theta) = \sum_{m=0,2,\ldots}^{\infty} \epsilon_m (-1)^{m/2} J_m(n\pi) \cos(m\theta) \ , \tag{6.25}$$

and

$$\sin(n\pi \cos\theta) = 2 \sum_{m=1,3,\ldots}^{\infty} (-1)^{\frac{m-1}{2}} J_m(n\pi) \cos(m\theta), \tag{6.26}$$

where J_m is the m^{th} order Bessel function of the first type. Substitution of Eqs. (6.25) and (6.26) into the integrals of Eq. (6.24) and interchanging orders of integration and summation gives

$$\int_o^\pi \cos(n\pi \cos\theta)\, \cos(k\theta)\, d\theta =$$

$$\sum_{m=0,2,\ldots}^{\infty} \epsilon_m (-1)^{m/2}\, J_m(n\pi) \int_o^\pi \cos(m\theta)\, \cos(k\theta)\, d\theta\ , \qquad (6.27)$$

and

$$\int_o^\pi \sin(n\pi \cos\theta)\, \cos(k\theta)\, d\theta =$$

$$2 \sum_{m=1,3,\ldots}^{\infty} (-1)^{\frac{m-1}{2}}\, J_m(n\pi) \int_o^\pi \cos(m\theta)\, \cos(k\theta)\, d\theta, \qquad (6.28)$$

which, upon evaluation, yield

$$\int_o^\pi \cos(n\pi \cos\theta)\, \cos(k\theta)\, d\theta = \begin{cases} \pi(-1)^{k/2}\, J_k(n\pi), & k \text{ even} \\ 0, & k \text{ odd}, \end{cases} \qquad (6.29)$$

and

$$\int_o^\pi \sin(n\pi \cos\theta)\, \cos(k\theta)\, d\theta = \begin{cases} 0, & k \text{ even} \\ \pi(-1)^{(k-1)/2} J_k(n\pi), & k \text{ odd}. \end{cases} \qquad (6.30)$$

Substitution of these results in Eq. (6.24) gives

$$b_k = (-1)^{k/2} \sum_{n=o}^{\infty} \epsilon_n\, c_n\, J_k(n\pi)\ , \qquad (6.31)$$

for even k and

$$b_k = 2(-1)^{(k-1)/2} \sum_{n=o}^{\infty} d_n \, J_k(n\pi) \ , \tag{6.32}$$

for odd k, as the resulting expressions for the output harmonic coefficients.

Equations (6.31) and (6.32) can be rewritten as

$$b_k = \sum_{n=o}^{\infty} c_n \, g_{nk} \ , \tag{6.33}$$

for even k and

$$b_k = \sum_{n=o}^{\infty} d_n \, g_{nk} \ , \tag{6.34}$$

for odd k, where

$$g_{nk} = \begin{cases} \epsilon_n (-1)^{k/2} \, J_k(n\pi), & k \text{ even} \\ 2(-1)^{(k-1)/2} \, J_k(n\pi), & k \text{ odd.} \end{cases} \tag{6.35}$$

Table 6.2 shows the g_{nk} for $k \leq 5$ and $n \leq 10$.

6.4 Fourier Series - Method B

A Fourier series expression for f(x) on [-1,1] may be obtained by defining a related function g(x) on [-2,2]. On [0,2], g(x) is the translation of f(x) given by

$$g(x) = f(x - 1). \tag{6.36}$$

On [-2,0], g(x) is extended evenly. Because of the evenness property, Fourier series expansion of g(x) on [-2,2] contains only cosine terms. This expression is then given by

Table 6.2 Coefficients g_{nk} for the Fourier series expansion method A with $k \leq 5$ and $n \leq 10$

n \ k	0	1	2	3	4	5
0	1.0000	0.0	0.0	0.0	0.0	0.0
1	- .6085	.5692	- .9707	- .6669	.3028	.1043
2	.4406	- .4248	.5758	- .0582	.6314	.7456
3	- .3624	.3535	- .4374	.1678	- .5443	- .2942
4	.3150	- .3091	.3642	- .1931	.4564	.0974
5	- .2824	.2781	- .3178	.1971	- .3931	- .0030
6	.2581	- .2548	.2852	- .1943	.3470	- .0470
7	- .2392	.2366	- .2607	.1892	- .3123	.0755
8	.2239	- .2218	.2416	- .1833	.2853	- .0925
9	- .2112	.2094	- .2261	.1774	- .2637	.1028
10	.2005	- .1989	.2132	- .1718	.2460	- .1092

$$g(x) = \frac{1}{2} \sum_{n=0}^{\infty} e_n \, a_n \cos\left(\frac{n\pi}{2} x\right), \tag{6.37}$$

where

$$a_n = \int_0^2 g(x) \cos\left(\frac{n\pi x}{2}\right) dx. \tag{6.38}$$

If $f(x)$ is continuous and square integrable on $[-1,1]$, the series (6.37) converges on $[-1,1]$ (Jackson, 1941). The coefficients a_n can be evaluated in terms of $f(x)$ as

$$a_n = \int_{-1}^{1} f(x) \cos[\tfrac{n\pi}{2}(x + 1)] \, dx \, . \qquad (6.39)$$

Replacing x by (x + 1) in Eq. (6.37) and using Eq. (6.36) gives

$$f(x) = \tfrac{1}{2} \sum_{n=o}^{\infty} \epsilon_n a_n \cos[\tfrac{n\pi}{2}(x + 1)] \qquad (6.40)$$

or

$$f(x) = \tfrac{1}{2} \sum_{n=o}^{\infty} \epsilon_n a_n \left[\cos(\tfrac{n\pi}{2}) \cos(\tfrac{n\pi x}{2}) - \sin(\tfrac{n\pi}{2}) \sin(\tfrac{n\pi x}{2})\right]. \qquad (6.41)$$

Substituting cos θ for x in this expression and using the resulting series in the equation for the k^{th} output Fourier coefficient gives

$$b_k = \tfrac{1}{\pi} \int_o^{\pi} \Big\{ \sum_{n=o}^{\infty} \epsilon_n \, a_n \left[\cos(\tfrac{n\pi}{2}) \cos(\tfrac{n\pi}{2} \cos \theta) - \sin(\tfrac{n\pi}{2}) \sin(\tfrac{n\pi}{2} \cos \theta)\right]\Big\} \cos(k\theta) \, d\theta \, . \qquad (6.42)$$

Interchanging the order of integration and summation yields

$$b_k = \tfrac{1}{\pi} \sum_{n=o}^{\infty} \epsilon_n \, a_n \left[\cos(\tfrac{n\pi}{2}) \int_o^{\pi} \cos(\tfrac{n\pi}{2}\cos \theta) \cos(k\theta) \, d\theta - \sin(\tfrac{n\pi}{2}) \int_o^{\pi} \sin(\tfrac{n\pi}{2}\cos \theta) \cos(k\theta) \, d\theta\right] . \qquad (6.43)$$

The integrals in this expression may be evaluated with the

help of the expansions (6.25) and (6.26) where $n\pi$ is replaced by $\frac{n\pi}{2}$. Using these as in the previous derivation gives

$$\int_0^{\pi} \cos\left(\frac{n\pi}{2}\cos\theta\right)\cos(k\theta)\,d\theta = \begin{cases} (-1)^{k/2}\pi\, J_k\left(\frac{n\pi}{2}\right), & k \text{ even} \\ 0, & k \text{ odd}, \end{cases} \tag{6.44}$$

and

$$\int_0^{\pi} \sin\left(\frac{n\pi}{2}\cos\theta\right)\cos(k\theta)\,d\theta = \begin{cases} 0, & k \text{ even} \\ (-1)^{(k-1)/2}\pi\, J_k\left(\frac{n\pi}{2}\right), & k \text{ odd}. \end{cases} \tag{6.45}$$

Substituting these results in (6.43) gives the equations for the output harmonic coefficients:

$$b_k = (-1)^{k/2} \sum_{n=0,2,\ldots}^{\infty} \epsilon_n\, a_n (-1)^{n/2} J_k\left(\frac{n\pi}{2}\right), \tag{6.46}$$

for even k and

$$b_k = 2(-1)^{(k-1)/2} \sum_{n=1,3,\ldots}^{\infty} a_n (-1)^{(n-1)/2} J_k\left(\frac{n\pi}{2}\right), \tag{6.47}$$

for odd k.

These equations can be rewritten as

$$b_k = \sum_{n=0,2,\ldots}^{\infty} a_n\, g_{nk}, \tag{6.48}$$

for even k and

$$b_k = \sum_{n=1,3,\ldots}^{\infty} a_n\, g_{nk}, \tag{6.49}$$

for odd k where

$$g_{nk} = \begin{cases} \varepsilon_n (-1)^{\frac{n+k}{2}} J_k(\frac{n\pi}{2}); & n,k \text{ both even} \\ 2(-1)^{\frac{n+k-2}{2}} J_k(\frac{n\pi}{2}); & n,k \text{ both odd} \\ 0; & \text{otherwise.} \end{cases} \tag{6.50}$$

The non-vanishing g_{nk} for $k \leq 5$, $n \leq 10$ are shown in Table 6.3.

Table 6.3. Non-vanishing coefficients g_{nk} for the Fourier series expansion method B with $k \leq 5$ and $n \leq 10$

n \ k	0	1	2	3	4	5
0	1.0000					
1		1.1336		-.1381		.0045
2	.6085		.9709		-.3028	
3		.5633		.8117		-.4460
4	.4406		.5758		.6314	
5		.4225		.5758		.4343
6	.3624		.4374		.5443	
7		.3522		.4540		.4774
8	.3150		.3642		.4564	
9		.3082		.3815		.4365
10	.2824		.3178		.3931	

6.5 Legendre Series

The Legendre series expansion of f(x) on [-1,1] (Kaplan, 1952) is given by

$$f(x) = \sum_{n=0}^{\infty} a_n P_n(x), \tag{6.51}$$

where

$$a_n = \frac{2n+1}{2} \int_{-1}^{1} f(x) P_n(x) dx, \tag{6.52}$$

and P_n is the Legendre polynomial of order n. A sufficient condition for the convergence of (6.51) on [-1,1] is that f(x) is bounded, continuous, and integrable on [-1,1] (Sansone, 1959). The Legendre polynomials are defined by

$$P_0(x) = 1, \tag{6.53}$$

$$P_1(x) = x, \tag{6.54}$$

and the recurrence relation

$$P_{n+1}(x) = \frac{2n+1}{n+1} xP_n(x) - \frac{n}{n+1} P_{n-1}(x), \tag{6.55}$$

or by the Rodregues formula

$$P_n(x) = \frac{1}{2^n n!} \frac{d^n}{dx^n} [(x^2 - 1)^n]. \tag{6.56}$$

Replacing x by cos θ in Eq. (6.51) gives

$$f(\cos \theta) = \sum_{n=0}^{\infty} a_n P_n(\cos \theta), \tag{6.57}$$

which is convergent for $0 \leq \theta \leq \pi$. Substituting this expression

into the expression (6.4) for the k^{th} output harmonic coefficient gives

$$b_k = \frac{2}{\pi} \sum_{n=o}^{\infty} a_n \left[\int_o^{\pi} P_n(\cos\theta) \cos(k\theta)\, d\theta \right], \tag{6.58}$$

after interchanging the order of integration and summation. The integrals in (6.58) can be evaluated by using the expansions (Mangulis, 1965)

$$P_n(\cos\theta) = \frac{1}{\pi} \sum_{m=0,2,\ldots}^{n} \epsilon_m \frac{\Gamma(\frac{n-m+1}{2})\ \Gamma(\frac{n+m+1}{2})}{(\frac{n-m}{2})!\ (\frac{n+m}{2})!} \cos(m\theta), \tag{6.59}$$

for even n and

$$P_n(\cos\theta) = \frac{2}{\pi} \sum_{m=1,3,\ldots}^{n} \frac{\Gamma(\frac{n-m+1}{2})\ \Gamma(\frac{n+m+1}{2})}{(\frac{n-m}{2})!\ (\frac{n+m}{2})!} \cos(m\theta), \tag{6.60}$$

for odd n, where Γ represents the gamma function. Substituting these expansions into the integrals of (6.58) and again interchanging the order of integration and summation gives

$$\int_o^{\pi} P_n(\cos\theta) \cos(k\theta)\, d\theta =$$

$$\frac{1}{\pi} \sum_{m=0,2,\ldots}^{n} \epsilon_m \frac{\Gamma(\frac{n-m+1}{2})\ \Gamma(\frac{n+m+1}{2})}{(\frac{n-m}{2})!\ (\frac{n+m}{2})!} \int_o^{\pi} \cos(m\theta) \cos(k\theta)\, d\theta, \tag{6.61}$$

for even n and

$$\int_0^{\pi} P_n(\cos\theta)\,\cos(k\theta)\,d\theta =$$

$$\frac{2}{\pi}\sum_{m=1,3,\ldots}^{n} \frac{\Gamma\left(\frac{n-m+1}{2}\right)\,\Gamma\left(\frac{n+m+1}{2}\right)}{\left(\frac{n-m}{2}\right)!\;\left(\frac{n+m}{2}\right)!} \int_0^{\pi}\cos(m\theta)\,\cos(k\theta)\,d\theta, \tag{6.62}$$

for odd n. Evaluation of the integrals in these expressions gives

$$\int_0^{\pi} P_n(\cos\theta)\,\cos(k\theta)\,d\theta =$$

$$\begin{cases} 0, & n < k \\ \dfrac{\Gamma\left(\frac{n-k+1}{2}\right)\,\Gamma\left(\frac{n+k+1}{2}\right)}{\left(\frac{n-k}{2}\right)!\;\left(\frac{n+k}{2}\right)!}, & n \geq k, \end{cases} \tag{6.63}$$

for all n. Substitution of this result in (6.58) gives

$$b_k = \frac{2}{\pi}\sum_{n=k,k+2,\ldots}^{\infty} a_n \frac{\Gamma\left(\frac{n-k+1}{2}\right)\,\Gamma\left(\frac{n+k+1}{2}\right)}{\left(\frac{n-k}{2}\right)!\;\left(\frac{n+k}{2}\right)!} \tag{6.64}$$

which is the desired expression, relating the harmonic coefficients b_k to the Legendre coefficients a_n.

Equation (6.64) can be written as

$$b_k = \sum_{n=k,k+2,\ldots}^{\infty} a_n\, g_{nk}, \tag{6.65}$$

where

$$g_{nk} = \begin{cases} \frac{2}{\pi} \frac{\Gamma\left(\frac{n-k+1}{2}\right)\ \Gamma\left(\frac{n+k+1}{2}\right)}{\left(\frac{n-k}{2}\right)!\ \left(\frac{n+k}{2}\right)!}, & (n-k) \text{ even and non negative} \\ 0, \text{ otherwise} \end{cases} \tag{6.66}$$

Table 6.4 shows the non-vanishing g_{nk} for $k \leq 5$ and $n \leq 10$.

Table 6.4. Non-vanishing coefficients g_{nk} for the Legendre series expansion method with $k \leq 5$ and $n \leq 10$.

n \ k	0	1	2	3	4	5
0	2.0000					
1		1.0000				
2	.5000		.7500			
3		.3750		.6250		
4	.2812		.3125		.5469	
5		.2344		.2734		.4922
6	.1953		.2051		.2461	
7		.1709		.1846		.2256
8	.1495		.1538		.1692	
9		.1346		.1410		.1571
10	.1211		.1234		.1309	

6.6 Tchebyscheff Series

The Tchebyscheff expansion of f(x) on [-1,1] is given by (Snyder, 1966)

$$f(x) = \frac{1}{2} \sum_{n=o}^{\infty} \epsilon_n \, a_n \, T_n(x) \ , \tag{6.67}$$

where

$$a_n = \frac{2}{\pi} \int_{-1}^{1} \frac{f(x) \ T_n(x)}{\sqrt{1 - x^2}} \ dx \ , \tag{6.68}$$

and T_n represents the Tchebyscheff polynomial of order n. A sufficient condition for convergence of the series (6.67) is that f(x) is bounded, continuous, and square intergrable on [-1,1] (Courant, 1953). The Tchebyscheff polynomials can be defined by

$$T_o(x) = 1 \ , \tag{6.69}$$

$$T_1(x) = x \ , \tag{6.70}$$

and the recurrence relation

$$T_{n+1}(x) = 2x \ T_n(x) - T_{n-1}(x), \tag{6.71}$$

or by the "Rodrigues" formula

$$T_n(x) = \frac{(-1)^n \ 2^n n!}{(2n)!} \ (1-x^2)^{\frac{1}{2}} \ \frac{d^n}{dx^n} \left[(1-x^2)^{\frac{2n-1}{2}} \right] \ . \tag{6.72}$$

They can be alternately expressed as

$$T_n(x) = \cos(n \cos^{-1} x), \tag{6.73}$$

so that when x is replaced by cos θ

$$T_n(\cos\theta) = \cos(n\theta) \ . \tag{6.74}$$

Making this change of variable in (6.67) and (6.68) gives

$$f(\cos\theta) = \frac{1}{2} \sum_{n=o}^{\infty} \epsilon_n \, a_n \cos(n\theta) \ , \tag{6.75}$$

and

$$a_n = \frac{2}{\pi} \int_0^{\pi} f(\cos\theta) \cos(n\theta) d\theta \ . \tag{6.76}$$

These equations are recognized as those of the harmonic expansion of the output of the nonlinear device. The Tchebyscheff polynomials which form the expansion of f(x) thus correspond to the harmonics of the output signal. The harmonic coefficients b_k are given simply by

$$b_k = a_k \ . \tag{6.77}$$

Because of this unique property, the harmonic coefficients of the output can be obtained directly from the Tchebyscheff expansion. The equivalence of the Tchebyscheff and harmonic coefficients exists, however, only when the change of variable x to cos θ is made. When the expansion is to be applied to an interval other than [-1,1], an appropriate normalization is required.

6.7 Applications of the Expansion Methods

In the preceding sections, equations for the output harmonic coefficients of a sinusoidally excited, zero-memory,

nonlinear device were developed in terms of Taylor, Fourier, Legendre, and Tchebyscheff expansion coefficients of the characteristic function. Each of these expansion methods can be used when the characteristic meets the stated conditions which insure the convergence of the corresponding series.

The Taylor series method has been applied, as described in the literature review, to characteristics given both analytically and empirically. When a characteristic is given analytically, the derivative operations corresponding to Eq. (6.7) are usually simpler to perform than computation of the definite integrals required by the other methods. Many analytic functions can be well approximated over limited regions with a small number of terms of a Taylor series; and in such applications, this method can be effectively employed. Many characteristics, however, may not meet the continuity conditions stated in section 2, and direct computation of the Taylor expansion cannot be accomplished. A characteristic given in the form of a graph or a table of functional values also presents problems. Numerical differentiation procedures are susceptible to noise effects and in many instances, can be used to obtain, at most, several derivatives (Hildebrand, 1956). In applications where the Taylor series coefficients cannot be obtained directly, curve-fitting procedures such as the method of least-squares can be used to obtain polynomial approximations to characteristics. The coefficients of the fitted polynomials become approximations to the Taylor series

coefficients. A version of this method was used by Wilczyuski (1961). Least-squares methods used to obtain high order approximations, however, can, in some cases, fail to converge (Hildebrand, 1956); and their use for empirically obtained functions is questionable. These versions of the Taylor series method thus do not appear to be suitable for general analysis purposes.

The Fourier series expansion methods developed in sections 3 and 4 can be applied to characteristic functions given in either analytic or empirical form. The expansion coefficients of these methods are given by definite integrals which can be evaluated numerically. The Fourier expansions converge with minimum restrictions on the form of the characteristic function. In applications, method B has the advantages of more rapid convergence described in section 1. If, in addition, the first derivative of the characteristic is continuous, the method described by Lanczos (1956) can be used to obtain even faster convergence. Tables 6.2 and 6.3 show that each of the harmonic coefficients of the output of a nonlinear device depends on an infinite series of Fourier coefficients involving consecutive or alternate orders. In applications, however, convergence of the Fourier expansion allows these series to be truncated; and approximations to lower order harmonic coefficients can be obtained from the resulting finite series. Thus, although the computational procedures can become rather involved, the Fourier series methods can be used for general analysis purposes.

In the Legendre series method, the expansion coefficients are given by definite integrals which are similar in form to those of the Fourier methods. The integrals can be evaluated numerically, and the method can be used to analyze both analytic and empirical characteristics. As with the Fourier series, the Legendre expansions converge with minimum restrictions on the form of the characteristic function. In contrast to the Fourier methods, boundary conditions such as (6.1) do not directly affect the rate of convergence of the Legendre series; and modifications of the expansion method are unnecessary. Table 6.4 shows that each harmonic coefficient depends on the Legendre coefficients of equal and higher orders. The convergence of the Legendre expansion, however, allows truncation of the coefficient series; harmonic coefficients of lower orders can be approximated in this manner. The Legendre series method, thus, appears to be suitable for general analysis purposes.

In the Tchebyscheff method, the expansion coefficients are given by the definite integrals (6.68) and (6.70). The form (6.68) is inappropriate for numeric integration since the factor in the denominator vanishes as the endpoints of the interval [-1,1] are approached. This singularity does not appear in (6.70), however, and numerical methods can be used to evaluate the coefficients in this form. The restrictions on the characteristic function stated in section 6 are sufficiently general to allow the Tchebyscheff method to be

applied to a wide class of characteristics. Applications can be made to characteristics given both analytically and empirically, and the method can be used for general analysis purposes. Since the Tchebyscheff coefficients are, in fact, the harmonic coefficients of the output signal, the computational procedures are simplified. The summations required by the other methods are avoided and the convergence of the harmonic expansion is in direct evidence. In the following chapters, methods of application of the Tchebyscheff expansion method are developed in detail. The choice of this method was based on the straightforwardness of the computational procedure and the ease with which errors in the computations can be related to the resulting harmonic coefficients.

7. A NUMERICAL METHOD FOR COMPUTING TCHEBYSCHEFF COEFFICIENTS

7.1 Introduction

In Chapter 5 some of the advantages of using the Tchebyscheff expansion for the computation of the output harmonic coefficients of a sinusoidally excited nonlinear device were described. This chapter presents a numerical method through which the Tchebyscheff expansion can be applied to actual nonlinear characteristics. Section 7.2 describes the mathematical development of the method. In section 7.3, the method is formulated in the form of a digital computer program. The program is used to evaluate the expansion method and determine its accuracy under various conditions of use. The method is also compared with the other expansion methods described in Chapter 5.

7.2 The Numerical Method

In the study of nonlinear devices, the characteristic function (or transfer characteristic) may be given either analytically, graphically, or numerically. The method of computing Tchebyscheff expansions presented here can be used with characteristics given in any of these forms. It consists of representing the characteristic by a piecewise linear approximation and computing the Tchebyscheff coefficients of the representation. Since the only approximations introduced are those in the piecewise representation

of the characteristic, the method seems to have advantages over the direct application of numerical integration.

Figure 7.1 shows a typical nonlinear characteristic f(x) and a region where the Tchebyscheff expansion is desired. The region is given by

$$\left|x - x_o\right| \leq A. \tag{7.1}$$

Making the change of variable

$$u = \frac{x-x_o}{A} , \tag{7.2}$$

the region in u is

$$\left|u\right| \leq 1. \tag{7.3}$$

The expansion coefficients are then given by either

$$a_n(A,x_o) = \frac{2}{\pi} \int_{-1}^{1} \frac{f(au + x_o)\ T_n(u)}{\sqrt{1-u^2}}\, du , \tag{7.4}$$

or

$$a_n(A,x_o) = \frac{2}{\pi} \int_{o}^{\pi} f(A \cos\theta + x_o)\ \cos(n\theta)\ d\theta , \tag{7.5}$$

as was shown previously. These equations can be simplified by defining

$$g(u) = f(Au + x_o) , \tag{7.6}$$

in the region given by (7.3). Equations (7.4) and (7.5) then become

$$a_n(A,x_o) = \frac{2}{\pi} \int_{-1}^{1} \frac{s(u)\ T_n(u)}{\sqrt{1-u^2}}\, du , \tag{7.7}$$

and

$$a_n(A,x_o) = \frac{2}{\pi}\int_o^{\pi} g(\cos\theta)\,\cos(n\theta)\,d\theta \ . \qquad (7.8)$$

The function g(u) can be represented by a piecewise linear approximation consisting of N segments as shown in Figure 7.2. When g(u) is continuous, the error in the approximation can be made arbitrarily small by increasing the number of segments N such that the length of each becomes small. If a set of N + 1 values of u and g(u) (including the endpoints of the interval $|u| \leq 1$) are known, the equations of the corresponding segments can be computed. Denoting these values by u_i and $g(u_i)$, where $1 \leq i \leq N+1$, the Tchebyscheff expansion coefficients for the approximation to g(u) are given by

$$a_n = \frac{2}{\pi}\sum_{i=1}^{N}\int_{u_i}^{u_{i+1}} \frac{(c_i + d_i u)T_n(u)}{\sqrt{1-u^2}}\,du \ , \qquad (7.9)$$

where $(c_i + d_i u)$ represents the equation for the i^{th} segment. The constants c_i and d_i can be computed for each segment by solving the simultaneous equations

$$c_i + d_i u = g(u_i) \ , \qquad (7.10)$$

and

$$c_i + du_{i+1} = g(u_{i+1}) \ . \qquad (7.11)$$

The solution yields

$$c_i = \frac{g(u_i)\,u_{i+1} - g(u_{i+1})\,u_i}{u_{i+1} - u_i} \ , \qquad (7.12)$$

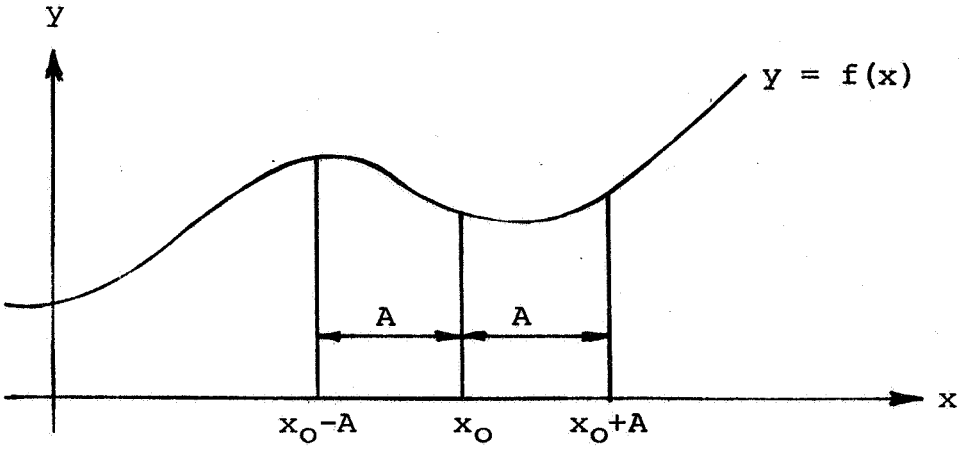

Figure 7.1 Typical characteristic and desired expansion region

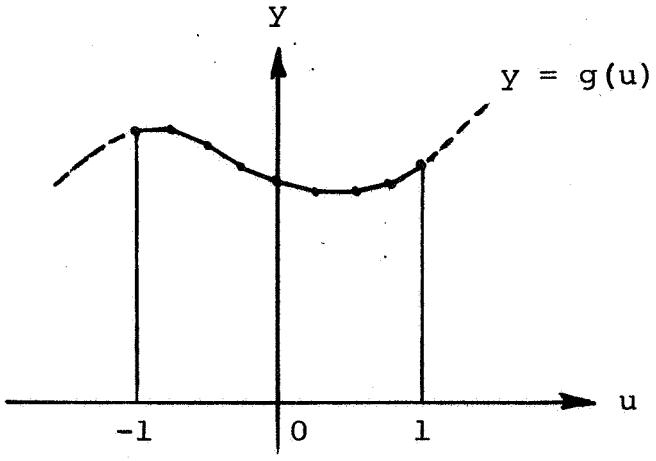

Figure 7.2 A piecewise linear approximation to the characteristic

and

$$d_i = \frac{g(u_{i+1}) - g(u_i)}{u_{i+1} - u_i} \quad . \tag{7.13}$$

Equation (7.9) can be evaluated by making the change of variable

$$u = \cos\theta \ , \tag{7.13}$$

so that it becomes

$$a_n = \frac{2}{\pi} \sum_{i=1}^{N} \int_{\cos^{-1}(u_{i+1})}^{\cos^{-1}(u_i)} (c_i + d_i \cos\theta)\cos(n\theta)\,d\theta \ . \tag{7.15}$$

Expansion of the cosine products allows this expression to be rewritten as

$$a_o = \frac{2}{\pi} \sum_{i=1}^{N} \int_{\cos^{-1}(u_{i+1})}^{\cos^{-1}(u_i)} (c_i + d_i \cos\theta)\,d\theta \ , \tag{7.16}$$

$$a_1 = \frac{2}{\pi} \sum_{i=1}^{N} \int_{\cos^{-1}(u_{i+1})}^{\cos^{-1}(u_i)} [\tfrac{1}{2}d_i + c_i \cos\theta + \tfrac{1}{2}d \cos(2\theta)]\,d\theta \ , \tag{7.17}$$

and

$$a_n = \frac{2}{\pi} \sum_{i=1}^{N} \int_{\cos^{-1}(u_{i+1})}^{\cos^{-1}(u_i)} \left\{ \tfrac{1}{2} d_i \cos[(n-1)\theta] + c_i \cos(n\theta) \right.$$

$$\left. + \tfrac{1}{2} d_i \cos[(n+1)\theta] \right\} d\theta \ , \tag{7.18}$$

for $n \geq 2$.

The integrals in these expressions can be evaluated so that

$$a_o = \frac{2}{\pi} \sum_{i=1}^{N} \left[c_i\theta + d_i \sin\theta \right]_{\cos^{-1}(u_{i+1})}^{\cos^{-1}(u_i)} , \tag{7.19}$$

$$a_1 = \frac{2}{\pi} \sum_{i=1}^{N} \left[\tfrac{1}{2} d_i\theta + c_i \sin\theta + \tfrac{1}{4} d_i \sin(2\theta) \right]_{\cos^{-1}(u_{i+1})}^{\cos^{-1}(u_i)} , \tag{7.20}$$

and

$$a_n = \frac{2}{\pi} \sum_{i=1}^{N} \left\{ \frac{d_i \sin\left[(n-1)\theta \right]}{2(n-1)} + \frac{c_i \sin(n\theta)}{n} \right.$$

$$\left. + \frac{d_i \sin\left[(n+1)\theta \right]}{2(n+1)} \right\}_{\cos^{-1}(u_{i+1})}^{\cos^{-1}(u_i)} , \tag{7.21}$$

for $n \leq 2$. The Tchebyscheff expansion of the piecewise linear approximation to $g(u)$ can thus be computed from Eqs. (7.12), (7.13), and (7.19) through (7.21). The applicability of this method to numeric data is evident. The data points simply become the u_i and $g(u_i)$. If the data are given in graphic or analytic form, the u_i and $g(u_i)$ can be respectively measured or computed.

7.3 Evaluation of the Numerical Method

7.3.1 Computer Programs

In order to evaluate the Tchebyscheff expansion method described in the previous section, several digital computer programs were written. The programs allowed determination

of the accuracy of the expansion method under various conditions of use. They also allowed comparison of the harmonic coefficients obtained by the method to those obtained by the Taylor, Fourier, and Legendre series methods presented in the previous chapter. The programs were written in FORTRAN IV language and were run on an IBM-360 series, Model 75 computer.[1/]

The program ODP-10 is reproduced in the Appendix and a flow chart is shown in Figure 7.3. The four digit numbers in the blocks of the flow chart correspond to statement numbers in the program. The statements within each block perform the operations indicated by the title of the block. The program computes approximations to the Taylor (LMS), Legendre (LEG), and Tchebyscheff (TCH) expansions of functions on the range [-1,1]. For each function that is expanded, the program input requires a data set consisting of N equally spaced argument values and the corresponding functional values. The argument values are normalized to the range [-1,1]. Approximations to the Taylor series coefficients are obtained by fitting polynomials to the data set by the method of least squares. The Legendre coefficients are obtained by approximating the integrals

$$\int_{-1}^{1} f(x)\ P_n(x)\ dx\ , \tag{7.22}$$

[1/] Triangle Universities Computation Center, Research Triangle Park, Research Triangle, North Carolina.

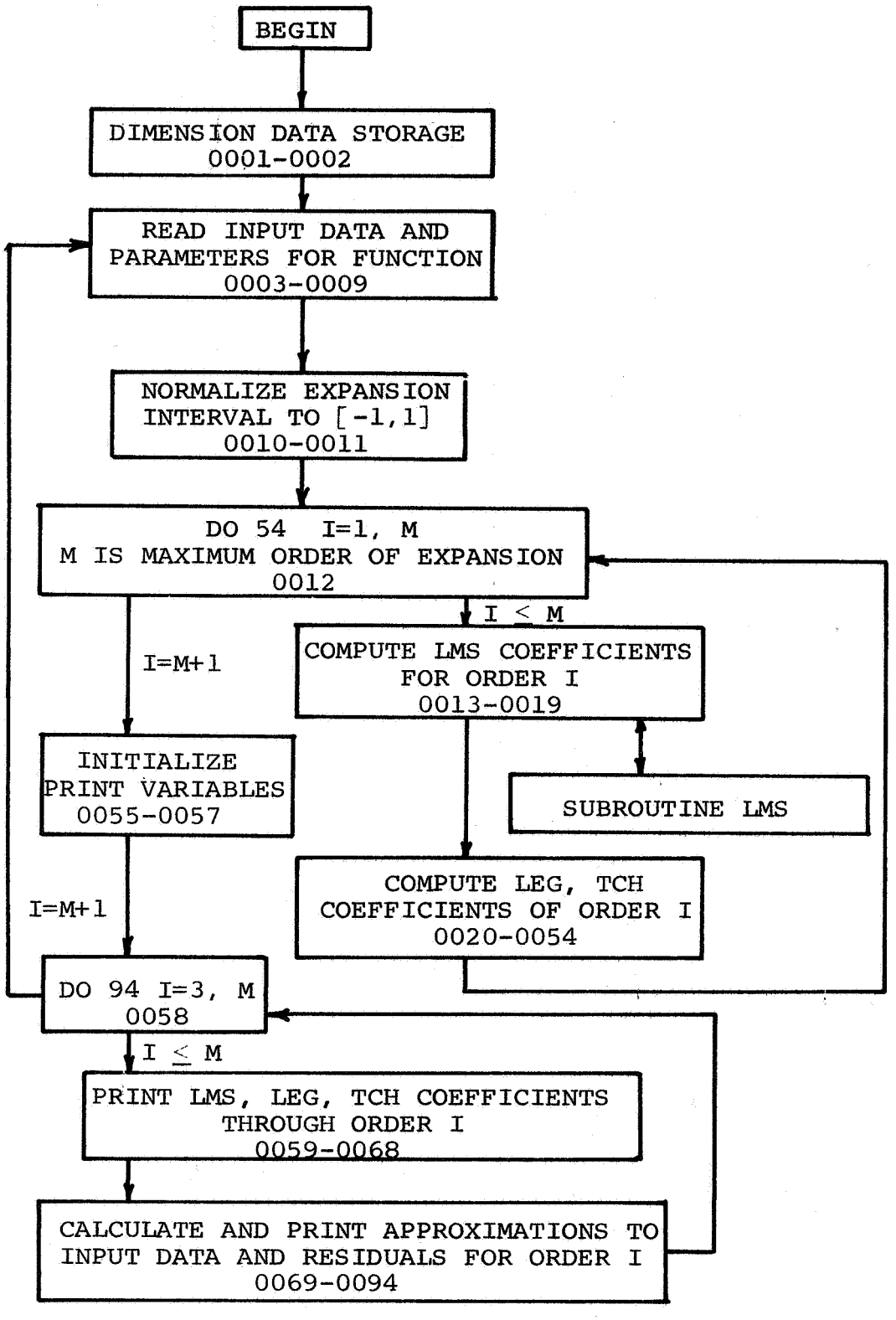

Figure 7.3 Flow chart for program ODP-10

(see section 6.5 and Eq. (6.52)) by the sums

$$\frac{1}{(N-1)} \sum_{i=1}^{N-1} f(x_i)\ P_n(x_i)\ , \qquad (7.23)$$

where $f(x)$ is the function being expanded, P_n is the n^{th} order Legendre function, and the x_i correspond to the N values of the arguments of the input data set. Approximations to the Tchebyscheff coefficients are obtained by the expansion method described in the previous section.

Two programs (ODP-13, ODP-14) were written to compute expansions corresponding to the Fourier series methods A and B described in the previous chapter. The programs utilize the IBM Scientific Subroutine Package subroutine FORIT which computes Fourier expansions of tabulated functions. The programs consist of a direct application of the subroutine and are, therefore, not included in the Appendix.

7.3.2 Expansions of Analytic Functions

When the Tchebyscheff expansion method described in section two is applied to an actual nonlinear characteristic, errors in the piecewise linear approximation produce errors in the computed Tchebyscheff coefficients. The magnitude of the errors depends both on the form of the function being expanded and the number of segments in the piecewise linear approximation. In order to determine the magnitude of the errors obtained under various conditions of use of the expansion method, several functions having known Tchebyscheff coefficients

were expanded. The program ODP-10 was used to compute the expansions.

The first function considered was

$$f(x) = \frac{(1-x)}{2} . \tag{7.24}$$

Expansions were computed on the range [-1,1]. Since the function is linear, the only nonvanishing Tchebyscheff coefficients are those of zero and first order. Because of the linearity, piecewise linear approximations to the function become exact. A data set consisting of 101 equidistant points was generated for the function and subsequently used as an input to the program ODP-10. The results of the expansion are shown in Table 7.1. Errors in the coefficients can be attributed to approximations, truncation, and roundoff within the program. The maximum absolute error in any of the coefficients is 10^{-5}. Since the program is written with single precision statements, seven significant figures are retained in the computations. Errors of the order of 10^{-5} may thus arise from the repetitive calculations involved in the computation of the coefficients.

The second function considered was

$$f(x) = e^{k(x-1)}, \tag{7.25}$$

where k is a constant. Its Tchebyscheff expansion on [-1,1] is given by (Snyder, 1966)

$$e^{k(x-1)} = 2e^{-k} \sum_{n=0}^{\infty} \epsilon_n I_n(k) T_n(x), \tag{7.26}$$

Table 7.1 Tchebyscheff coefficients for $\frac{(1-x)}{2}$ on [-1,1]

Order	Analytic Coefficient	ODP-10 (101 Points)	Error
0	1.0	1.0000	10^{-4}
1	-0.5	-.5000	10^{-4}
2	0.0	$-.1793 \times 10^{-5}$	10^{-5}
3	0.0	$.9323 \times 10^{-7}$	10^{-7}
4	0.0	$-.3027 \times 10^{-6}$	10^{-6}
5	0.0	$.7653 \times 10^{-6}$	10^{-6}
6	0.0	$-.8514 \times 10^{-6}$	10^{-6}
7	0.0	$.1039 \times 10^{-5}$	10^{-5}
8	0.0	$-.8324 \times 10^{-6}$	10^{-6}
9	0.0	$.7138 \times 10^{-6}$	10^{-6}

where I_n is the n^{th} order modified Bessel function of the first type and ϵ_n is the Neumann symbol (see Eqs. (6.5) and (6.6)). The function of Eq. (7.25) can be used to test the Tchebyscheff expansion method under a variety of conditions since the rate of convergence of the expansion of Eq. (7.26) depends on the value of the constant k. For smaller values the expansion is more quickly convergent. Expansions of the function were computed for k values of one, two, and five. Figure 7.4 shows the form of the function with these values. Results of using the program ODP-10 with input data sets consisting of 101 equidistant points are shown in Tables 7.2, 7.3, and 7.4.

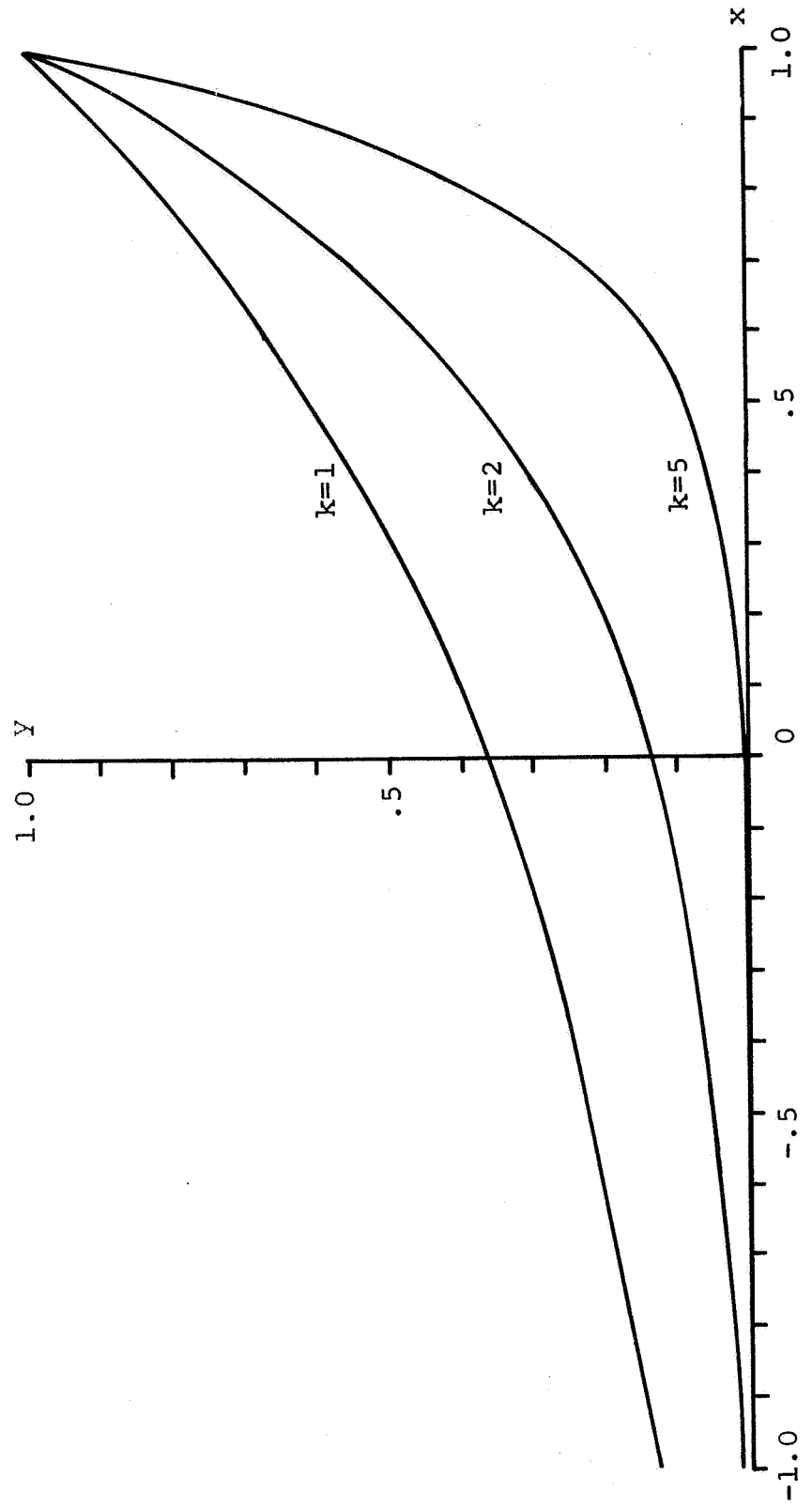

Figure 7.4 The function $e^{k(x-1)}$ with several values of k

Table 7.2 Tchebyscheff coefficients for $e^{(x-1)}$ on [-1,1]

Order	Analytic coefficient	ODP-10 (101 Points)	Error
0	.9315	.9315	10^{-4}
1	.4158	.4158	10^{-4}
2	$.9984 \times 10^{-1}$	$.9988 \times 10^{-1}$	4×10^{-5}
3	$.1630 \times 10^{-1}$	$.1631 \times 10^{-1}$	10^{-5}
4	$.2014 \times 10^{-2}$	$.2013 \times 10^{-2}$	10^{-6}
5	$.1997 \times 10^{-3}$	$.1990 \times 10^{-3}$	10^{-6}
6	$.1655 \times 10^{-4}$	$.1472 \times 10^{-4}$	2×10^{-6}
7	$.1176 \times 10^{-5}$	$.4553 \times 10^{-6}$	10^{-6}
8	$.7329 \times 10^{-7}$	$-.1442 \times 10^{-5}$	2×10^{-6}
9	$.4059 \times 10^{-8}$	$-.6830 \times 10^{-6}$	10^{-6}

Table 7.3 Tchebyscheff coefficients for $e^{2(x-1)}$ on [-1,1]

Order	Analytic coefficient	ODP-10 (101 Points)	Error
0	.6168	.6171	3×10^{-4}
1	.4304	.4306	2×10^{-4}
2	.1864	.1865	10^{-4}
3	$.5757 \times 10^{-1}$	$.5759 \times 10^{-1}$	2×10^{-5}
4	$.1373 \times 10^{-1}$	$.1373 \times 10^{-1}$	10^{-5}
5	$.2659 \times 10^{-2}$	$.2656 \times 10^{-2}$	3×10^{-6}
6	$.4331 \times 10^{-3}$	$.4292 \times 10^{-3}$	4×10^{-6}
7	$.6079 \times 10^{-4}$	$.5692 \times 10^{-4}$	4×10^{-6}
8	$.7498 \times 10^{-5}$	$.3301 \times 10^{-5}$	4×10^{-6}
9	$.8239 \times 10^{-6}$	$-.3225 \times 10^{-5}$	4×10^{-6}

Table 7.4 Tchebyscheff coefficients for $e^{5(x-1)}$ on [-1,1]

Order	Analytic coefficient	ODP-10 (101 Points)	Error
0	.3669	.3674	5×10^{-4}
1	.3278	.3282	4×10^{-4}
2	.2359	.2361	3×10^{-4}
3	.1392	.1393	10^{-4}
4	$.6883 \times 10^{-1}$	$.6887 \times 10^{-1}$	5×10^{-5}
5	$.2908 \times 10^{-1}$	$.2908 \times 10^{-1}$	10^{-5}
6	$.1068 \times 10^{-1}$	$.1066 \times 10^{-1}$	2×10^{-5}
7	$.3457 \times 10^{-2}$	$.3435 \times 10^{-2}$	3×10^{-5}
8	$.9988 \times 10^{-3}$	$.9752 \times 10^{-3}$	3×10^{-5}
9	$.2602 \times 10^{-3}$	$.2358 \times 10^{-3}$	3×10^{-5}

The analytic coefficient values shown were obtained by using Eq. (7.26) and tables of modified Bessel functions (Oliver, 1965). The results show that as the analytic expansion becomes more slowly convergent, additional errors occur in the approximations to the lower order coefficients. This can be seen by comparing the errors shown in the first several rows of the three tables. The results also show that the program is unable to evaluate coefficients of the order of 10^{-5} and less. This can be expected because of the limitations on the computational accuracy mentioned before.

In order to observe the errors introduced by the piecewise linear approximation, expansions of the exponential functions were computed from data sets containing various numbers of points. Results of using sets containing 11, 21, 41, and 81 equidistant points for the exponential with k=5 are shown in Table 7.5 Similar results were obtained for the other values of k. The results show the increased errors as the number of points diminishes. It can be seen, however, that approximations accurate to within three percent are obtained for the coefficients of orders zero through five with as few as 21 points.

Table 7.5 Tchebyscheff coefficients for $e^{5(x-1)}$ resulting from ODP-10 with various data sets

Order	Analytic coefficient	Points in data set			
		81	41	21	11
0	.3669	.3675	.3688	.3734	.3896
1	.3278	.3283	.3294	.3334	.3470
2	.2359	.2362	.2369	.2394	.2469
3	.1392	.1394	.1397	.1407	.1418
4	.0688	.0688	.0689	.0687	.0652
5	.0290	.0290	.0299	.0281	.0221
6	.0106	.0106	.0104	.0093	.0023
7	.0034	.0034	.0032	.0019	-.0049
8	.0009	.0009	.0007	-.0006	-.0006
9	.0002	.0002	-.0000	-.0013	-.0062

The results presented here indicate that the numerical expansion method formulated in the program ODP-10 is capable of providing good approximations to Tchebyscheff coefficients having magnitudes of 10^{-4} through unity. The results also indicate that even for functions such as $e^{5(x-1)}$ which have slowly convergent expansions, good approximations to the coefficients through fifth order can be obtained with as few as 21 equidistant data points.

7.3.3 Comparison with the Other Expansion Methods

The programs ODP-10, ODP-13, and ODP-14 were used to compute the Taylor, Fourier, Legendre, and Tchebyscheff expansions of several nonlinear characteristics. The expansion coefficients obtained were used in the expressions (derived in Chapter 6) for the output harmonic coefficients of a sinusoidally excited nonlinear device. By truncating the expansions at various orders, the approximations to the harmonic coefficients given by the Taylor, Fourier, and Legendre expansion methods could be compared to those given by the Tchebyscheff method described in section 2. Expansions of a number of functions were computed. The results presented here are typical of those obtained.

Figures 7.5 through 7.8 show results of the expansion of the function $e^{5(x-1)}$ with a data set consisting of 101 equidistant points on the range $[-1,1]$. Approximations to the harmonic coefficients of orders one (b_1) through four (b_4)

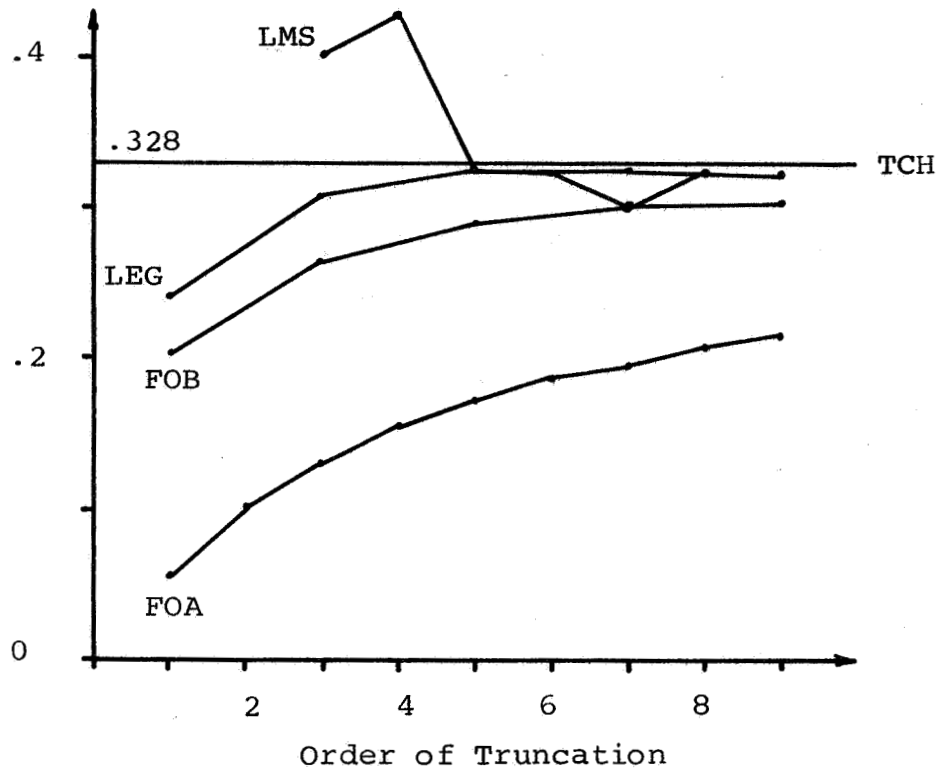

Figure 7.5 Approximations to the Harmonic Coefficient b_1

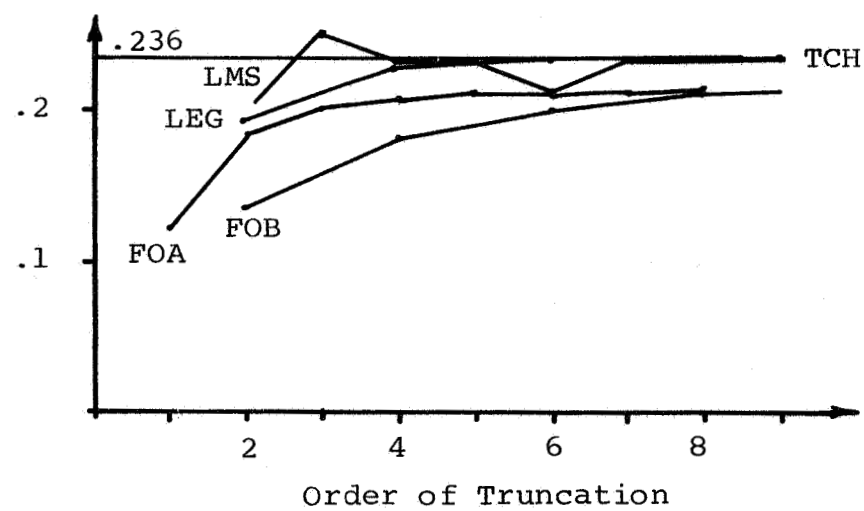

Figure 7.6 Approximations to the Harmonic Coefficient b_2

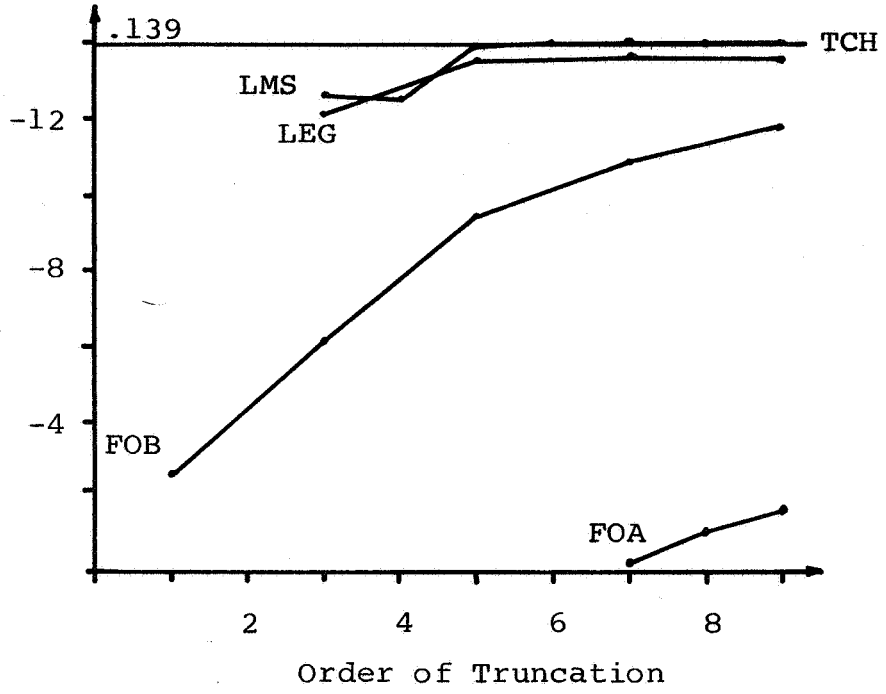

Figure 7.7 Approximations to the Harmonic Coefficient b_3

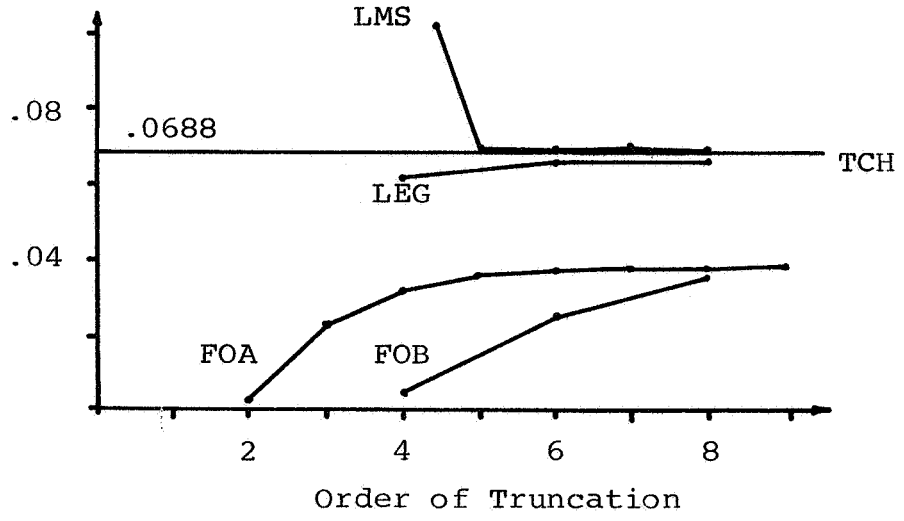

Figure 7.8 Approximations to the Harmonic Coefficient b_4

are shown. The various expansions were truncated at orders three through nine. The approximations to the coefficients given by the Taylor (LMS), Fourier A (FOA), Fourier B (FOB), and Legendre (LEG) methods show convergence to the values given by the Tchebyscheff (TCH) coefficients. The Fourier series methods showed relatively slow convergence as can be seen in the figures. The somewhat erratic behavior of the LMS method can be seen in Figure 7.5.

The results demonstrate advantages of using the Tchebyscheff expansion method. The approximation to a given harmonic coefficient is obtained directly from the TCH coefficient of corresponding order. For a given order, higher orders of the Tchebyscheff expansion are necessary.

8. APPLICATIONS OF THE TCHEBYSCHEFF EXPANSION METHOD

8.1 A Fortran Program for the Analysis of Zero-Memory Nonlinear Characteristics

In order to apply the Tchebyscheff expansion method to the analysis of nonlinear characteristics, a computer program was written. The program (ODP-11) utilizes the numerical method presented in the previous chapter to compute Tchebyscheff expansions of subregions of a given nonlinear characteristic. The program also computes the equivalent noise-to-signal ratios of the subregions. Various subregions of a characteristic can thus be compared with respect to the signal distortions that they introduce and regions giving minimum distortion can be found. The program is reproduced in the Appendix and a flow chart is shown in Figure 8.1.

For each subregion the program output contains the Tchebyscheff expansion coefficients, the corresponding noise-to-signal ratio, an estimate of the accuracy of the noise-to-signal ratio, and identification data. The estimate of the accuracy of the noise-to-signal ratio is obtained by use of an error parameter. The parameter is part of the required program input for each characteristic. It corresponds to the accuracy to which of the functional values of the input data set are known. In the execution of the program, expansion coefficients less than this value are set equal to zero. The noise-to-signal ratios are computed as

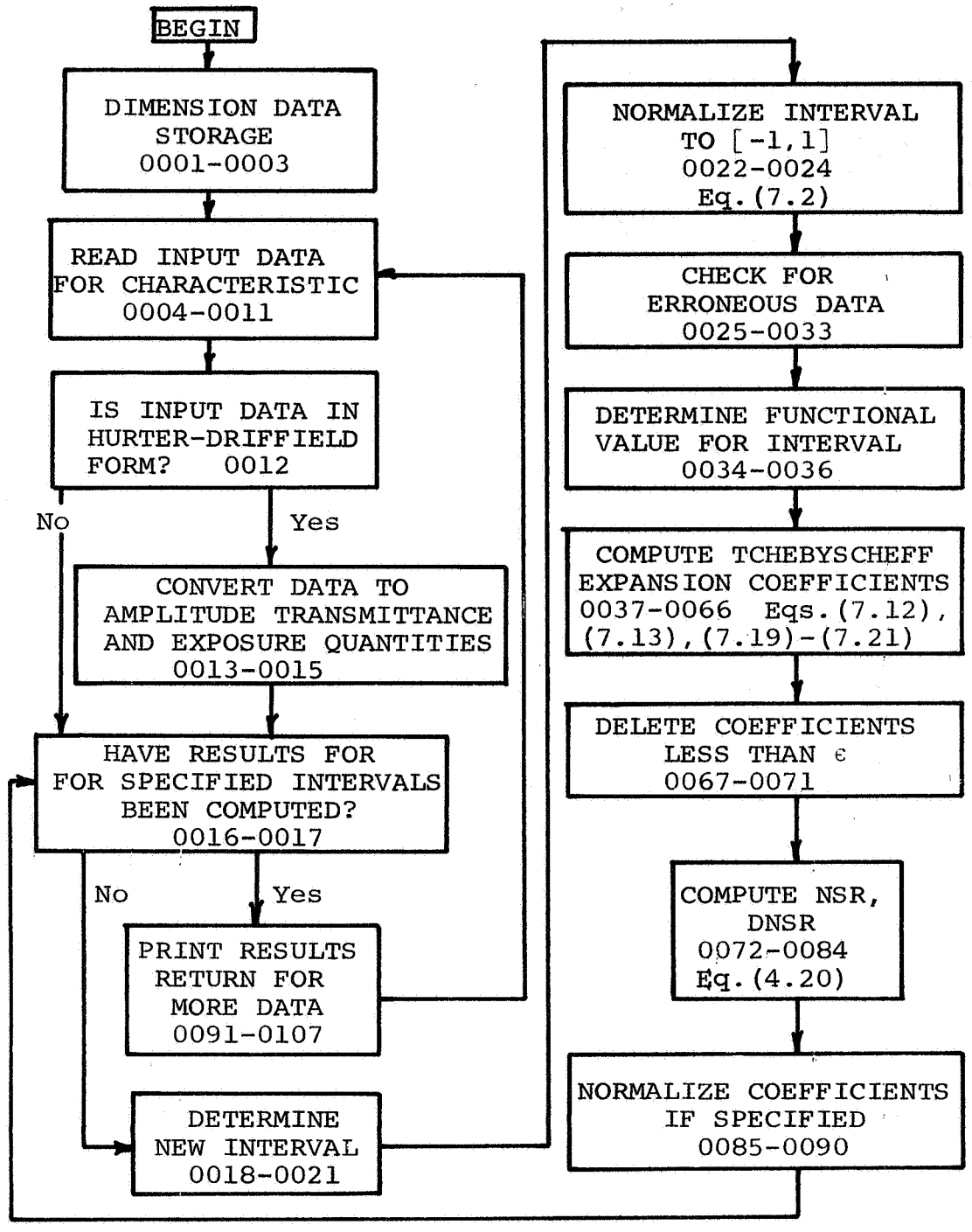

Figure 8.1 Flow chart for the program ODP-11

$$NSR = \frac{\sum_{n=2}^{M} b_n^2}{b_1^2} \tag{8.1}$$

where b_n represents the Tchebyscheff (harmonic coefficients and M represents the highest expansion order computed. The estimates of the accuracy of the noise-to-signal ratios are computed as

$$DNSR = \frac{\varepsilon^2}{b_1^2} \tag{8.2}$$

where ε represents the error parameter. This estimate, thus, corresponds to the change in the noise-to-signal ratio if a small random fluctuation having a root-mean-squared value of ε is added to the function that is being expanded.

For each characteristic, the subregions are determined by a list of amplitude parameters and a spacing parameter. These are part of the required program input and correspond numerically to numbers of points of the input data set. Thus, an amplitude parameter of ten corresponds to a region spanned by ten points of the input data set. If the data points are equally spaced, a specific amplitude parameter implies a fixed subregion length. For each amplitude parameter listed, the program varies the location of the subregion by increments corresponding to the spacing parameter. The process is begun at the beginning of the input data set and is continued until the region reaches the end of the set. This procedure is repeated for each listed amplitude parameter.

8.2 Analysis of the Characteristic Curves of Type 649-F Spectroscopic Plates

The fortran program ODP-11 was used to analyze the characteristic curves of Kodak, type 649-F spectroscopic plates. The analysis serves as an example of the use of the program outlined in the preceding section. The results reveal optimum exposure and development conditions for the use of the plates.

The curves were obtained in Hurter-Driffield form from a publication of the Eastman Kodak Company (Kodak, 1967). They represent 10 second exposure to tungsten illumination and development in Kodak developer D-19 at 68^{o}F. Each curve is identified by its corresponding development time. The curves were enlarged photographically to approximately 4" x 8" size. An accurate set of data was taken from each curve and the corresponding amplitude transmittance vs. exposure data was obtained using a simple fortran program. This data was then accurately plotted on graph paper. The resulting curves are shown in Figure 8.2. Final data for use in the program was taken from these curves. This procedure allowed the final data to be in equal interval form. Thus, a set number of consecutive data points corresponds to a specific region length.

In order to determine the accuracy of the data taking, three independent observations of 96 points on the 2 minute characteristic were made. A short fortran program was

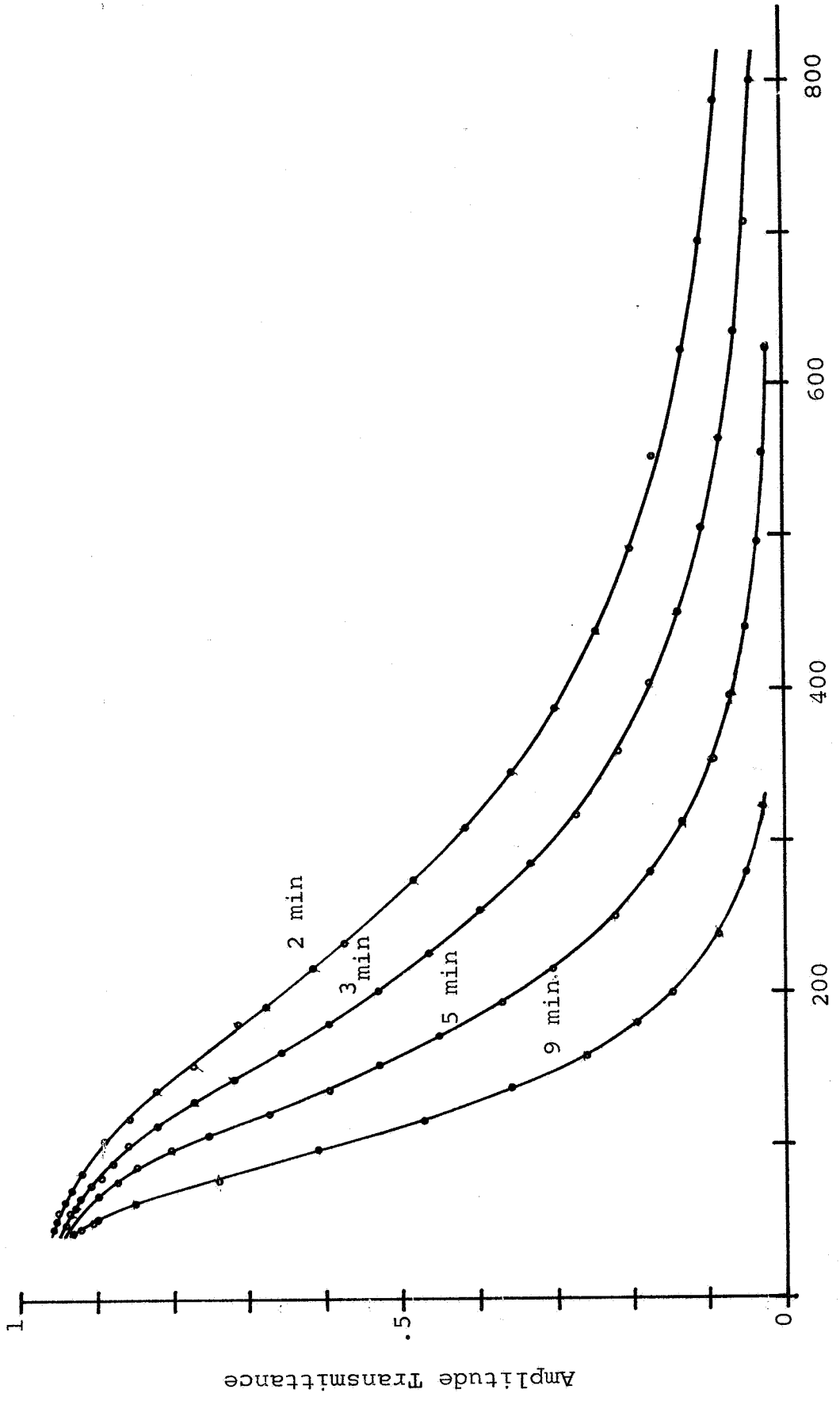

Figure 8.2 Characteristic curves for type 649-F spectroscopic plates

written to estimate the standard deviation of the observations. The resulting estimate was .0033. This estimate was subsequently used as the error parameter in the program.

The final data set for each of the 649-F characteristic curves consisted of approximately 90 points. The amplitude parameters used were 11, 21, 31, etc. and the step parameter was 5. Results from the program are shown in Figures 8.3 through 8.10. In the figures the input exposure is assumed to be of the form

$$E(x) = E_o + A \cos(w_x x), \tag{8.3}$$

where E_o is the bias level and A is the amplitude of the sinusoid, and w_x represents its spatial radian frequency. Figures 8.3 through 8.6 show the output fundamental (undistorted signal) amplitude as a function of bias level and input sinusoid amplitude A. Figures 8.7 through 8.10 show the output NSR as a function of bias level and input amplitude.

Results of the analysis of the characteristic curves of type 649-F spectroscopic plates show that the effects of the nonlinearities can be minimized for a given characteristic by choosing bias levels appropriate to the amplitude. In most cases, the optimum bias corresponds to the maximization of the output fundamental amplitude. Figure 8.11 shows the NSR's (at optimum bias) of the four characteristics as a function of this amplitude. It can be seen that under

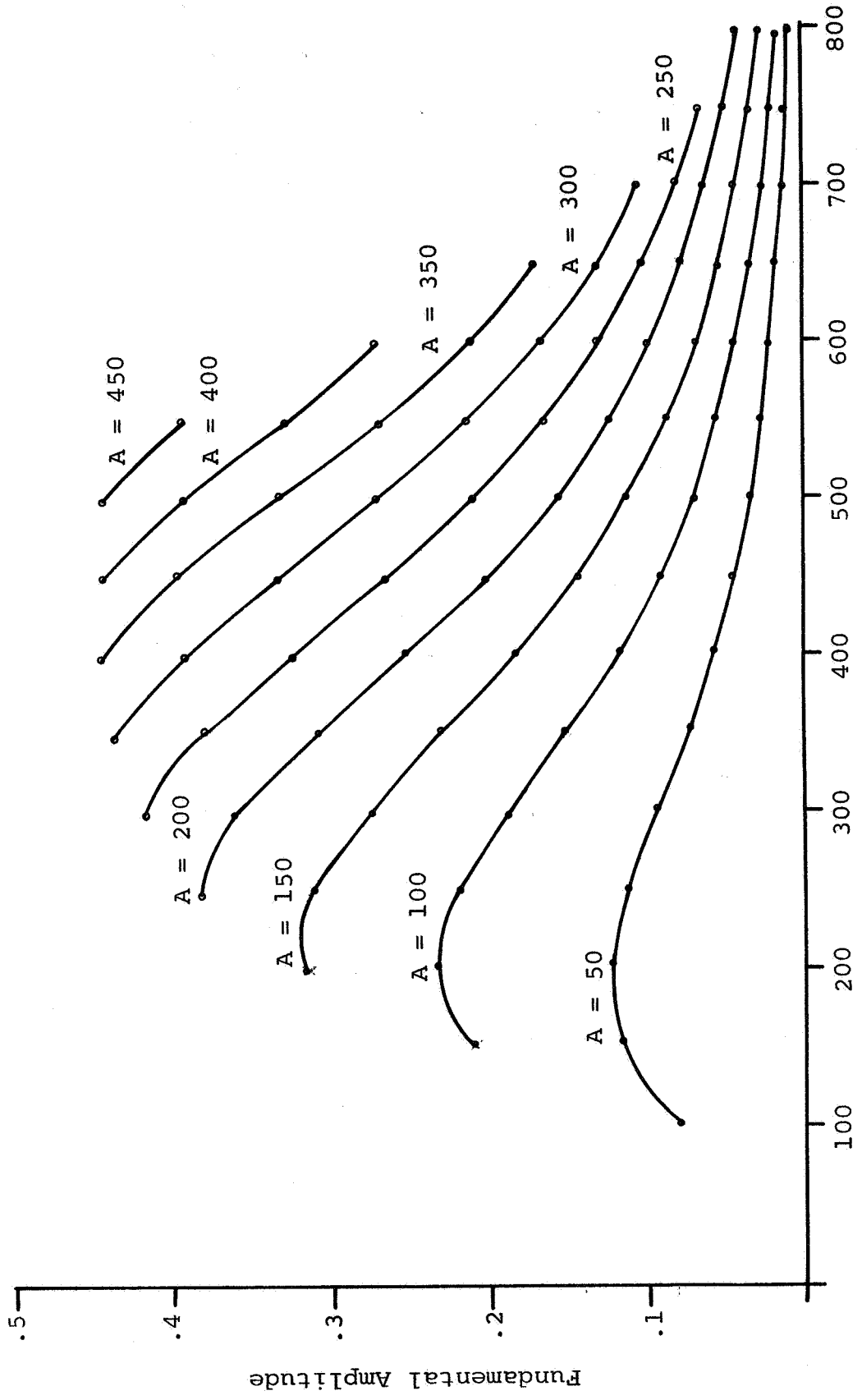

Figure 8.3 Output fundamental amplitudes for the 2 minute characteristic

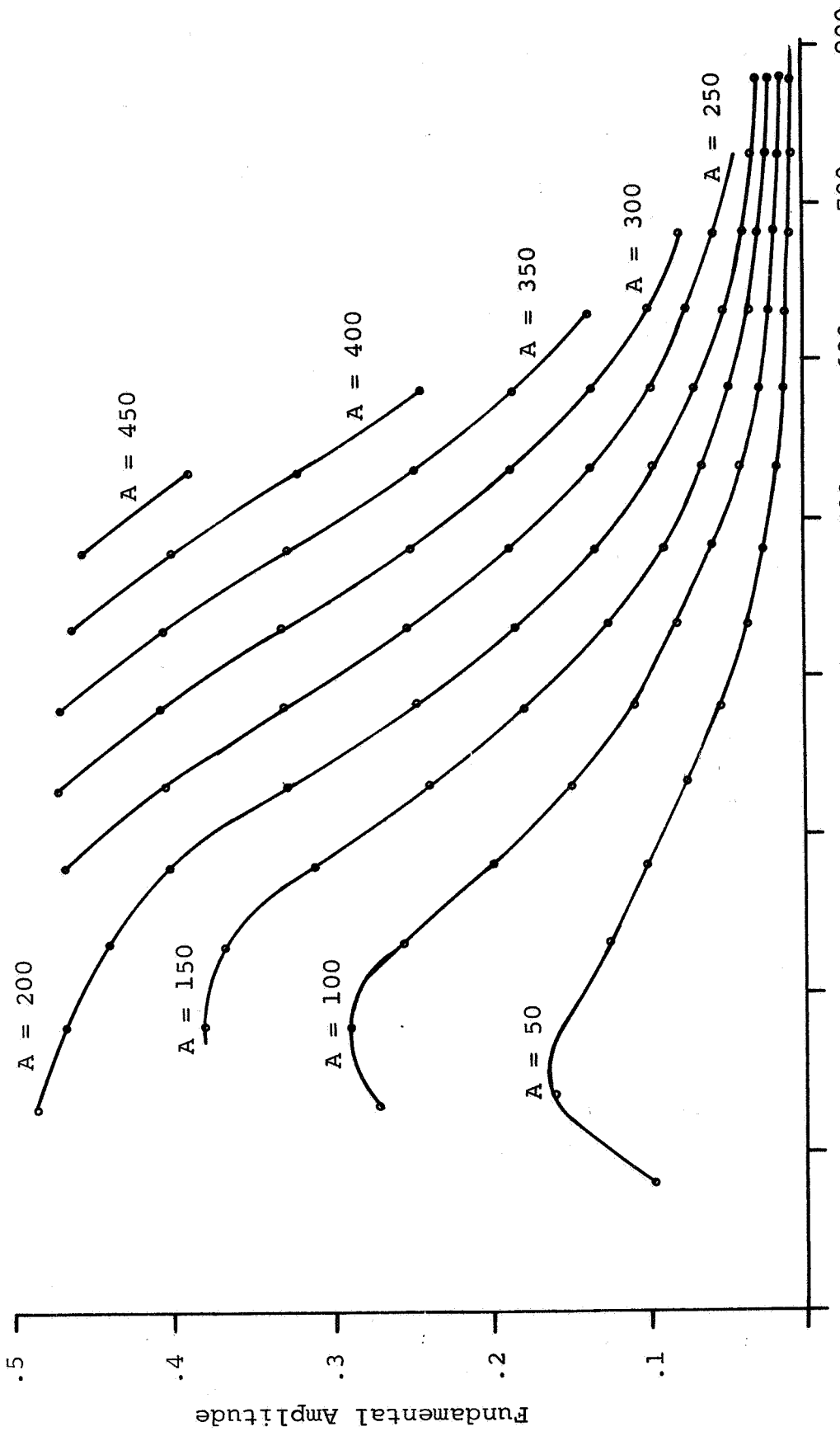

Figure 8.4 Output fundamental amplitudes for the 3 minute characteristic

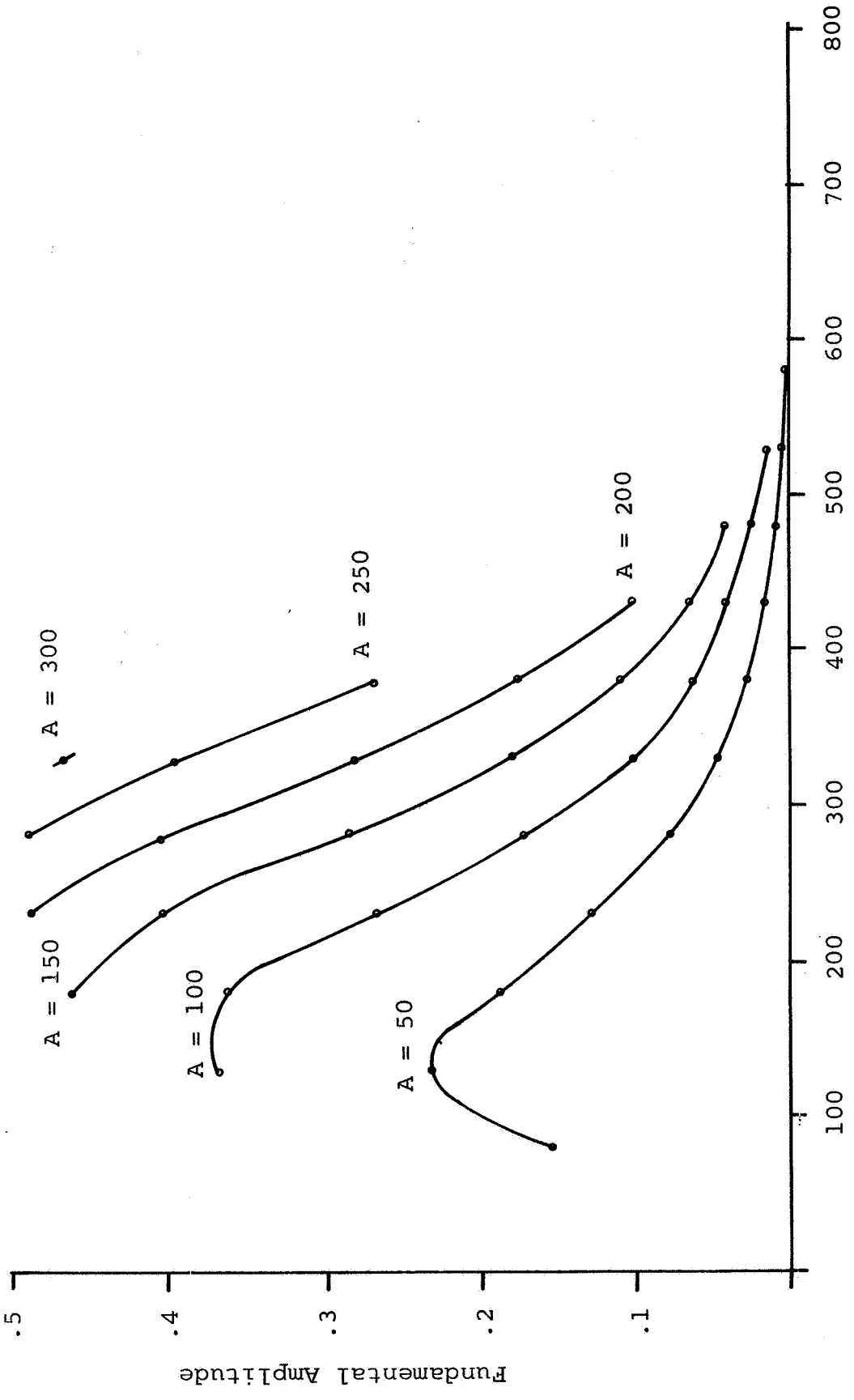

Figure 8.5 Output fundamental amplitudes for the 5 minute characteristic

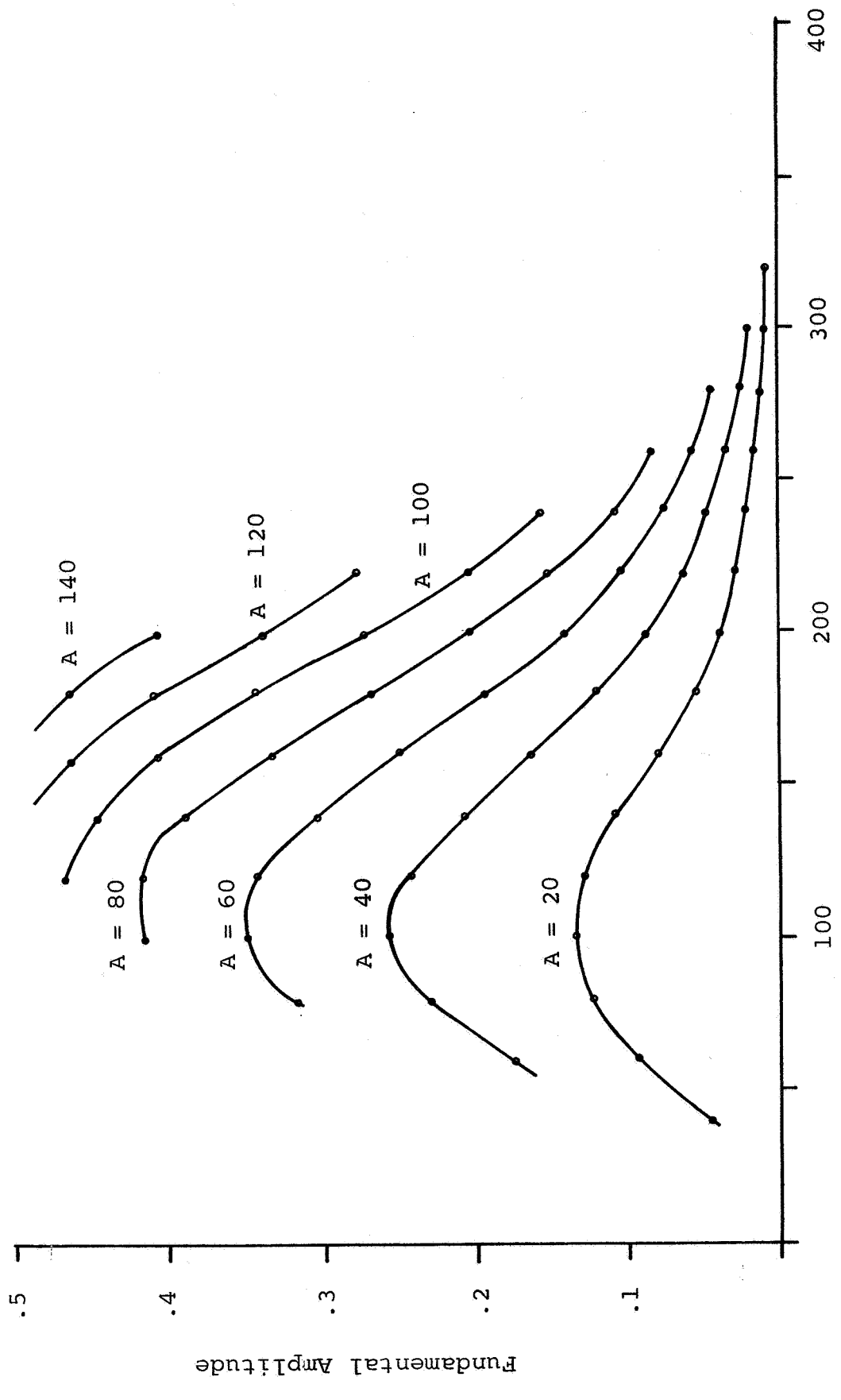

Figure 8.6 Output fundamental amplitudes for the 9 minute characteristic

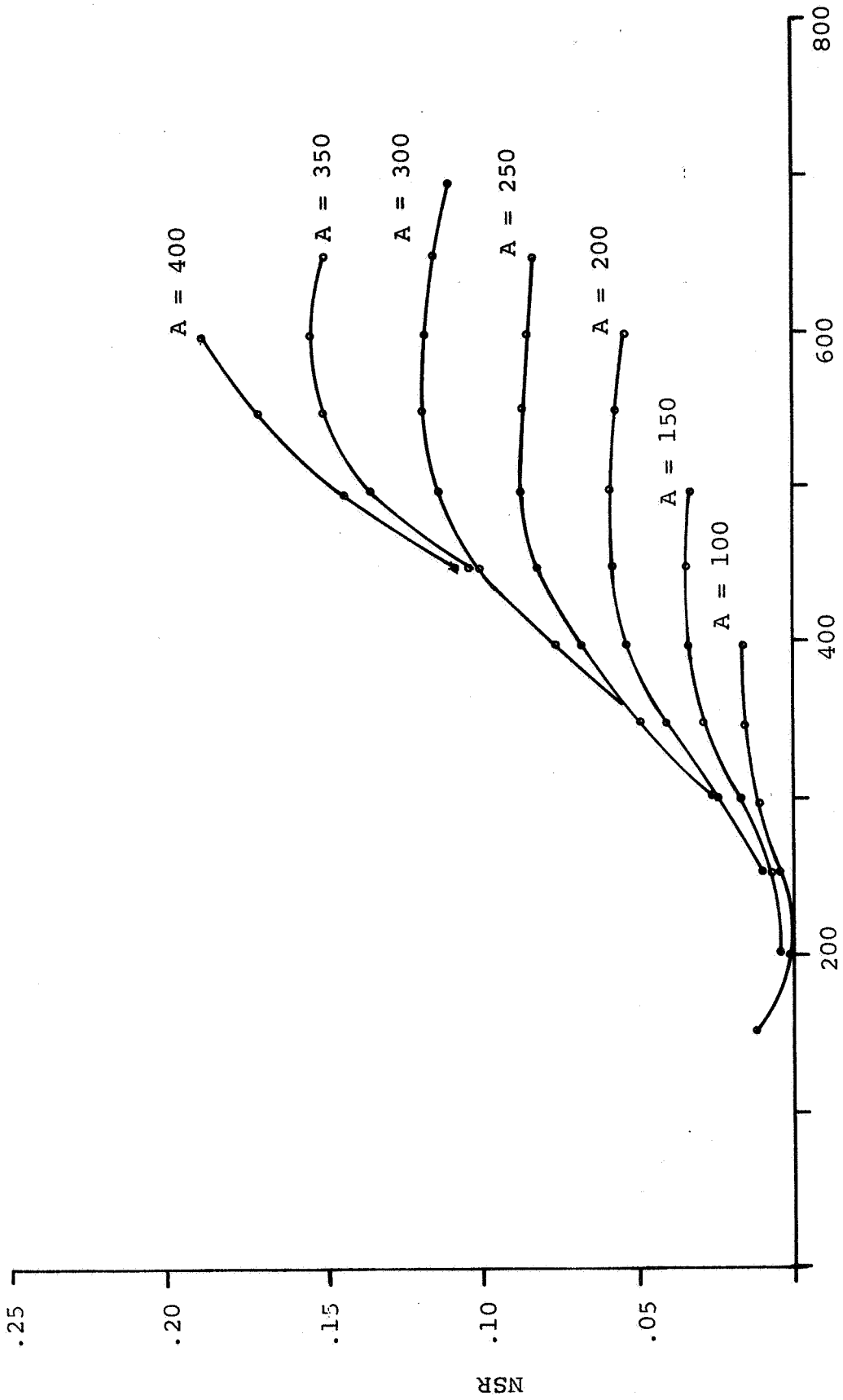

Figure 8.7 Noise-to-signal ratios for the 2 minute characteristic

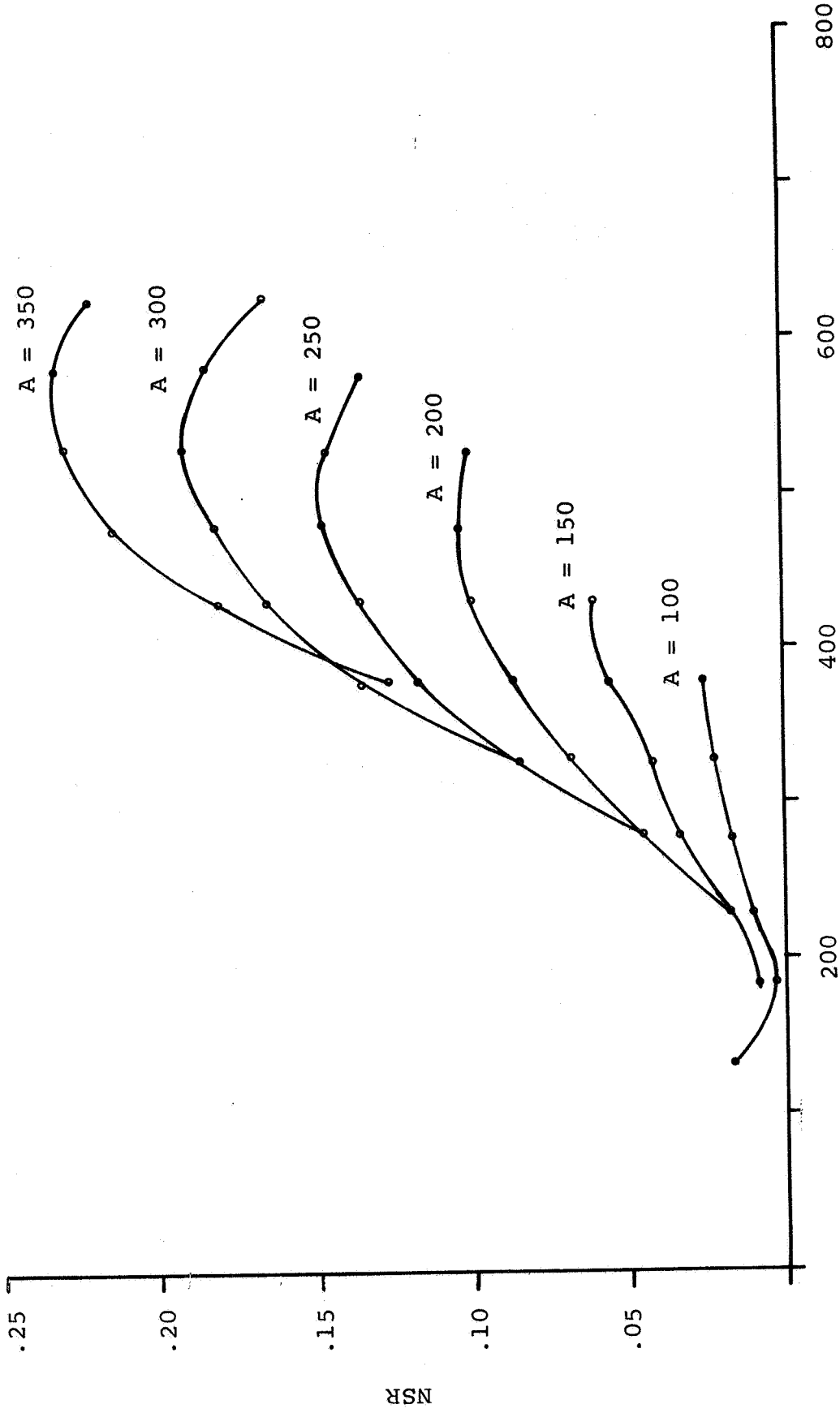

Figure 8.8 Noise-to-signal ratios for the 3 minute characteristic

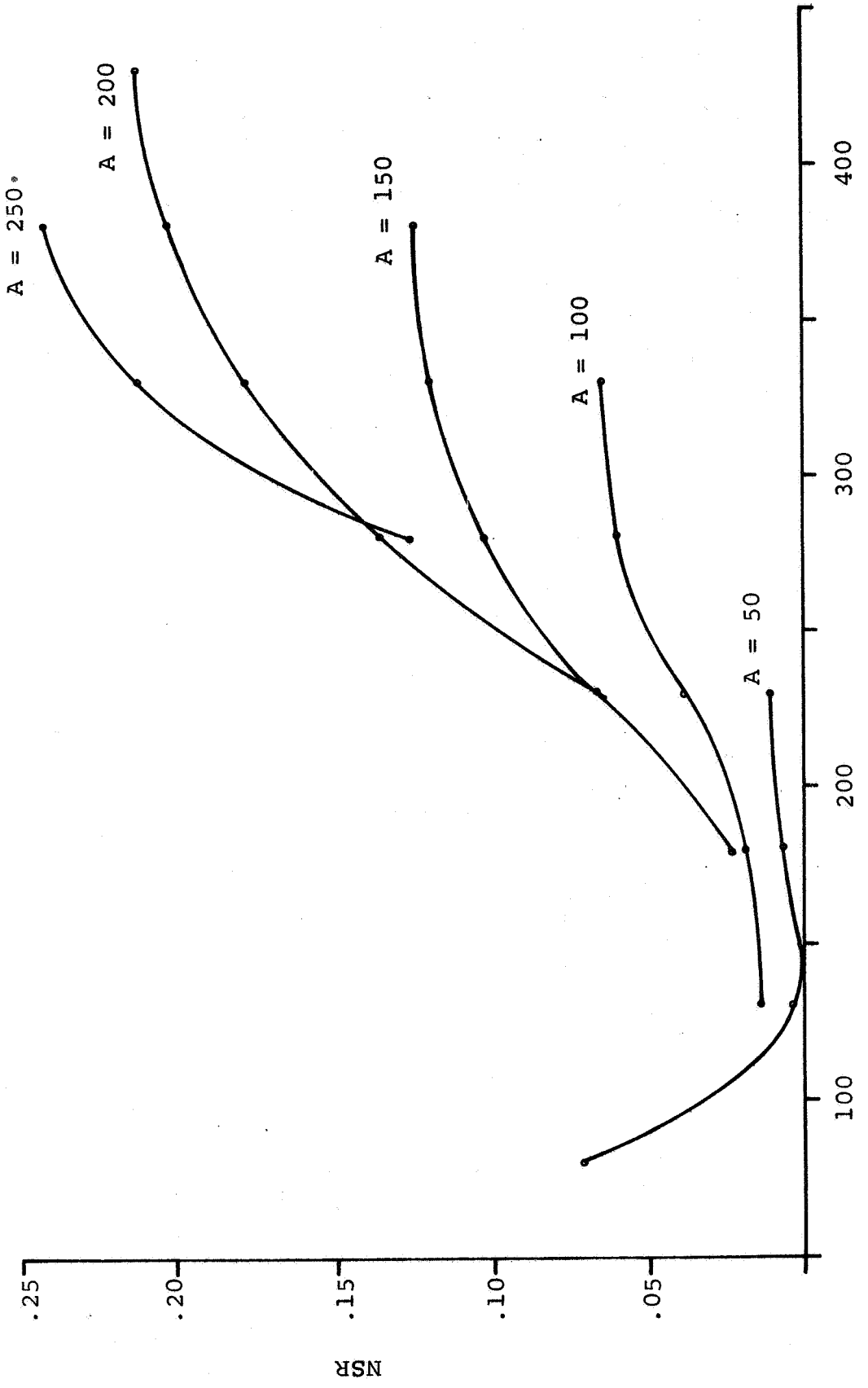

Figure 8.9 Noise-to-signal ratios for the 5 minute characteristic

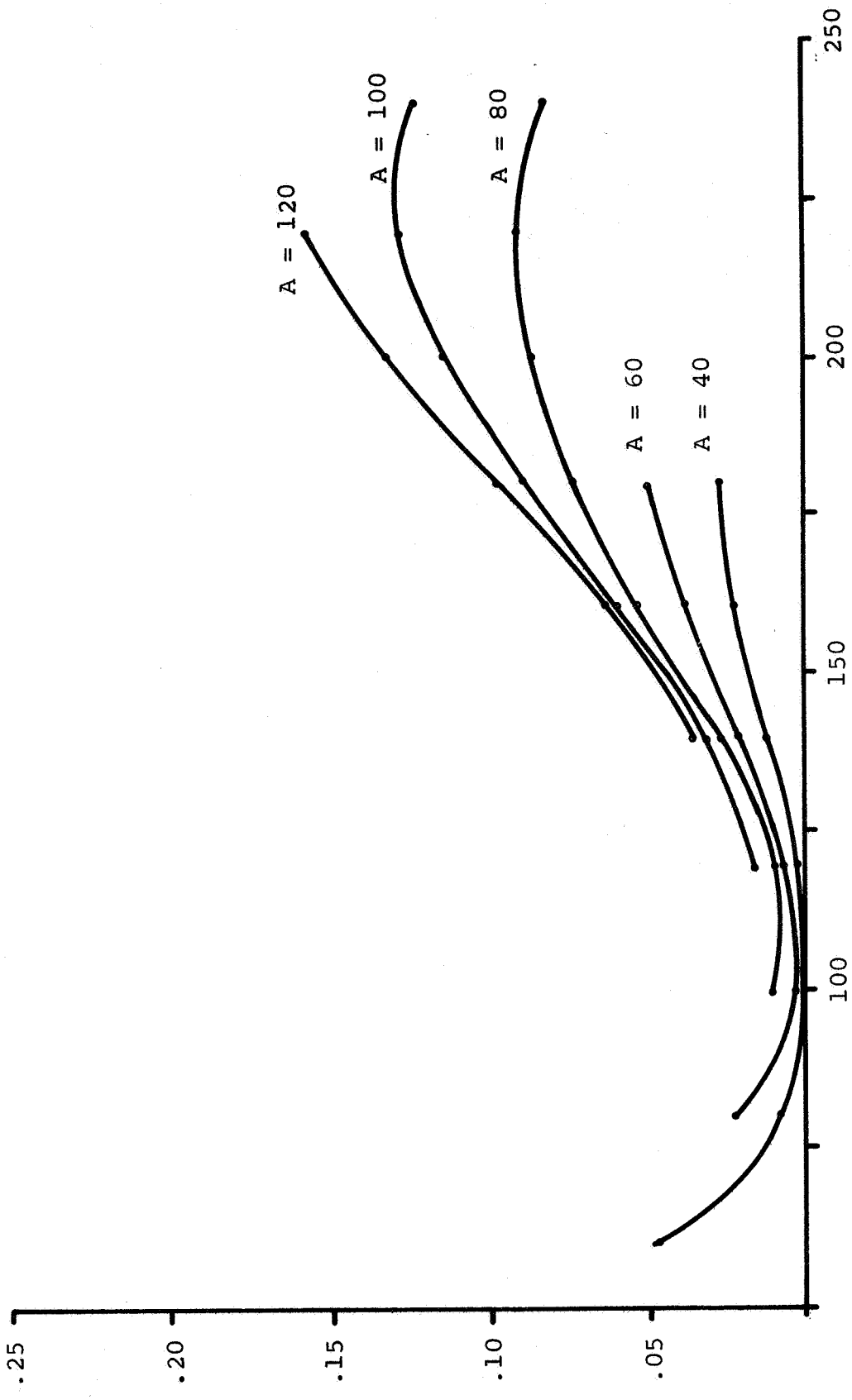

Figure 8.10 Noise-to-signal ratios for the 9 minute characteristic

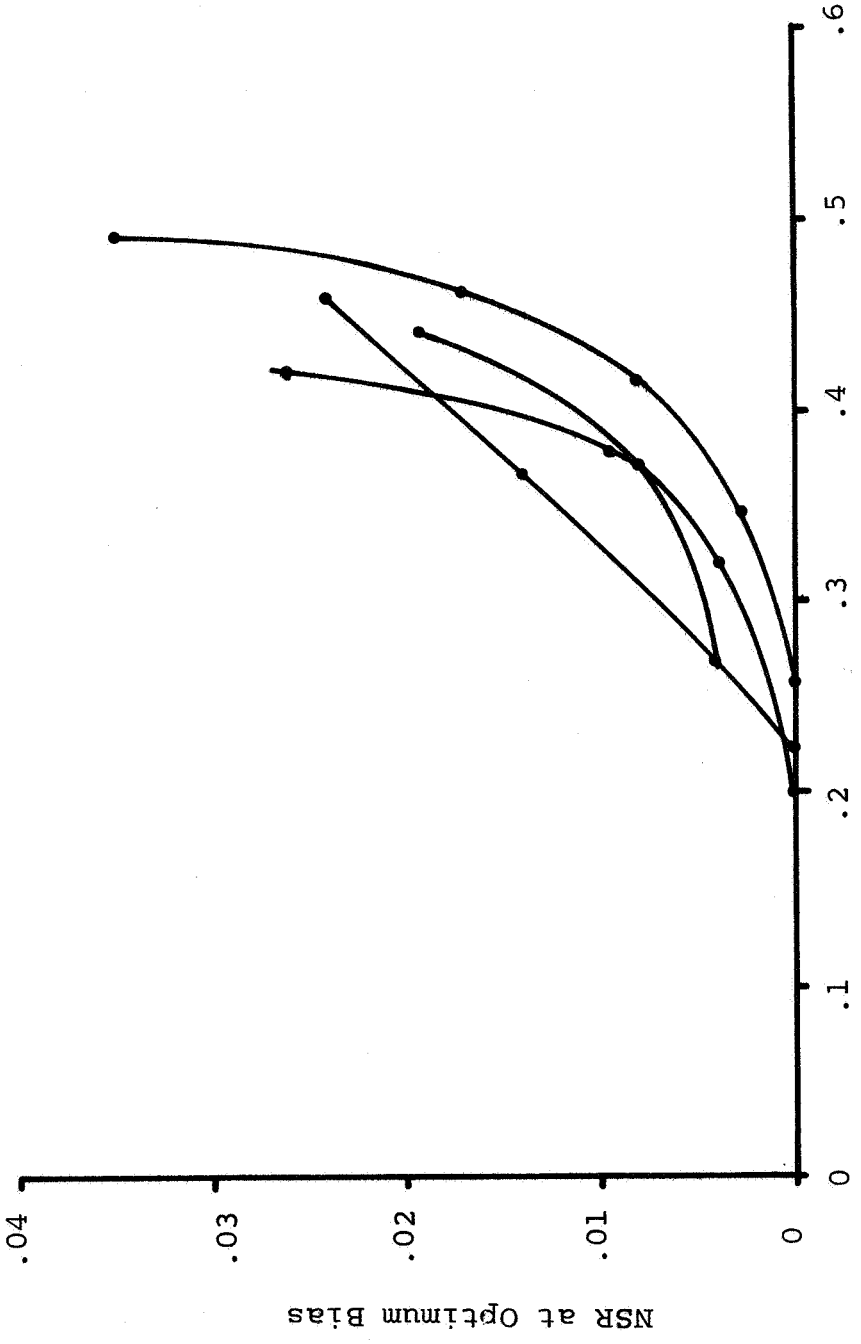

Figure 8.11 Optimum noise-to-signal ratios for the 649-F characertistic curves

optimum bias conditions the 9 minute characteristic exhibits minimum nonlinear effects. The output fundamental amplitude .4 represents a threshold value. For output amplitudes less than this, all of the characteristics give NSR's less than .02 with optimum bias. For output amplitudes greater than this, the NSR's increase rapidly.

9. CONCLUSION

9.1 Summary

Two sources of signal distortions in optical data processors employing coherent light were investigated. Small Deviations of the geometry of signal carrier surfaces within such processors were shown to create signal distortions corresponding to attenuation, frequency shifts, and, and phase errors in electronic systems. Geometric deviations of actual signal carrier surfaces were represented by specific geometric models. These models allowed quantitative relations to be derived between the signal distortions and the parameters describing the geometry.

A method of analyzing the severity of signal distortions caused by zero-memory nonlinearities was developed. An equivalent noise-to-signal ratio was introduced for the description of the severity of nonlinear effects. Existing methods of computing sinusoidal signal distortions were compared with the Tchebyscheff methods. The Tchebyscheff method together with the noise-to-signal ratio description of nonlinear effects was formulated as a computer program. The program was used to analyze the nonlinear characteristics of type 649-F spectroscopic plates.

9.2 Findings

The results of the study of deviations of signal carrier surface geometry show that the primary signal distortions

introduced by small deviations are phase shifts. The attenuation and frequency shift distortions appear as second order effects. The equations relating the phase distortions to the parameters describing the various geometric deviations show that significant phase distortions exist, even for small deviations, if fairly high spatial frequencies occur in the signals being processed. The phase distortions increase as the square of the spatial frequency of the signals.

The comparison of quantities describing the severity of signal distortions caused by zero-memory nonlinearities shows the advantages of using the noise-to-signal ratio. If additional noise sources exist within an optical processor, the noise-to-signal ratios combine additively. The comparison of the expansion methods for determining the output harmonic coefficients of a sinusoidally excited nonlinear device demonstrates the advantages of the Tchebyscheff method. The harmonic coefficients are, in fact, the Tchebyscheff expansion coefficients of the characteristic representing the nonlinearity and thus their computation is simplified. The numerical method of obtaining Tchebyscheff coefficients described in Chapter 7 was found to give accurate approximations to coefficients of analytic functions.

The analysis of the characteristic curves of type 649-F spectroscopic plates reveals optimum exposure conditions for the minimization of nonlinear signal distortions. Recorded signals which modulate the amplitude transmittance by as much

as .8 can be obtained with equivalent noise-to-signal ratios as low as .01. When exposed properly, the plates are capable of yielding minimal nonlinear distortions.

The method of analyzing zero-memory nonlinearities developed herein can be used to determine the severity of nonlinear distortions both in optical data processing systems and other applications where such nonlinearities are encountered. The method can be used effectively in applications requiring either approximate or precise results.

10. LIST OF REFERENCES

Apostol, T. M. 1957. Mathematical Analysis. Addison-Wesley Publishing Company, Inc., Reading Massachusetts.

Born, M. and E. Wolf. 1965. Principles of Optics. Third Edition. Pergamon Press, London.

Chirlian, P. M. 1965. Analysis and Design of Electronic Circuits. McGraw-Hill Book Company, Inc., New York.

Cutrona, L. J. 1964. Optical Computing Techniques. IEEE Spectrum 1(10):101-108.

Cutrona, L. J., E. N. Leith, C. J. Palermo, and L. J. Porcello. 1960. Optical Data Processing and Filtering Systems. I.R.E. Trans. Inf. Theory IT-6:386-400.

Davenport, W. B., Jr., and W. L. Root. 1958. Introduction to Random Signals and Noise. McGraw-Hill Book Company, Inc., New York.

Eastman Kodak Company. 1967. Kodak Plates and Films for Science and Industry (Kodak Data Book P-9). Eastman Kodak Company, Rochester, New York.

Espley, D. C. 1933. The Calculation of Harmonic Production in Thermionic Valves with Resistive Loads. Proc. Inst. Radio Engrs. 21:1439-1446.

Friesem, A. A., and J. S. Zelenka. 1967. Effects of Film Nonlinearities in Holography. Appl. Opt. 6:1755-1759.

Hildebrand, F. B. 1956. Introduction to Numerical Analysis. McGraw-Hill Book Company, Inc., New York.

Jackson, D. 1941. Fourier Series and Orthogonal Polynomials. The Mathematical Association of America, Menasha, Wisconsin.

Kelly, D. H. 1960. Systems Analysis of the Photographic Process. I. A Three-State Model. J. opt. Soc. Am. 50: 269-276.

Kozma, A. 1966. Photographic Recording of Spatially Modulated Coherent Light. J. opt. Soc. Am. 56:428-432.

Lamberts, R. L. 1961. Sine-Wave Response Techniques in Photographic Printing. J. opt. Soc. Am. 51:982-987.

LIST OF REFERENCES (continued)

Lanczos, C. 1956. Applied Analysis. Prentice Hall, Inc., Englewood Cliffs, New Jersey.

Lanczos, C. 1966. Discourse on Fourier Series. Hafner Publishing Company, New York.

Little, R. E. 1966. The Suppression of Harmonic Distortion in Photographic Images. Optica Acta 13:31-40.

Mangulis, V. 1965. Handbook of Series for Scientists and Engineers. Academic Press, New York.

Middleton, D. 1960. An Introduction to Statistical Communication Theory. McGraw-Hill Book Company, Inc., New York.

Oliver, F. W. J. 1965. Bessel Functions of Integer Order, pp. 355-433. In M. Abramowitz and I. A. Stegun (ed.), Handbook of Mathematical Functions. Dover Publications, Inc., New York.

Preston, K., Jr. 1965. Computing at the Speed of Light. Electronics 38(18):72-83.

Rhodes, J. E., Jr. 1953. Analysis and Synthesis of Optical Images. Am. J. Phy. 21:337-343.

Rochelle, R. W. 1963. Pulse-Frequency-Modulation Telemetry, Unpublished PhD thesis, Department of Electrical Engineering, University of Maryland. University Microfilm, Ann Arbor, Michigan.

Ryder, J. D. 1964. Electronic Fundamentals and Applications. Third Edition. Prentice-Hall Inc., Englewood Cliffs, New Jersey.

Sansone, G. 1959. Orthogonal Functions. Interscience Publishers, Inc., New York.

Schwartz, M. 1959. Information Transmission, Modulation, and Noise. McGraw-Hill Book Company, Inc., New York.

Snyder, M. A. 1966. Chebyshev Methods in Numerical Approximation. Prentice-Hall Inc., Englewood Cliffs, New Jersey.

Tischer, F. J. 1965. Basic Theory of Space Communications. D. Van Nostrand Co., Inc., Princeton, New Jersey.

LIST OF REFERENCES (continued)

Vander Lugt, A. 1967. The Effects of Small Displacements of Spatial Filters. Appl. Opt. 6:1221-1225.

Wilczynski, J. S. 1961. Some Properties of Photographic Image Recording. Proc. phy. Soc. (London) 77:17-35.

11. APPENDIX

11.1 The Fortran Program ODP-10

```
      C       ODP10  LMS,LEGENDRE,TCHEBYSCHEFF EXPANSIONS
      C
0001          DIMENSION X(120),Y(120),XN(120),AP(15,15),
             *AL(15),AT(15),F2(120)
0002          DIMENSION F3(120),PLMS(15),A(15,15),B(15)
      C
      C       X=EXPOSURE (INTENSITY)
      C       Y=AMPLITUDE TRANSMITTANCE
      C       XN=NORMALIZED X (-1,1)
      C       AP(I,J) = LMS COEFFICIENT J FOR ORDER I-1
      C       AL(I) = LEGENDRE COEFFICIENT FOR ORDER I-1
      C       AT (I) = TCHEBYSCHEFF COEFFICIENT FOR ORDER I-1
      C       PR = FLIM IDENTIFICATION
      C       N = NUMBER OF POINTS
      C       NORD=HIGHEST ORDER COMPUTED
      C
      C       READ DATA
      C
0003          DO 400 NA1=1,100
0004          READ(1,20)PR,PR1,PR2,N,NORD
0005       20 FORMAT(2A4,A2,2I5)
0006          M=NORD+1
0007          DO 1 I=1,N
0008        1 READ(1,21) X(I),Y(I)
0009       21 FORMAT (2F10.4)
      C
      C       NORMALIZE X
      C
0010          DO 2 I=1,N
0011        2 XN(I)=(2.*X(I)-X(N)-X(1)/(X(N)-X(1))
      C
      C       COMPUTE EXPANSIONS
      C
0012          DO 3 I=1,M
0013          IF(I-3) 6,4,4
0014        4 CALL LMS (XN,Y,I,N,PLMS,ILMS)
0015          DO 10 J=1,I
0016       10 AP(I,J)=PLMS(J)
0017          IF(ILMS)7,6,7
0018        7 WRITE(3,22) I,ILMS
0019       22 FORMAT(' ','ORD+1=',I2,' ERROR(LMS)=',I2)
0020        6 N1=N-1
0021          AL(I)=0.
0022          AT(I)=0.
0023          I1=I-1
0024          DO 60 J=1,N1
```

```
0025          DEL=XN(J+1)-XN(J)
0026          X1=(XN(J)+XN(J+1))/2.
0027          CALL LEGEN (X1,I1,PLI,ILEG)
0028          IF (ILEG) 8,9,8
0029        8 WRITE(3,23) I,J,ILEG
0030       23 FORMAT(' ','ORD+1=',' PT NUM=',14,' ERROR(LEG)=
          *',I2)
0031        9 AL(I)=AL(I)+(Y(J)+Y(J+1))*PLI*DEL
0032          IF (XN(J)) 301,100,101
0033      301 ARG1=ATAN(SQRT(1.-XN(J)*XN(J))/XN(J))+3.141593
0034          GO TO 104
0035      100 ARG1=1.570796
0036          GO TO 104
0037      101 ARG1=ATAN(SQRT(1.-XN(J)*XN(J))/XN(J))
0038      104 IF(XN(J+1)) 303,102,103
0039      303 ARG2=ATAN(SQRT(1.-XN(J+1)*XN(J+1))/XN(J+1))+
          *3.141593
0040          GO TO 105
0041      102 ARG2=1.570796
0042          GO TO 105
0043      103 ARG2=ATAN(SQRT(1.-XN(J+1)*XN(J+1))/XN(J+1))
0044      105 CONTINUE
0045          AO=(Y(J)*XN(J+1)-Y(J+1)*XN(J))/(XN(J+1)-XN(J))
0046          AL=(Y(J+1)-Y(J))/(XN(J+1)-XN(J))
0047          IF (I-2) 107,108,109
0048      107 AT(I)=AT(I)+(AO*(ARG1-ARG2)+A1*(SIN(ARG1)-SIN
          *(ARG2)))
0049          GO TO 60
0050      108 AT(I)=AT(I)+(.5*A1*(ARG1-ARG2)+A0*(SIN(ARG1)-
          *SIN(ARG2))+.25*A1*(SIN(2.*ARG1)-SIN(2.*ARG2)))
0051          GO TO 60
0052      109 AT(I)=AT(I)+(.5*A1*(SIN((I1-1)*ARG1)-SIN((I1-1)*
          *ARG2))/(I1-1)+AO*(SIN(I1*ARG1)-SIN(I1*ARG2))/I1+
          *.5*A1*(SIN((I1+1)*ARG1)-SIN((I1+1)*ARG2))/(I1+1))
0053       60 CONTINUE
0054          AL(I)=AL(I)*(.5*I1+.25)
0055        3 AT(I)=AT(I)/1.570796
      C
      C       PRINT COEFFICIENTS
      C
0056          DO 14 K=1,N
0057          F2(K)=AL(1)+AL(2)*XN(K)
0058       14 F3(K)=AT(1)/2.+AT(2)*XN(K)
      C
0059          DO 99 I=3,M
0060          I1=I-1
0061          WRITE(3,24)PR,PR1,PR2,I1
0062       24 FORMAT('1',2A4,A2,' ORDER=',I2//)
0063          WRITE(3,25) (AP(I,J),J=1,I)
0064       25 FORMAT(' ','LMS ',10(E11.4,1X))
0065          WRITE(3,26) (AL(J),J=1,I)
```

```
0066       26 FORMAT(' ','LEG ',10(E11.4,1X))
0067          WRITE(3,27) (AT(J),J=1,I)
0068       27 FORMAT('1','TCH ',10(E11.4,1X)//)
       C
       C       PRINT APPROXIMATIONS
       C
0069          WRITE(3,29)
0070       29 FORMAT(' ',4X,'X',9X,'XN',8X,'Y',8X,'LMS',7X'
          *LEG',7X'TCH')
       C
0071          SLMS=0.
0072          SLEG=0.
0073          STCH=0.
0074          DO 13 K=1,N
0075          F1=AP(I,1)
0076          DO 16 L=2,I
0077       16 F1=F1+AP(I,L)*XN(K)**(L-1)
0078       15 CALL LEGEN (XN(K),I1,FLEG,ILEG)
0079          F2(K)=F2(K)+AL(I)*FLEG
0080          IF (XN(K)) 200,202,201
0081      200 F3(K)=F3(K)+AT(I)*COS(I1*(ATAN(SQRT(1.-XN(K)*
             *XN(K))/XN(K))+3.141593))
0082          GO TO 203
0083      202 F3(K)=F3(K)+AT(I)*COS(I1*1.570796)
0084          GO TO 203
0085      201 F3(K)=F3(K)+AT(I)*COS(I1*ATAN(SQRT(1.-XN(K)*
             *XN(K))/XN(K)))
0086      203 R1=Y(K)-F1
0087          R2=Y(K)-F2(K)
0088          R3=Y(K)-F3(K)
0089          SLMS+SLMS+ABS(R1)
0090          SLEG=SLEG+ABS(R2)
0091          STCH=STCH+ABS(R3)
0092       13 WRITE(3,28) X(K),Y(K),F1,F2(K),F3(K),R1,R2,R3
0093       28 FORMAT(' ',9(F8.4,2X))
0094       99 WRITE(3,30) SLMS,SLEG,STCH
0095       30 FORMAT(' ','SUM OF RESIDUALS',3(E11.4,5X))
0096      400 CONTINUE
0097          STOP
0098          END
```

```
0001          SUBROUTINE LMS (X,Y,M,N,PCLMS,ILMS)
       C
       C       X=ARGUMENT
       C       Y=FUNCTION FITTED
       C       M=ORDER+1
       C       N=NUMBER OF POINTS
```

```
      C       PCLMS=RESULTING COEFFICIENTS
      C       IER=0=NO ERROR
      C       IER=1=SOLUN IN SIMQ WAS SINGULAR
      C       A=DUMMY
      C       B=DUMMY
      C
0002          DIMENSION A(15,15),B(15),X(200),Y(200),PCLMS(15)
             *,AA(225)
      C
      C       INITIALIZE
      C
0003          DO 2 I=1,15
0004          DO 2 J=1,15
0005          A(I,J)=0.
0006        2 B(J)=0.
      C
      C       COMPUTE MATRIX
      C
0007          DO 4 I=1,M
0008          DO 4 J=1,M
0009          DO 4 K=1,N
0010          IF (I+J-2) 12,1,12
0011        1 A(I,J)=A(I,J)+1.
0012          GO TO 4
0013       12 A(I,J)=A(I,J)+X(K)**(I+J-2)
0014        4 CONTINUE
      C
      C       COMPUTE VECTOR
      C
0015          DO 3 I=1,M
0016          DO 3 K=1,N
0017          IF (I-1) 6,5,6
0018        5 B(I)=B(I)+Y(K)
0019          GO TO 3
0020        6 B(I)=B(I)+Y(K)*X(K)**(I-1)
0021        3 CONTINUE
      C
      C       SOLVE
      C
0022          CALL ARRAY(2,M,M,15,15,AA,A)
0023          CALL SIMQ (AA,B,M,IER)
0024          DO 8 I=1,M
0025        8 PCLMS (I)=B(I)
0026          ILMS=IER
0027          RETURN
0028          END
```

11.2 The Fortran Program ODP-11

```
      C     ODP11:  NONLINEAR CHARACTERISTIC ANALYSIS
      C             PROGRAM
      C
0001        DIMENSION NP(15),NORD(15),X(105),YIN(105),
           *XN(105),AT(15,105,10)
0002        DIMENSION Y(105),XO(15,105),LSAVE(105)
           *FER(15,105),SNR(15,105)
0003        DIMENSION ERPS(15,105)
      C
      C     READ INPUT DATA
      C
0004    500 READ(1,20) PR,PR1,PR2,NTYPE,N,NAMP,NSTEP,NORM
           *,ERR
0005     20 FORMAT(2A4,A2,5I5,F10.4)
0006        READ(1,21) (NP(I),I=1,NAMP)
0007        READ(1,21) (NORD(I),I=1,NAMP)
0008     21 FORMAT(20I5)
      C
      C     PR= IDENTIFICATION SYMBOLS
      C     NTYPE=0=INPUT DATA IS FUNCTION TO BE EXPANDED
      C     NTYPE=1=INPUT DATA IS IN HURTER-DRIFFIELD FORM
      C     N=NUMBER OF DATA POINTS
      C     NAMP=NUMBER OF AMPLITUDES
      C     NSTEP=NUMBER OF INTERVALS IN STEP
      C     NORM=0=COEFFICIENTS ARE PRINTED
      C     NORM=1=HIGHER ORDER COEFFICIENTS ARE NORMALIZED
      C     TO FIRST ORDER
      C     ERR=NOISE LEVEL OF DATA (SET=0 IF NOT USED)
      C     NP(I)= NUMBER OF POINTS IN ITH AMPLITUDE
      C     NORD(I)= HIGHEST ORDER TO BE FITTED TO ITH
      C     AMPLITUDE
      C
0009        DO 1 I=1,N
0010      1 READ(1,22) X(I), YIN(I)
0011     22 FORMAT(2F10.4)
0012        IF (NTYPE-1) 30,31,30
0013     31 DO 32 I=1,N
0014        X(I)=10.**X(I)
0015     32 YIN(I)=10.**(-YIN(I)/2.)
      C
      C     X=EXPOSURE VARIABLE
      C     YIN=DENSITY VARIABLE
      C
      C     DETERMINE LOCAL INTERVALS
      C
0016     30 DO 9 K=1,NAMP
0017        DO 8 L=1,N
0018        NP1=NP(K)
```

```
0019          NB=(L-1)*NSTEP+1
0020          NE=NB+NP(K)-1
0021          IF(NE-N) 3,3,9
      C
      C       NORMALIZE LOCAL INTERVAL TO (-1,1)
      C
0022        3 DO 2 I=NB,NE
0023          NUM1=I-NB+1
0024        2 XN(NUM1)=(2.*X(I)-X(NE)-X(NB))/(X(NE)-X(NB))
      C
      C       SEARCH FOR XN OUTSIDE (-1,1)
0025          DO 201 I=1,NP1
0026          IF (1.-XN(I)*XN(I)) 200,201,201
0027      200 WRITE (3,202) I,XN(I),L,K
0028      202 FORMAT (' ', XN(',I3,')=',E11.4,' IN LINE',I3,'
             *OF AMPLITUDE',I3)
0029          IF(XN(I)) 203,203,204
0030      204 XN(I)=.999999
0031          GO TO 201
0032      203 XN(I)=-.999999
0033      201 CONTINUE
      C
      C       ADJUST Y VALUES
      C
0034          DO 4 J=1,NP1
0035          NUM2=NB+J-1
0036          4Y(J)=YIN(NUM2)
      C
      C       COMPUTE EXPANSION
      C
0037          M=NORD(K)+1
0038          DO 5 I=1,M
0039          N1=NP(K)-1
0040          AT(K,L,I)=0
      C
      C       AT(K,L,I)=TCHEB COEFF FOR AMP(K),INTERVAL(L)
      C        ORDER+1=I
      C
0041          I1=I-1
0042          I2=I-2
      C
0043          DO60 J=1,N1
0044          IF(XN(J)) 301,100,101
0045      301 ARG1=ATAN(SQRT(1.-XN(J)*XN(J))/XN(J))+3.
             *141592
0046          GO TO 104
0047      100 ARG1=1.570796
0048          GO TO 104
0049      101 ARG1=ATAN(SQRT(1.-XN(J)*XN(J))/XN(J))
0050      104 IF(XN(J+1)) 303,102,103
```

```
0051      303 ARG2=ATAN(SQRT(1.-XN(J+1)*XN(J+1))/XN(J+1))
              *+3.141592
0052          GO TO 105
0053      102 ARG2=1.570796
0054          GO TO 105
0055      103 ARG2=ATAN(SQRT(1.-XN(J+1)*XN(J+1))/XN(J+1))
0056      105 AO=(Y(J)*XN(J+1)-Y(J+1)*XN(J))/(XN(J+1)-XN(J))
0057          A1=(Y(J+1)-Y(J))/(XN(J+1)-XN(J))
0058          IF (I-2) 107,108,109
0059      107 AT(K.L.I)=AT(K,L,I)+(AO*(ARG1-ARG2)+A1*(SIN
              *ARG1)-SIN(ARG2)))
0060          GO TO 60
0061      108 AT(K,L,I)=AT(K,L,I)+(.5*A1*(ARG1-ARG2)+AO*(
              *SIN(ARG1)-SIN(ARG2))+1.2.5*A1*(SIN(2.*ARG1)-
              *SIN(2.*ARG2)))
0062          GO TO 60
0063      109 AT(K,L,I)=AT(K,L,I)+(.5*A1*(SIN(I2*ARG1)-SIN
              *(I2*ARG2))/I2
              1+AO*(SIN(I1*ARG1)-SIN(I1*ARG2))/I1
              2+.5*A1*SIN(I*ARG1)-SIN(I*ARG2))/I)
0064       60 CONTINUE
0065        5 AT(K,L,I)=AT(K,L,I)/1.570796
0066          XO(K,L)=.5*(X(NB)+X(NE))
      C
      C       CHECK FOR COEFFICIENTS LESS THAN NOISE LEVEL
      C
0067          DO 7 I=1,M
0068          ATAB=ABS(AT(K,L,I))
0069          IF (ATAB-ERR) 6,7,7
0070        6 AT(K,L,I)=0.0
0071        7 CONTINUE
      C
      C       COMPUTE NSR,1/S
      C
      C       ERPS(K,L)=ESTIMATE OF NUMERICAL ERROR IN FER(K,L)
      C       SNR(K,L)=RECIPROCAL OF SQUARED FUNDAMENTAL
      C       AMPLITUDE
      C       FER(K,L)=NOISE TO SIGNAL RATIO
0072          SIG2=AT(K,L,2)*AT(K,L,2)
0073          HAR2=0.0
0074          DO 13 I=3,M
0075       13 HAR2=HAR2+AT(K,L,I)*AT(K,L,I)
0076          IF(SIG2) 15,14,15
0077       14 FER(K,L)=0.0
0078          ERPS(K,L)=0.0
0079          SNR(K,L)=0.0
0080          GO TO 8
0081       15 FER(K,L)=HAR2/SIG2
0082          SNR(K,L)-1./SIG2
0083          ERR1=ERR*ERR
0084          ERPS(K,L)=ERR1/SIG2
```

```
      C
      C      NORMALIZE COEFFICIENTS IF SPECIFIED
      C
0085          IF (NORM-1) 8,18,8
0086       18 IF (AT(K,L,2)) 16,8,16
0087       16 DO 17 I=3,M
0088       17 AT(K,L,I)=AT(K,L,I)/AT(K,L,2)
0089        8 LSAVE(K)=L
0090        9 CONTINUE
      C
      C      WRITE RESULTS
      C
0091          DO 11 I=1,NAMP
0092          NUM3=NP(I)
0093          AMP=X(NUM3)-X(1)
0094          WRITE(3,24) PR,PR1,PR2,N,NP(I),NORM,ERR
0095       24 FORMAT('1',2A4,A2,' N=',I3,' NP=',I3,' NORM=',
             *I2,' ERR=',E10.3)
0096          WRITE(3,25)
0097       25 FORMAT(' ','NB',4X,'XZRO',5X,'XINT',5X,
             *'YINT',5X,'NSR',9X,
             1'DNSR',8X,'1/S',9X,'TCHEBYSCHEFF EXPANSION
             *COEFFICIENTS')
0098          MM=NORD(I)+1
0099          LS=LSAVE(I)
0100          DO 11 J=1,LS
0101          NB=(J-1)*NSTEP+1
0102          NE=NB+NP(I)-1
0103          XINT=X(NE)-X(NB)
0104          YINT=YIN(NE)-YIN(NB)
0105       11 WRITE(3,26) NB,XO(I,J),XINT,YINT,FER(I,J),
             *ERPS(I,J),SNR(I,J)
             1(AT(I,J,K),K=1,MM)
0106       26 FORMAT('0',I3,1X,3F9.3,1X,8(E11.4,1X)/69X,
             *5(E11.4,1X))
0107          GO TO 500
0108          END
```